Spring 1-1-2011

Probabilistic Assessment of Building Response to Simulated and Recorded Ground Motions

Kristen Leigh Rowe
University of Colorado at Boulder, Kristen.Rowe@colorado.edu

UNIVERSITY OF COLORADO AT BOULDER

Probabilistic Assessment of Building Response to Simulated and Recorded Ground Motions

By
Kristen Rowe
B.S./M.S., University of Colorado at Boulder, 2011

A Thesis Submitted to the Faculty of the Graduate School of the University of Colorado at Boulder in Partial Fulfillment of the Requirements for a Master's of Science
Department of Civil, Environmental and Architectural Engineering
2011

This Thesis entitled:

Probabilistic Assessment of Building Response to Simulated and Recorded Ground Motions

Written by Kristen Rowe

Has been approved for the department of Civil, Environmental and Architectural Engineering

---

Abbie Liel – Principal Advisor

Keith Porter

Nicolas Luco

Date December 7, 2011

The final copy of this thesis has been examined by the signatories, and we find that both the content and the form meet acceptable presentation standards of scholarly work for the Department of Civil, Environmental and Architectural Engineering

Abstract

Rowe, Kristen (M.S., Civil Environmental and Architectural Engineering)
Probabilistic Assessment of Building Response to Simulated and Recorded Ground Motions
Thesis directed by Assistant Professor Abbie Liel

This study examines the response of reinforced concrete (RC) frame buildings to both, physics-based ground motion simulations and recorded ground motions time histories. Nonlinear dynamic analysis is used to evaluate the response of six archetypical RC frame buildings to a set of three simulated and three recorded earthquakes. Using probabilistic analysis, building response is examined and statistically compared to determine whether the broadband ground motion simulations and the recorded ground motion time histories yield similar distributions for building response. Important aspects of the ground motion time histories which may cause differences in building response are then examined to attempt and explain the source of any dissimilarity in response. This study also examines the potential of applying the probabilistic analysis outlined in this study to the broader area of seismic risk analysis and potentially offers a new framework with which to evaluate building vulnerability to seismic events.

Results indicate that, when examined based on the elastic spectral response and inelastic spectral response, there are not significant statistical differences in building response. The long period energy content of the ground motions was found to play a key role in any differences which do exist. Higher mode effects, earthquake duration, energy content and rate of energy accruement were not found to have a significant effect on differences in building response.

Acknowledgments

I would first like to thank my research advisor Professor Abbie Liel. From taking me on as an undergraduate and encouraging me to attend graduate school, to spending countless hours with me planning, developing and revising this thesis, she has been an integral part of my college education. Without her drive, enthusiasm and insight this research would not have been possible. I would also like to thank Professor Keith Porter and Dr Nicolas Luco for agreeing to sit on my committee and offering their time to help me further develop this thesis.

A warm thank you to the researchers of the USGS, SCEC and other organizations that have helped develop the earthquake simulations used for this research. In particular thank you to Brad Aagaard and Robert Graves for providing me with data and kindly answering questions regarding their simulations.

Financial support for this research and my graduate education was provided by mainly SCEC with additional support from the CU Boulder department of Civil, Environmental and Architectural Engineering. This support was greatly appreciated.

Most importantly I would like to thank my family and friends for their continual support and love.

Table of Contents

List of Tables

List of Figures

Chapter 1: Introduction

1.1 Background

In recent years, researchers have developed a number of simulated earthquake scenarios using physics-based models of seismic wave propagation and attenuation. These simulated earthquake scenarios offer important information about regional risk, particularly because of a scarcity of groups of recorded ground motion time histories for large magnitude earthquakes. Simulated earthquake scenarios could also potentially add considerably to the available inventory of ground motions used for analyzing building response during a seismic event, particularly over an entire urban area. However, there are concerns that the response of multiple degree of freedom systems (MDOFs) when subjected to these simulated ground motions has not been systematically validated to show that comparable results are obtained from both the recorded ground motion time histories and the simulated earthquake scenario ground motion time histories.

1.2 Objectives

This study attempts to evaluate the use of simulated ground motions for nonlinear analysis of building response by examining, probabilistically, building responses to both simulated earthquake scenarios and recorded ground motion time histories. It attempts to quantitatively and qualitatively explain the differences that exist in the building response of archetypical reinforced concrete buildings to simulated and recorded ground motions. Building response is analyzed using the metrics of: interstory drift, probability of collapse and probability of exceeding given drift levels. Further, it attempts to explain why these differences in building response exist by examining ground motion input and structural response in both the frequency and time domains. Finally, it looks at the broader implications of applying scenario versus record time histories in terms of seismic risk assessment.

1.3 Scope and Organization

While the probabilistic assessment of building response used in this study has applications across multiple types of structures and geological areas, this research focuses on developing and applying a probabilistic method for evaluating the building response of reinforced concrete

frames subjected to simulated and recorded earthquakes in the California region. Using three simulated scenarios and ground motion time histories from three recorded events, as well as a general set of records developed from large magnitude events, this study uses probabilistic analysis in an attempt to quantify the differences in building response to the simulated and recorded ground motions. We also try to examine what features of the ground motion time history are causing the difference in building response by examining features in both the time and frequency domains of the various ground motions. These include: the response spectra, inelastic response, higher mode effects and energy content. Lastly, we examine the implications of ground motion selection in seismic risk assessment by looking at predicting building response using the probabilistic assessment approach rather than a scenario simulation approach.

Chapter 2 discusses the physics-based ground motion simulations. It first addresses the general process of simulation, including important input parameters, and also examines each of the three simulations used for this work in more detail. Assumptions and limitations which exist in the ground motion simulation process are also addressed. Additionally, this chapter examines literature which relates to important aspects of this study to provide a context for where this research fits into the broader spectrum of examining building response to simulated ground motions.

Chapter 3 outlines the research approach. It includes information about what recorded ground motions were selected, and what metrics will be used to compare the building response to the various ground motions. It also outlines what aspects of the ground motion will be examined to determine why the differences in building response exist. This chapter also contains a discussion on the limitations and assumptions of the study.

Chapter 4 describes the nonlinear building models, including the methodology and assumptions behind creating the nonlinear building models, and the important aspects of the building models, including geometry and material properties.

Chapter 5 outlines results of the nonlinear analysis as well as the key findings from the results in the context of one of the buildings. It also looks at the ground motion time histories and response spectra to attempt to explain the trends in the results. Lastly, Chapter 5 examines the broader implications of the research in terms of seismic risk assessment.

Chapter 2: Ground Motion Simulations

This study evaluates building response due to three different simulated earthquake scenarios: a repeat of the 1906 San Francisco earthquake developed by Aagaard et al. (2009), the ShakeOut Scenario created by Graves et al. (2008) and the Puente Hills scenario developed by Graves at al. (2005). Important aspects of each simulation are discussed in the sections below. A brief review of the simulation process is also provided here, as well as assumptions and limitations that inherently exist in the modeling process and may affect structural response.

Ground motion simulation is an increasing area of research for seismologists. Using physics-based models of seismic wave propagation and attenuation, researchers have developed broadband ground motion predictions for numerous simulated earthquake scenarios for faults in California and elsewhere. The predicted ground motion intensity and frequency content at each site from these simulated earthquake events depends on effects of earthquake magnitude, proximity to the fault, and site soil conditions as well as directivity and rupture patterns, which depend on the orientation of the fault and the direction of rupture (Jones, et al., 2008). In current physics-based ground motion simulations, modelers develop the ground motions simulations from input parameters including: fault geometry, rock and soil properties, ground topography, a fault rupture scenario, and a slip distribution.

For each simulation, a detailed model of the subsurface makeup of the region is an important input because the properties of the soil through which the seismic waves propagate determines how the seismic waves travel as well as the shaking characteristics at each site (USGS 2009). Rock properties can also affect seismic wave reflection and refraction, which affects the intensity of ground shaking. **Figure 1** shows an example of such a model taken from the simulation of a repeat of the 1906 San Francisco earthquake. In an effort to more accurately model the ground shaking for the 1906 San Francisco earthquake, the United States Geological Survey (USGS) developed this three dimensional (3-D) geological model of the area. This 3-D model contains data about the types of rock and seismic properties for the upper 45 meters of the Earth's crust and was developed based on core samples taken from hundreds of bore holes, in addition to gravitational and magnetic testing compiled by the USGS National Cooperative Geologic Mapping Program (USGS 2009). Similar 3-D models were developed for all three of the simulations used in this study. The 3-D models also contain information about fault

geometry and location and about sedimentary deposits, known as basins, which tend to reflect waves and also experience high levels of shaking intensity. An accurate geological model of the simulated region is an important aspect of developing robust simulated ground motions.

The fault rupture defines the rupture velocity during the simulated earthquake event. It is derived using previous observations as well as other forms of physics-based modeling such as full waveform tomography.

Defining a slip distribution, or the amount of horizontal displacement experienced at each point along the fault as a function of time, when the earthquake occurs is also an important factor in simulating an earthquake event. The slip distribution is generally based on the integral of the far-field time function, which is developed from the assumed effective stress stored in the fault which, when released, will accelerate each side of the fault (Aagaard, et. al, 2009). **Figure 2** shows a slip distribution along the entire rupture length developed for the 1906 earthquake.

Next, researchers create a wave propagation code by combining the fault rupture model, the detailed 3-D geological model and the slip distribution with basic physics wave propagation equations to create an earthquake rupture scenario. The physics-based wave propagation code allows researchers to numerically simulate the ground shaking at various sites across the region, creating the ground velocity time histories that are used in this study.

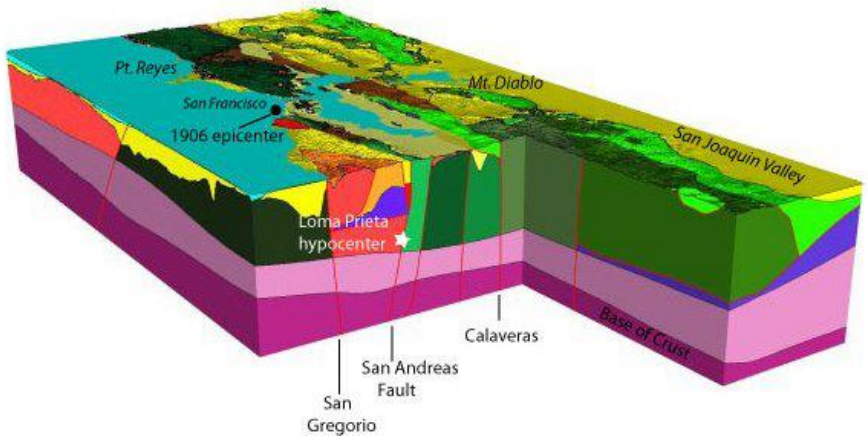

Figure 1: *3-D geological model developed for simulations of the 1906 San Francisco earthquake* (from USGS <http://earthquake.usgs.gov/regional/nca/3Dgeologic>)

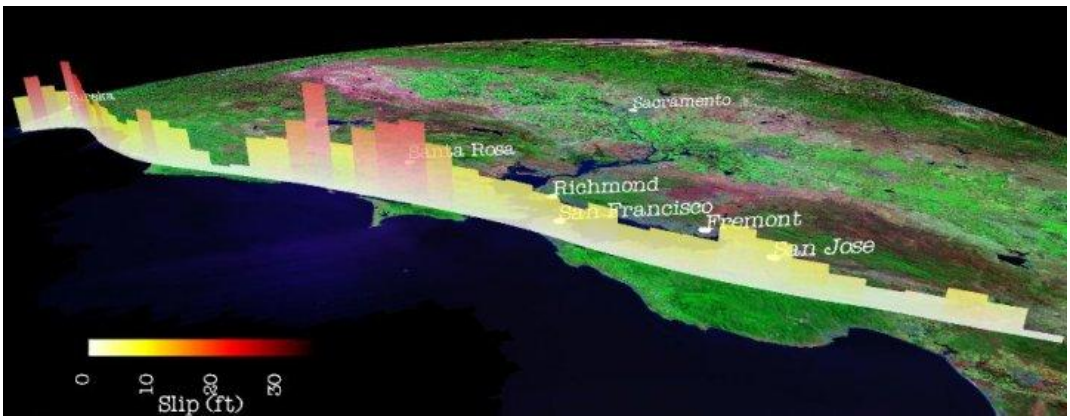

Figure 2: *Slip distribution for the 1906 earthquake simulation* (From USGS <http://earthquake.usgs.gov/regional/nca/1906/simulations/slipmodel.php>)

2.1.1 1906 San Francisco earthquake simulation

Broadband simulations for a repeat of the 1906 San Francisco earthquake were developed by multiple parties; this study utilizes the ground motions developed by Aagaard et al. (2008). This simulation of the 1906 earthquake produces a 7.8 M_w event which ruptures approximately 300 miles of the Northern San Andreas Fault (Aagaard, et al., 2009). The simulation was based on the SongMod scenario, the preferred source model for the 1906 earthquake, and is modified from the source model by Song et al. (2008). Ground motion time histories were developed for 1400 sites, seen in **Figure 3**, for the San Francisco area. The sites were selected to include both intensity sites chosen by Boatwright and Bundock (2005) and centroids of census tracks. The hypocenter for the SongMod scenario is located offshore from San Francisco at a depth of 10 kilometer. The SongMod scenario was modified from the Song source model by adding shorter-scale variations in slip and rupture speed which was modified such that waves propagate more quickly in regions of larger slip (Aagaard, et al., 2009).

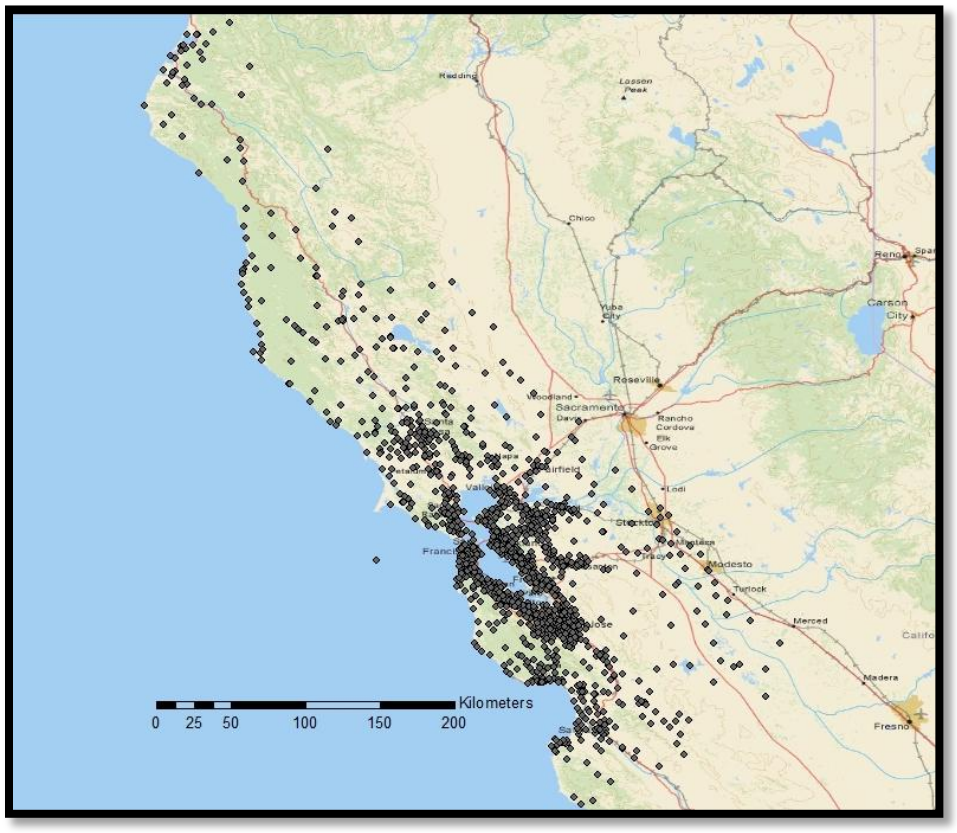

Figure 3: *Simulated ground motion time history sites for the 1906 San Francisco Earthquake*

Ground motions developed by Aagaard *et al.* for the SongMod simulation are bandlimited to low frequencies (<0.5 Hz). The slip distribution used varies along the fault rupture with an average slip of 3.0 m and the slip-time function is based on Brune's far-field time function. The material properties for the rock used in the Aagaard SongMod scenario were derived from the USGS Bay Area Velocity model, version 05.1.0, which attempts to define a 3D geological model of the Northern California region based on boreholes, surface outcrops, gravity and magnetic data (Brocher 2006). The simulation also takes into consideration surface topography of the rupture area, including the presence of basins and mountains. The seismic wave propagation for the SongMod scenario was modeled using an unstructured finite-element code that is composed of 4-node tetrahedral elements. The element size varies depending on the local shear wave wavelength with a minimum shear velocity of 70 m/s. The fault surface is represented by an internal boundary within the finite-element mesh which is smoothed by applying a Laplacian transformation and the slip is represented as a displacement discontinuity on the fault surface (Aagaard et al., 2008).

The 1906 SongMod simulation was validated in two ways: first by using the 1989 Loma Prieta earthquake simulation and comparing the simulated ground motions to actual recorded results, and second by comparing estimated shaking intensities to the ShakeMap developed by Boatwright and Boondock (2005). In performing this validation, Aagaard et al. (2009) determined that the long-period simulation, on average, under-predicted the shaking intensities by approximately one-half Modified Mercalli Intensity units (MMI) or about 25%-35% in peak ground velocity (PGV). MMI is a measure of ground motion intensity on a scale from 1 to 12 with 1 being nearly imperceptible ground shaking and 12 being total destruction of nearly all structures and including significant ground distortion. This discrepancy likely arises from the assumptions regarding geological structure and wave propagation as well as limitations in the modeling process and resolution. Overall, the validation with the Loma Prieta earthquake suggests that the simulation model fairly successfully captures key aspects and trends of the ground motion at various sites. **Figure 4** shows the observed and simulated wave forms for two of the stations. The validation found that waveforms, particularly at sites close to the rupture reproduced amplitude and duration of the recorded motions (Aagaard, Brocher, et al., 2008). Validation using the Boatwright and Boondock ShakeMap, which estimated shaking intensities from detailed reports of the 1906 earthquake, showed that the 1906 simulation generally over-predicted shaking intensities by 0.1 to 0.5 MMI units or about 6%-35% (Aagaard, et al., 2008).

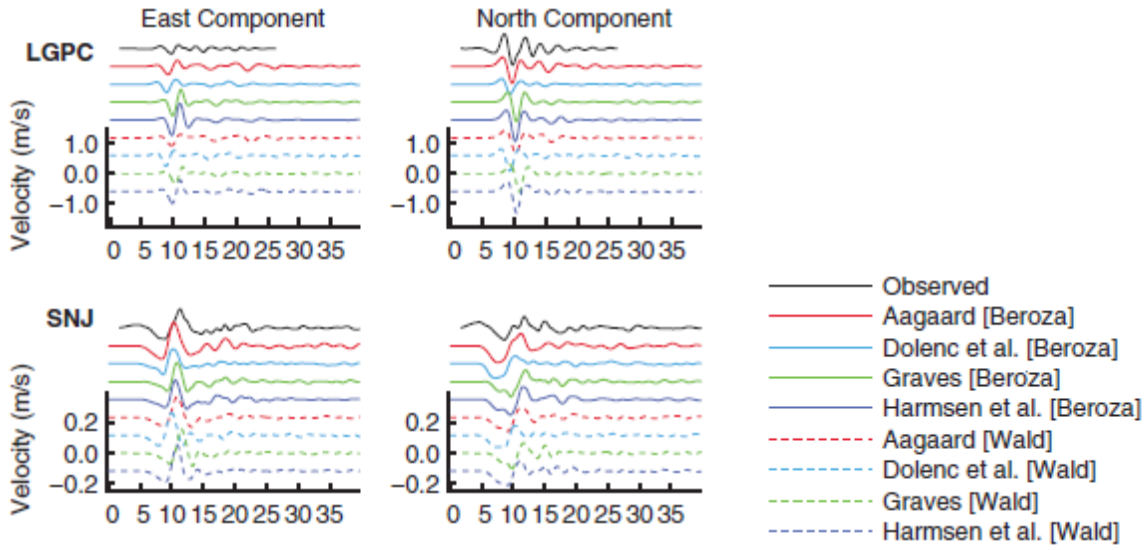

Figure 4: *Velocity waveforms for two sites developed for the 1989 Loma Prieta simulation and compared to recorded results (Aagaard, 2008)*

2.1.2 ShakeOut scenario earthquake simulation

Broadband simulations for the ShakeOut scenario were developed by Graves et al. (2008) for a 7.8 M_w earthquake on the Southern San Andreas Fault. Three different rupture scenarios were developed; this study uses the ShakeOut scenario earthquake which is a south-to-north rupture which produces the largest shaking intensities in the Los Angeles Basin. The scenario rupture extends for 300 kilometers from Bombay Beach to Lake Hughes along the southern most portion of the San Andreas Fault. Ground motion time histories from the 736 sites, are shown in **Figure 5**.

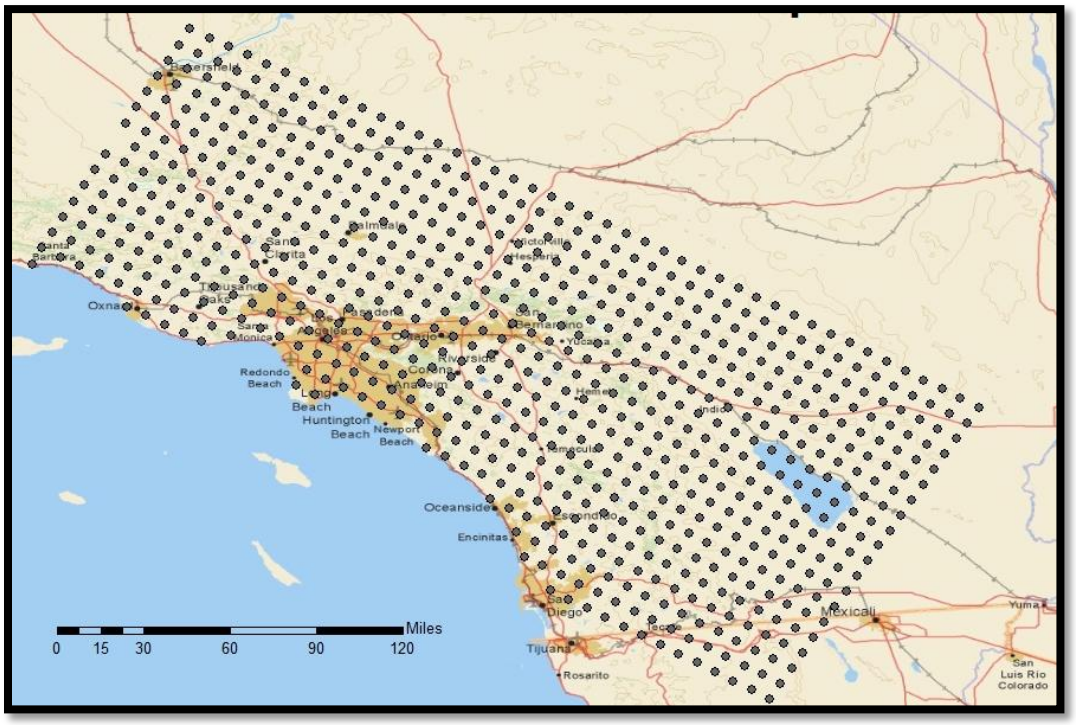

Figure 5: *Simulated ground motion time history sites for the ShakeOut simulation*

The broadband ground motions (0-10 Hz), were developed by combining a 3-D deterministic approach at low frequencies with a semi-stochastic approach at high frequencies. The ShakeOut scenario slip distribution produces an average slip along the fault of 4.6 meters. The slip distribution function is based on two models: the slip-predictable model from Jones et al. (2008) for large scales and a random-phased slip model from Mai and Beroza (2002) for smaller scales. The slip function is based on Brune's far-field time function. Rupture speed was assumed to be varied linearly based on the local shear wave velocity (V_s). Fault geometry was

modeled using 3D models developed by the Southern California Earthquake Center (SCEC) including the SCEC Community Fault Model and the SCEC 3D Community Velocity Model.

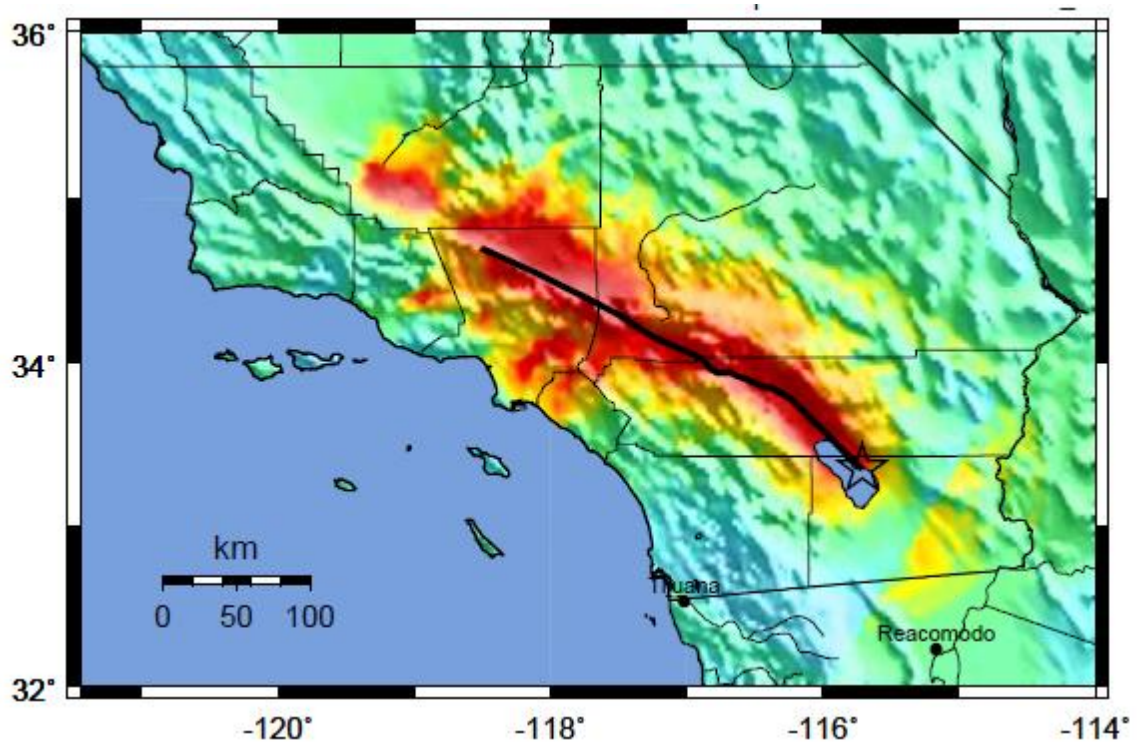

Figure 6: *Shaking intensities (MMI) for the ShakeOut simulation on the San Andreas Fault (fault location in black, hypocenter indicated by star)* (from the USGS <http://urbanearth.gps.caltech.edu/scenario08/shakeout_media>)

In validating the ShakeOut scenario, Graves et al. (2008) examined the shaking intensities (seen in **Figure 6** in units of MMI), peak ground acceleration (PGA), peak ground velocity (PGV) and peak ground displacement (PGD). The shaking intensities were compared to four Ground Motion Prediction Equations (GMPEs): Campbell and Bozorgnia (2008), Abrahamson and Silva (2008), Boore and Atkinson (2008), and Chiou and Youngs (2008). The GMPEs provide the median expected shaking intensity. Because the GMPEs are developed based on observed data, they are limited in that few large earthquakes have occurred for this fault and rupture type so they may not accurately represent the shaking experienced for large magnitude earthquakes. When comparing the ShakeOut simulation results with the GMPEs, it was determined that the simulations results were usually at or below the median GMPE estimates for periods $T < 2.0$s but they were found to be higher for periods between $3.0 < T < 5.0$s. This discrepancy is assumed to occur because of basin and directivity effects that are strongest in this

frequency band. The comparison for the long-period ground motions are also affected by the fault slip distribution which creates larger shaking intensities at long periods (Star, et al., 2008).

2.1.3 Puente Hills scenario earthquake simulation

The Puente Hills simulation developed by Graves et al. (2005) consists of three different scenarios rupturing the Puente Hills Fault near the Los Angeles Basin. A major earthquake on the Puente Hills fault could cause substantial damage in the Los Angeles area and is of particular interest for this reason. Puente Hills is a blind thrust fault and the hypocenter, for this simulation, is north of the Los Angeles Basin. The rupture for this scenario earthquake propagates south funneling energy directly into the Los Angeles Basin, causing large ground motions due to directivity and basin effects. For this study, ground motion simulations from the R-2 rupture scenario were used; this scenario produces a 7.2 M_w event which ruptures the entire length of the Puente Hills Fault system. Due to the directivity effects, the R-2 simulation produces the largest ground motion effects in the Los Angeles Basin, motivating its choice for this study. Ground motions time histories from 875 sites, shown in **Figure 7**.

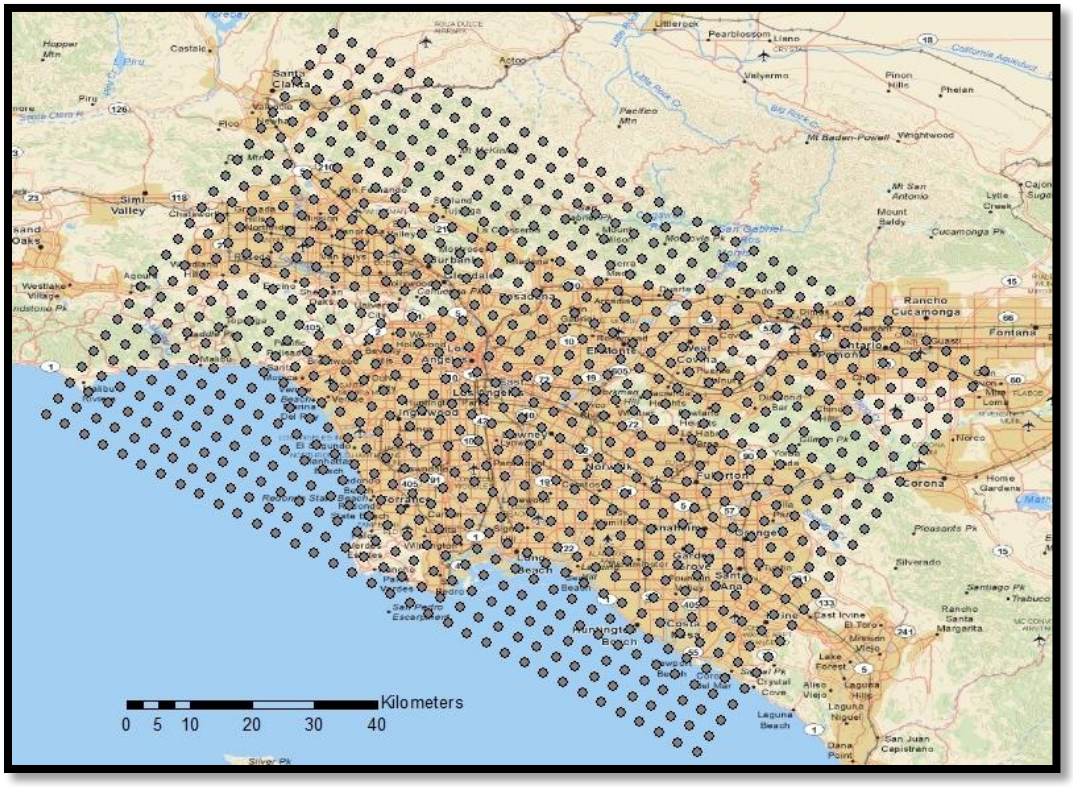

Figure 7: *Simulated ground motion time history sites for the Puente Hills*

Broadband (1-10Hz) ground motions were simulated for the Puente Hills scenario using two different procedures. For low frequencies (f<1Hz) a deterministic method was used carrying out the calculation using a 3-D viscoelastic finite-difference algorithm to combine the source rupture, wave propagation and 3-D geologic model. For high frequencies (f>1Hz), a stochastic method is used in which the simulation sums the response from each subfault which is allowed to rupture with a moment weighting proportional to the final slip for that subfault. Further information about the stochastic process is referenced in Boore et. al (1983). The simulation produces broadband (0-10Hz) ground motions at 66,000 sites near the LA area. For this simulation, slip distribution varies from 0 to 3 meters along the length of the fault (Graves, 2005).

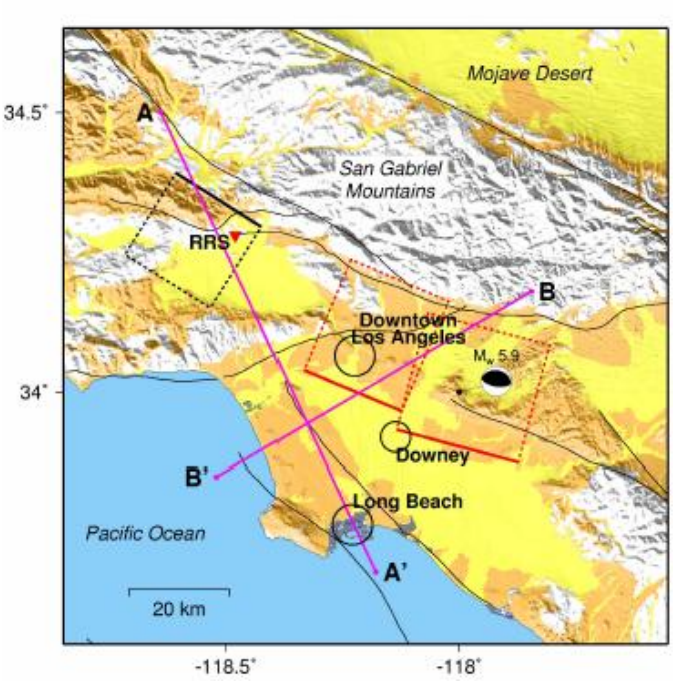

Figure 8: *The Puente Hills Fault system (indicated in red)* (Graves, 2005)

Stewart et. al. (2008) validate the Puente Hills simulation using four Next Generation Attenuation (NGA) developed empirical GMPEs which were used to validate the ShakeOut simulation. This study concludes that the simulated ground motions attenuate more rapidly than those from the empirical model particularly for longer spectral periods, but draws no other conclusions as to the validation of the Puente Hills simulation.

2.1 Limitations of ground motion simulation

As with any modeling effort, numerous limitations and approximations inherently exist in the modeling process for earthquake scenario events. The size of the modeling domain, the spatial resolution within the modeling domain, the bandwidth, as well as other features which are included in the models are all restricted due to computational and numerical limitations. Uncertainties also exist regarding the slip-time function, fault geometry, rock properties and wave propagation. Slip-time functions can vary drastically among researchers and while models are always validated, the slip distribution offers a large area of uncertainty in the modeling process (Aagaard, et al., 2008). Also, particularly for simulations of large magnitude earthquakes at sites near the fault, current data regarding wave propagation and attenuation are uncertain. Derived empirically from data recorded during actual earthquakes, these attenuation functions are limited to the current data set of actual recorded earthquakes. Therefore, for large ground motions, the accuracy of existing ground motion prediction equations is not well known. These uncertainties and limitations may affect the accuracy of the simulated events and their applicability to use for analyzing building response.

2.2 Literature review: Structural response to simulated ground motions

2.2.1 Building response due to simulated earthquakes

In recent years, multiple studies have examined building response due to simulated earthquakes. Using computer models of various structural systems and building types, researchers have analyzed the vulnerability of certain types of buildings to large ground motions. These studies offer important information about regional risk exposure and also vulnerability of certain types of structures to large ground motions, and demonstrate the importance of having a simulated ground motion set with which to evaluate building response. Having sets of simulated ground motions is important because of a lack of comprehensive recorded data for large ground motions near the fault. By simulating earthquake ruptures, researchers can provide engineers with ground motion time histories in evenly spaced grids particularly for areas of interest, including highly populated areas. They can also provide these ground motion time histories for much larger earthquakes than we currently have recorded, offering important information for

testing structural response. Of particular interest for this study, a number of papers have examined the response of buildings to simulated events in California.

For example, Olsen et al. (2008) evaluated the response of 20-story steel moment resisting frames (MRFs) with both ductile and brittle welds when excited by various simulated earthquakes including: the 1989 Loma Prieta earthquake simulation, the 1906 San Francisco earthquake simulation and two 7.8 M_w events on the Northern San Andreas Fault with hypocenters north and south of San Francisco. This study used simulated ground motions because it offers important information about regional risk to large ground motions for steel frame buildings in highly populated areas. Findings indicated that, when using peak interstory drift ratio (IDR) as the performance measure, the stiffer buildings with ductile welds outperformed the more flexible structures, as well as those with brittle welds. The study also found that the smaller 1989 Loma Prieta earthquake event produces much lower responses than the 1906 style simulation, implying that buildings which survived the 1989 Loma Prieta earthquake may still be susceptible to an event similar to the 1906 earthquake. This study also showed that the Bay Area is susceptible to large ground motions possibly causing damage to these types of buildings.

Krishnan et al. (2006) examined the response of 18-story steel MRFs when subjected to two of the ShakeOut rupture scenarios, again using simulated ground motions to examine regional risk exposure in urban areas. This study indicates that the Los Angeles Basin and San Fernando Valley are particularly susceptible to large ground motions and damage to tall steel moment frame structures. The two different scenarios considered, which ruptured in opposite directions, produced significantly different results in terms of building response. Based on this, research also concludes that directivity plays an extremely important role in structural response and regional risk exposure.

Lynch et al. (2011) examined the response of reinforced concrete frames to the simulated ShakeOut scenario. This study looked at the susceptibility of archetypical non-ductile and ductile reinforced concrete MRFs subjected to the ShakeOut rupture scenario. Results show that the non-ductile frames are significantly more susceptible to collapse during this scenario event particularly in Los Angeles, Palm Springs and San Bernardino. Results also indicate that even modern code-conforming buildings may be susceptible in the Los Angeles Basin due to basin and directivity effects.

While a multitude of other research efforts have been conducted regarding building response to simulated earthquake events, these studies were of particular interest because they examined structural response to the particular simulations used in this study. They demonstrate the importance of using the scenarios developed for California to analyze various types of structures and structural systems. These types of studies can, conceivably, determine regional areas which may be at risk due to large ground motions for various types of structures which exist in the California building inventory. They could also to provide city officials and disaster response teams with information about the structural vulnerability of urban areas in California.

2.2.2 Simulated versus recorded ground motions

Validating the use of these types of simulated ground motions is an important, but insufficiently researched, topic. Few studies have examined the response of structures to simulated ground motions in comparison to either recorded or modified ground motion time histories. Atkinson and Goda (2010) examined the response of single degree of freedom (SDOF) systems to scaled, modified and simulated ground motions for the Cascadia subduction zone, in an attempt to examine the validity of simulating and modifying ground motions and to identify the key factors that may affect structural response. Scaled records are those which retain the original spectral shape but are either scaled up or down to achieve a desired spectral acceleration for a particular period. Modified records are real records which have had the spectral shape altered through the removal of peaks and troughs using a spectrum matching technique and calibrating to a generated record. They observed that, for the nonlinear response of SDOF systems, if the peaks and troughs and spectral shape of the real and modified records are carefully selected, the simulated records adequately predict peak inelastic response of the system. This and previous studies (Luco and Bazzurro, 2007) find that two important features must be considered when selecting records to modify including: the effects of peaks and troughs in the spectra as well as the response spectra shape. Atkinson and Goda (2010) also conclude that, depending on the similarity of the peaks and troughs and response spectral shape, the nonlinear response for the simulated and modified records provides similar and satisfactory matches for peak inelastic response. However, that study is limited to SDOF structures and does not account for biases that may be inherent in the scaled and modified ground motions. Depending on the method of scaling, the process itself may introduce biases affecting the structural response of

MDOFs. Research regarding the biases introduced in scaling and what factors affect these biases is addressed below.

Ongoing work by Zareian and Jones (2010) is also examining the effects of simulated and recorded ground motions on building response using three 42-story buildings. The building types examined are: a concrete core, dual concrete and a steel moment resisting frame. They analyzed the response of these three building models to simulated ground motions in the Los Angeles area and compared them to a subset of large recorded ground motions taken from the NGA database. Preliminary results indicate that, despite possessing similar energy in the primary modes of vibration, the general set of ground motions yield different results in structural behavior in terms of interstory drift. They concluded that this is likely due to different phasing of modal contributions in the structural response between the two sets of ground motions. Research is ongoing to explore the cause for the difference in structural response. This study is also limited in that they scaled the NGA ground motions which may introduce biases into the response. To limit these biases, the maximum scale factor they used was 5.0 and the scale factor used for each ground motion was the one which introduced the smallest weighted error between the target spectrum and the geometric mean spectrum (Zareian and Jones 2010).

Lastly, current work by Jayaram, Shome and Krawinkler (2010) looks at the statistical analysis of the response of tall buildings to recorded and simulated ground motions. Using tall buildings (40-story) steel MRFs, they are analyzing structural response to the Puente Hills simulation and a general set of large ground motions from the PEER-NGA database. Using statistical methods, such as hypothesis testing, they compare important building response parameters for the simulated and recorded ground motions. They conclude that there are significant differences in some of the building response metrics including interstory drift, peak floor acceleration, and residual drifts. This study is limited to long period (6.4 s) structural response to ground motions.

2.2.3 Parameters which may affect building response

While little investigation has been performed regarding the effects of using simulated versus recorded ground motions on building response, numerous studies have examined the effects on building response using scaled and unscaled recorded ground motions time histories. Traditionally, ground motion records were selected for scaling based on similar magnitude and distance from the fault. Yet recent research has revealed that selecting and scaling ground

motions, without consideration of certain factors, may introduce significant biases into the building response. These studies have also revealed numerous areas of importance regarding the selection and scaling of ground motions. These spectral characteristics may also prove important when looking at possible biases introduced to structural response due to simulated earthquake scenarios. These include: the spectral acceleration, the spectral shape, the importance of peaks and troughs, and the building period and strength reduction factors. This section highlights several key parameters that research has revealed should be considered when using scaled ground motions.

When using ground motions to evaluate building response, spectral acceleration at the first mode building period $Sa(T_1)$ plays an important role in the response. Engineers and researchers often scale ground motions to reach a certain spectral acceleration value for particular periods in which they are interested. This scaling is important to estimate building response for a certain spectral acceleration. Often records do not exist with the needed level of spectral acceleration at key periods which will generally produce lower damage estimates when evaluating building response, requiring upscaling of current records. However, there are other parameters which can significantly affect the building response, in particular the spectral shape.

The spectral shape of the ground motion used has been found to be one of the key factors which can produce biases into the building response when scaling ground motions. Baker & Cornell (2006) evaluated selection and scaling ground motion records based on multiple parameters including: distance from fault, magnitude and the ground motion parameter epsilon (ε). Epsilon is a term used to quantify spectral shape and represents the difference between the spectra of the ground motion record and the median prediction from an attenuation function. They proposed a new way of selecting ground motions for scaling based on the conditional mean spectrum considering epsilon (CMS-ε). **Figure 9** shows an individual earthquake record and also a graphical representation of ε for a magnitude 7 earthquake 12 km from the fault. CMS-ε is a target spectrum obtained by considering both magnitude and distance from the fault and also including values of ε that are likely to cause a target ground motion intensity. They concluded that records selected by looking at ε and the CMS-ε produced scaled records which did not introduce biases into the structural response, whereas records chosen only by their distance from fault or magnitude, produced results which were determined to be biased in their structural response. Therefore, carefully matching the value of ε or calculating an appropriate value of

CMS-ε for the period of interest is important in avoiding biases when scaling ground motions. Luco and Bazzuro (2006) examined the response of SDOF systems to real records, considering amplitude-scaled records and spectrum scaled records. Amplitude-scaling is defined as when a real record is uniformly scaled so that the resulting spectrum has the desired amplitude at the period of interest, usually the fundamental period of the structure being examined. Spectrum scaling is when a real record's frequency content and phasing is modified to match a smooth target spectrum. They drew the conclusion that for SDOFs using near-source records, amplitude up-scaling tended to make the records more aggressive than the unscaled records at the same spectral acceleration level. This happens for a few reasons: first, upscaling the amplitude of the record increases the long period energy which, when looking at inelastic response, can cause much more damage as the building period increases. Second, rare ground motions, particularly in California, tend to have large values of epsilon implying they have large peaks and troughs. Upscaling causes an increase in the peaks causing an increase in intensity of the ground motion at periods which may be important for building response. Alternatively, spectrum-matched records were more benign than the corresponding real records likely because of the smoothing of peaks and troughs which can decrease intensity for periods that may affect structural response.

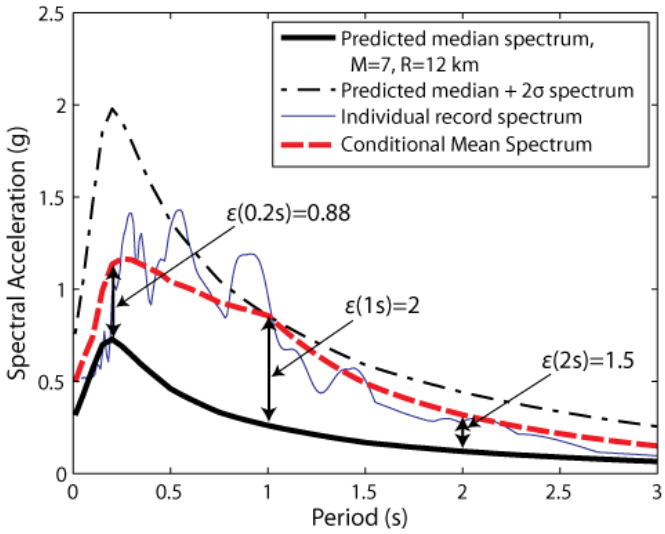

Figure 9: *Response spectra, illustrating calculation of epsilon* **(Baker 2011)**

Numerous studies have demonstrated the importance of matching peaks and troughs when scaling ground motions. Luco and Bazzurro (2007) analyzed the drift responses of SDOF and MDOF systems subjected to scaled and unscaled ground motion records using nonlinear

dynamic analysis. This study drew the conclusion that scaling of records with a trough at the period of interest produced results biased-high in the spectral displacement response relative to an unscaled record. However, if a record exhibits a peak at the period of interest and is therefore scaled down, it will result in a biased-low displacement response. Therefore, it is important when selecting ground motions to scale, the peaks and or troughs of the ground motion are considered. Atkinson and Goda (2010) also analyzed the response of SDOF structures to scaled records and drew a similar conclusion to Luco and Bazzurro (2007); if care is used in selecting records by looking at peaks and troughs, scaling of ground motions can result in relatively unbiased peak inelastic response.

Building properties themselves also affect the validity of scaling ground motion records. Luco and Bazzurro (2007) examined scaling of ground motion records by evaluating both SDOF and MDOF nonlinear drift response. Results demonstrated that, scaling randomly selected records introduced a bias into the median structural response, and that this bias increased with the degree of scaling. The amount of bias depends on numerous parameters including the fundamental period of vibration, the strength of the structure and the sensitivity of the structural response to higher modes of vibration. The study concluded that if the structural response is more sensitive to higher modes, the scaled record will produce more bias because of the difference in spectral shape of the scaled ground motion at periods relating to the higher modes.

Chapter 3: Research Approach

3.1 Overview

In order to systematically evaluate the use of simulated ground motions to predict the structural response of MDOFs, this study uses nonlinear dynamic analysis to evaluate building response for six computational simulation models of reinforced concrete frame structures. These building models, which will be discussed in detail in Chapter 4, are modeled in the OpenSees software platform and capture key aspects of nonlinear behavior. As the ground motion time history is applied and nonlinear behavior ensues, the stiffness of the model is constantly updated. Nonlinear dynamic analysis is performed for all six building models using both the simulated and recorded ground motions. Important metrics of building response including interstory drift, collapse, and building displaced shape are recorded for all ground motions and buildings. By analyzing these important response metrics, conclusions can be drawn as to what differences exist in the building response to simulated and recorded ground motions and whether these differences lie within an acceptable range of variability. The parameters and methods used to determine whether significant differences exist in building response are discussed in more detail in Section 3.3. If the response metrics indicate that significant differences exist between building response to simulated and recorded ground motions, it is important to then determine what causes these differences.

3.2 Selection and processing of simulated and recorded ground motions

This study focuses on the investigation of earthquake simulations created for California. California simulations in particular were selected because of the large number of simulations created for the area, as well a high number of recorded ground motions existing in a comprehensive database for this region. Three simulated events and three recorded events, as well as a generalized set of ground motions, were selected for use. The details of the simulated events were discussed in depth previously in Chapter 2. **Table 1** summarizes general information for both the recorded and simulated ground motions used in this study.

Table 1: *Simulated and recorded ground motion summary*

	Earthquake	M_W	# of Sites	Study Area [miles x miles]	Min PGA [g]	Max PGA [g]	Average PGA [g]
Recorded	Northridge	6.7	313	100x50	0.028	1.78	0.219
	Loma Prieta	6.9	163	160x40	0.005	1.16	0.121
	Chi-Chi	7.6	838	155x75	0.005	1.16	0.108
	Generalized	6.5-7.6	35	N/A	0.210	0.82	0.418
Simulated	ShakeOut	7.8	736	75x50	0.009	1.31	0.169
	Puente Hills	7.2	875	75x62	0.097	1.45	0.342
	1906 - San Francisco	7.8	1318	325x100	0.045	0.948	0.261

3.2.1 Simulated ground motions editing

All the simulated ground motion time histories were received as ground velocity time histories. To run the building models it was necessary to convert the velocity time history into an acceleration time history. This was accomplished using the linear approximation over each time step:

$$a(t) = \frac{v_2 - v_1}{t_2 - t_1}$$

This approximation is deemed to be reasonable because of the small time steps provided in the simulation.

After the ground motion velocity time histories were converted to accelerations, it was important to trim the length of the simulations to decrease the computational time required to run the building models with the simulated earthquakes. The simulated records contained the entire time length of rupture, often hundreds of seconds of which contained very little energy. The simulated ground acceleration time histories were trimmed to include only the significant duration of the earthquake, in this case the portion of the ground motion time history which contained 99% of the shaking energy. This was accomplished by calculating the Arias intensity, a measure of the ground motion intensity, and then normalizing to create a Husid plot (Husid, 1969). The Husid plot represents the accumulation of energy throughout the duration of the earthquake. The earthquake records were trimmed using the time when the energy accumulation passes the threshold of 0.5% until the time it reaches 99.5%. This represented a significant decrease in the earthquake duration and, hence, the necessary computational time, but due to very low amounts of lost energy, it does not affect the building response.

3.2.2 Recorded ground motions set selection

Recorded ground motions were selected for a number of reasons including: the location, fault type, magnitude and number of records available. The records were acquired from the PEER-NGA database maintained by the Pacific Earthquake Engineering Research Center. From this database we selected mainly California recordings because they represent shallow crustal ruptures similar to those being modeled in the ground motion simulations.

The 6.9 M_w 1989 Loma Prieta earthquake caused significant damage to bridge and viaduct structures and wood and unreinforced masonry construction in the San Francisco region. Because this study uses the 1906 San Francisco simulation, which was validated using the Loma Prieta earthquake, we decided it was important to include the Loma Prieta earthquake in the set of analyzed recorded ground motions to represent wave propagation and earthquake attenuation patterns in the San Francisco bay area. Ideally, the soil and rock structure as well as wave propagation and earthquake attenuation for the Loma Prieta earthquake should match that developed for the Bay Area used in the 1906 San Francisco simulation.

In the Los Angeles area, a significant number of ground motion time histories exist for both the Whittier Narrows and the Northridge earthquakes. The 6.7 M_w 1994 Northridge earthquake was selected for this study because of its larger magnitude and the larger number of sites at which recordings exist. Presumably, the soil structure and attenuation is also similar for the Northridge earthquake and the Puente Hills and ShakeOut simulations. However, it is important to note that the Northridge earthquake had the strongest directivity effects channeled in the mountains north of the San Fernando basin, which is opposite of the Puente Hills and ShakeOut cases, where rupture channels directly into the LA basin. This makes a direct comparison between the recorded and simulated ground motions difficult as directivity plays a large role in shaking intensities.

The 7.6 M_w 1999 Chi-Chi Taiwan earthquake was also selected, despite the fact that it is a thrust fault, because of the large magnitude of the earthquake and also a very large number of recordings existing for this earthquake. Very little data exists in accessible databases for large magnitude earthquakes and since all the earthquake simulations evaluated in this study are large magnitude events, we decided that the Chi-Chi earthquake would offer valuable building response information for recorded ground motion time histories.

3.2.3 Generalized far-field ground motion set overview

This study also uses a suite of far-field ground motions as a comparison to assist in examining the variation of building response from a mean expected value. This set of ground motions is characterized by records from high magnitude events and moderate site-to-source distances. This set is comprised of recordings from 13 different earthquakes and is used as a mean estimation of building response to large magnitude earthquakes similar to those being simulated in the California simulations examined in this study. The far-field ground motions used are a sub-set of the far-field ground motion database from Federal Emergency Management Agency (FEMA) P695 (2008). These ground motions records were selected from the PEER NGA database using the following criteria:

Magnitude - Moment magnitude Mw ≥ 6.5

Source type - strike-slip or reverse thrust fault sources

Geologic site conditions - soft rock or stiff soil sites

Site-to-source distance - average distance to the fault plane, D ≥ 10 km

Strong ground motion records - peak ground acceleration PGA ≥ 0.2g and peak ground velocity, PGV ≥ 15 cm/s

This set of ground motions contains 22 records each with two horizontal components yielding 44 acceleration time histories. Details of each recording can be found in **Table 2**. However, based on results from Champion et al. (2010), nine acceleration records were removed, having been identified as having a large velocity pulse. Records which exhibit large pulses are known to affect the building response and so, to avoid skewing results in building response due to pulses, these records were removed from the generalized set.

Table 2: *Far-field ground motion suite summary*

Earthquake	M_W	Year	Recording Station	Average Distance (km)	PGA (g)	PGV (cm/s)
Northridge	6.7	1994	Beverly Hills - Mulhol	17.2	0.52	63
Northridge	6.7	1994	Canyon Country - WLC	12.4	0.48	45
Duzce, Turkey	7.1	1999	Bolu	12	0.82	62
Hector Mine	7.1	1999	Hector	11.7	0.34	42
Imperial Valley	6.5	1979	Delta	22	0.35	33
Imperial Valley	6.5	1979	El Centro Array #11	12.5	0.38	42
Kobe, Japan	6.9	1995	Nishi-Akashi	7.1	0.51	37
Kobe, Japan	6.9	1995	Shin-Osaka	19.2	0.24	38
Kocaeli, Turkey	7.5	1999	Duzce	15.4	0.36	59
Kocaeli, Turkey	7.5	1999	Arcelik	13.5	0.22	40
Landers	7.3	1992	Yermo Fire Station	23.6	0.24	52
Landers	7.3	1992	Coolwater	19.7	0.42	42
Loma Prieta	6.9	1989	Capitola	15.2	0.53	35
Loma Prieta	6.9	1989	Gilroy Array #3	12.8	0.56	45
Manjil, Iran	7.4	1990	Abbar	12.6	0.51	54
Superstition Hills	6.5	1987	El Centro Imp. Co.	35.8	0.36	46
Superstition Hills	6.5	1987	Poe Road (temp)	11.2	0.45	36
Chi-Chi, Taiwan	7.6	1999	TCU045	77.5	0.51	39
San Fernando	6.6	1971	LA - Hollywood Store	39.5	0.21	19
Friuli, Italy	6.5	1976	Tolmezzo	20.2	0.35	31

3.3 Comparison of recorded and simulated ground motions

3.3.1 Evaluating building response

After performing nonlinear analysis of a given building model, the next step in examining the simulated ground motions is to quantify differences in building response to the simulated and the recorded ground motions and then determine what features of the simulation process contribute to these differences. Important metrics of building response that are evaluated to determine if differences exist include: maximum interstory drift ratio, median spectral acceleration causing collapse, and probability of exceedance of given drift levels.

The interstory drift represents the ratio of the differential maximum horizontal displacement between two floors to the height of that story. Higher levels of interstory drift

represent greater displacement over the height of the floor, which usually indicates higher levels of damage in that particular story. Plots of interstory drift versus spectral acceleration, as seen in **Figure 10**, can be used to examine trends for each earthquake, including average spectral accelerations which will cause a given interstory drift. In **Figure 10**, each dot shows the ground motion intensity, represented by $Sa(T_1)$, and the corresponding maximum interstory drift in the structure. The solid line represents the average curve computed for various bins of interstory drifts. Dots with interstory drifts greater than 0.1 represent the collapsed records, the treatment of these sites will be described in more detail below.

The difficulty in comparing building response metrics, such as interstory drift, for earthquake simulations and recorded ground motions is quantifying an acceptable variability. Due to differences in frequency and time domain content, record to record responses can vary drastically even for the same event. Because of this, it is difficult to compare interstory drifts for different earthquakes. To take this into consideration we examine the plots of interstory drift normalized by *Sa* and attempt to draw comparisons this way.

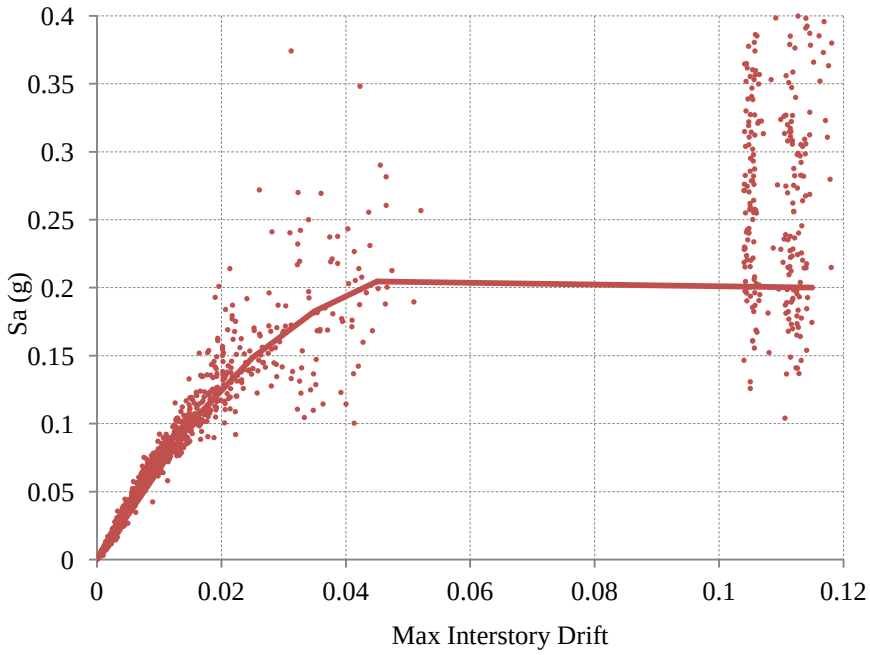

Figure 10: *Interstory drift vs. spectral acceleration for the ShakeOut simulation for an 8-story non-ductile concrete frame*

Fragility functions are also valuable for evaluating building response to a ground motion. The fragility function shows the probability of being in or exceeding a particular limit state, i.e. collapse, as a function of ground motion intensity, as shown in **Figure 11**. In this study, the fragility function is obtained from generalized linear regression created using a binomial distribution with the two outcomes, e.g. collapse (1) or non-collapse (0). These two outcomes are plotted on **Figure 11**. These fragility functions assume that the natural logarithm of the ground motion intensity causing the limit state exceedance is normally distributed. The fragility functions were created using the *glmfit* command in Matlab with a binomial distribution. The median spectral acceleration causing collapse can be easily determined from where the fragility function crosses the P[collapse] = 0.5.

Examining the variability in median spectral acceleration causing collapse for the real ground motions can give a range of typically experienced variability of building response to spectral acceleration. We can use this range of median spectral acceleration causing collapse to compare the simulated and recorded ground motions. This plot also provides information about the likelihood of collapse given a certain value of spectral acceleration. As an example, consider results from the 8-story non-ductile RC building subjected to the Northridge earthquake at a site with $Sa(T_1)$=0.2g. There is only about a 3% chance that the building will collapse while a building with $Sa(T_1)$=0.6g has approximately an 87% chance of collapse. This can allow engineers to offer valuable information to building owners and city officials about seismic risk of certain buildings including expected levels of damage for structural and non-structural components. Using this information, it is not necessary to explicitly create and analyze a building model to determine the collapse risk for a site as long as the expected ground shaking intensity is known.

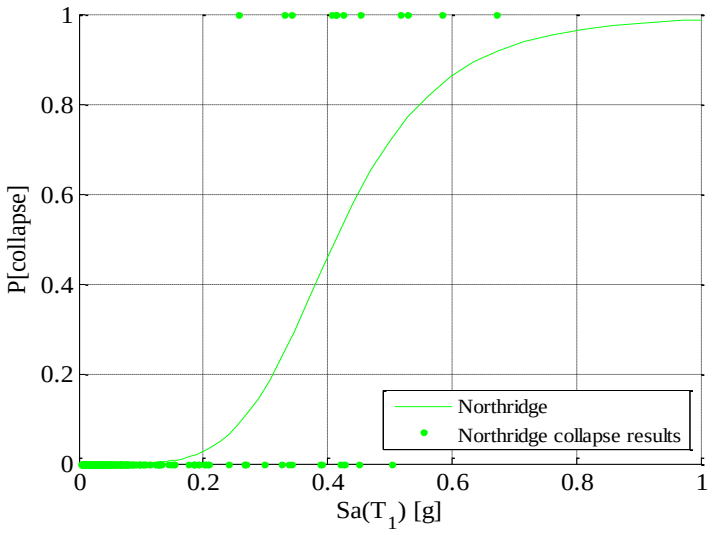

Figure 11: *Fragility function developed for the Northridge Earthquake for an 8-story non-ductile concrete frame (points at (0) represent non-collapsed at (1) represent collapse)*

It is also useful to develop fragility functions examining the probability of exceeding a given drift level for the same building model subjected to all the ground motions. **Figure 12** shows an example of the probability of exceeding 2 percent interstory drift for one earthquake. Similar to the collapse fragility curve, it is plotted using a binomial logistic regression with (0) representing a value equal to or under a given drift and (1) representing a value exceeding the given drift threshold. This curve offers information about whether the building response for the various earthquakes at lower drift levels offers the same trends as higher drift levels and collapse, which may be correlated to certain structural or nonstructural damage states. Probability of exceedance of various drift levels may also indicate whether differences exist in building response. **Figure 13** shows the probability of exceeding interstory drift levels of 2, 4, 6 and 8 percent for the same building and same earthquake. This plot can show the median value of spectral acceleration which will cause a building to exceed a given drift level. In this case, the 6 percent and 8 percent converge at approximately the same function of collapse indicating that, if this particular building subjected to the Northridge ground motion exceeds 6 percent story drift, it has collapsed as indicated by runaway interstory drifts in nonlinear simulation models.

This plot also provides information about probability of exceeding certain drift levels given a spectral acceleration value. For example, if a ground motion with $Sa(T_1)$=0.2g occurs, there is approximately a 40% chance that the drift will be less than 2 percent, a 55% chance it

will be between 2 and 4 percent, a 2% chance that it will be between 4 and 6 percent, and a 3% chance it will exceed 8% interstory drift. This information useful to building owners, insurance companies and city official concerned with the seismic risk to buildings associated with certain intensities of ground shaking. In this case, there would only be a 5% chance that interstory drifts would exceed 4%. This information can indicate the generally expected level of damage a building is likely to experience.

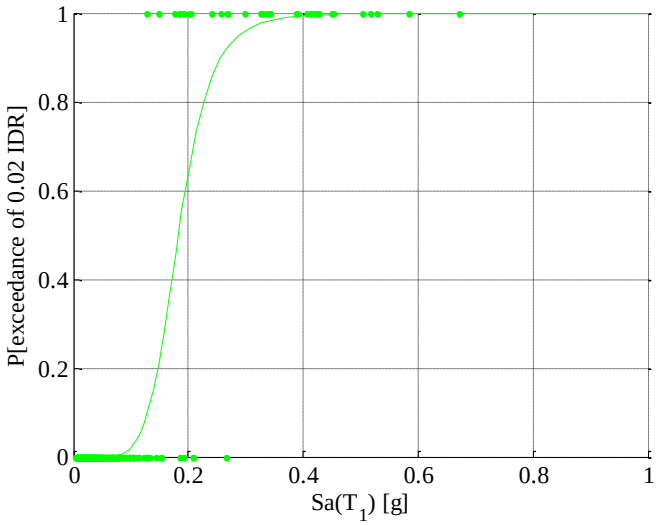

Figure 12: *Probability of exceeding 2% interstory drift for an 8-story non-ductile concrete frame (points at (0) represent ≤2% drift at (1) represent >2% drift. Data from the Northridge earthquake)*

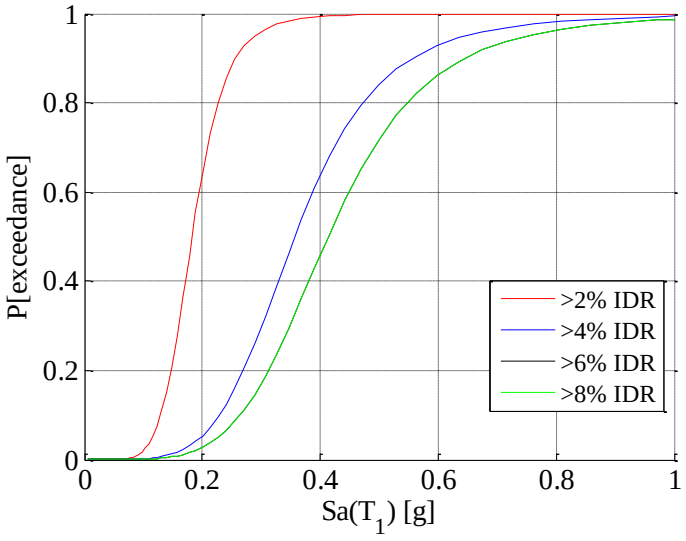

Figure 13: *Probability of exceedance of interstory drift levels for the Northridge earthquake for an 8-story non-ductile concrete frame*

The next step in analyzing the results is to determine whether the differences seen between simulated and recorded earthquakes is significant enough that it is affecting building response outside of the normal range seen in actual earthquakes. We expect some level of variability within the building response, even for real earthquakes, but quantifying whether the building response seen in this study is outside this acceptable range is important for validating the simulations. This comparison is accomplished through qualitative as well as statistical methods.

Qualitatively, comparing plots of building response similar to those discussed above can offer insight into the distribution of responses seen for recorded and simulated earthquakes. These plots can show trends in collapse and drift levels to help determine if a simulation is consistently giving results either below or above the range expected for real earthquakes. Examining these plots across all buildings and all earthquakes can help indicate whether a simulation is consistently biased in one direction and whether that bias is outside the typical range of building response.

Quantitatively, we use statistical methods to define confidence intervals which are then represented graphically on these fragility plots. These analyses offer valuable information about the level of confidence that the median response from simulations fall within an expected range of variability. By determining a percentage confidence interval based on the median response (taken to be the median of the generalized set of large ground motions) we can determine how confident we are that the simulated ground motions fall within an expected range.

3.2.4 Examining differences in building response

If it is determined that significant differences exist in the building response to the simulated and recorded ground motions, it is important to establish why these difference exist, so those people using them are aware of what biases the simulation process may introduce to building response. Various aspects of the ground motion time history may be responsible for any differences in building response including: spectral shape, time dependent characteristics such as energy content of the earthquake, or higher mode participation. Looking at the inelastic spectral displacement (S_{di}) can give an indication as to whether the differences exist due to a difference in spectral shape. Examining building displaced shape as a function of time can signify if higher mode effects are affecting the building response. Examining the energy content of the

earthquake can indicate whether it is time-dependent characteristics which are causing the differences.

Inelastic spectral displacement is an intensity measure that is better than conventional measures, such as elastic spectral acceleration or displacement, at representing the inelastic responses of MDOFs. Inelastic spectral displacement is computed using an undamped elastic period (T), and introducing a parameter, yield displacement (d_y), which represents the displacement required for an oscillator to remain elastic (F_e) and the yield strength (F_y). This parameter accounts for the yielding of the oscillator. Since yielding causes the structure to respond are periods longer than its fundamental building period, it allows us to create a spectral response parameter that accounts for energy content at more periods than only T. Looking at S_{di} can give a better idea of whether differences seen between ground motions are the result of the long period content of the spectra used or whether other aspects of the ground motion need to be examined. If the building response parameters yield more similar results when plotted with S_{di} for different earthquakes, it is a good indication that the differences seen in building response is a product of the elastic spectra. If however, the building response examined with S_{di} still yields different results, it indicates that the differences may be related to other components of the ground motion, namely time-dependent effects such as energy content or higher mode effects.

If examining building response using S_{di} still gives significantly different results for the simulated and recorded ground motions, we can also compare time domain differences in the records and their impacts on structural response. The amount of energy and where it is concentrated during the duration of the ground motion can have an effect on building response. If the energy content of the recorded ground motions occurs within a short burst of time while the simulated motion does not not, or vice versa, significant differences may be seen in building response. To look at the energy content of an earthquake, we can use the Arias intensity which is the square of the integral of the acceleration curve up to the point of interest. An example of an Arias intensity plot can be seen below in **Figure 14a**. Plotting the energy content over time shows the time period over which the majority of the energy was concentrated. This can offer important information about whether the energy content of the earthquake is related to differences seen in the building response to simulated and recorded earthquakes. Normalizing the Arias intensity at each point by the total Arias intensity gives the energy accumulation and is called a Husid plot. The Husid plot is shown in **Figure 14b**, also normalized by total duration, corresponding to the Arias intensity in **Figure 14a.**

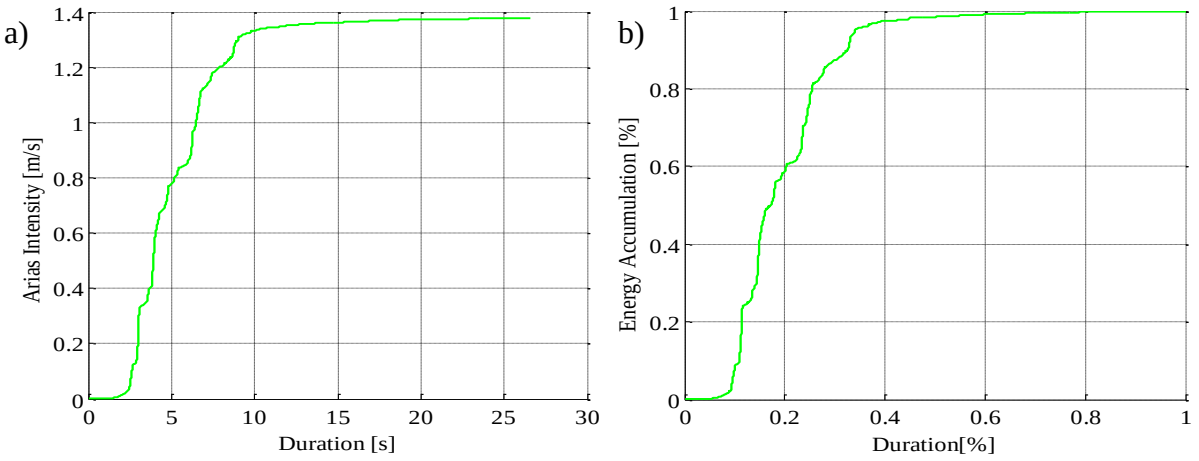

Figure 14: *a) Arias intensity and b) Husid plot for 8-story non-ductile building subjected to Northridge ground motion*

Higher mode effects should also be examined if building response using S_{di} gives different results for the simulated and recorded ground motions. In fact, Zariean and Jones (2010) attributed some of the observed differences in response between simulated and recorded ground motions to these factors. Higher mode effects are examined by looking at the building displaced shape at discreet time intervals during the earthquake. If the first mode dominates the building response, we expect to see a shape similar to the first mode shape seen in **Figure 15a**. However, if higher modes contribute more to the building response, the displaced shape will exhibit characteristics of the higher mode shapes such as the second and third mode shapes seen in **Figure 15b** and **Figure 15c**. Building displacement for discrete time intervals will be plotted over total building height as seen in **Figure 16**. These images illustrate what the building displaced shape looks like and whether higher mode effects are contributing to the difference in building response, as well as how these effects vary over time.

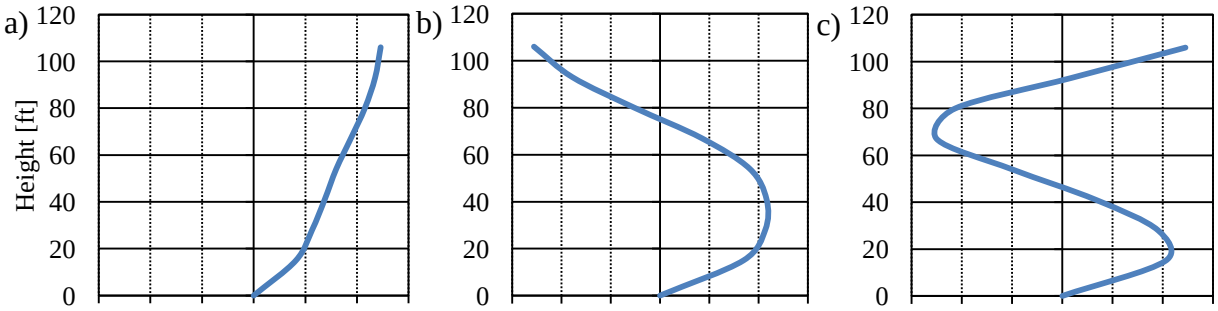

Figure 15: *8-Story non-ductile frame a) first mode shape b) second mode shape c) third mode shape*

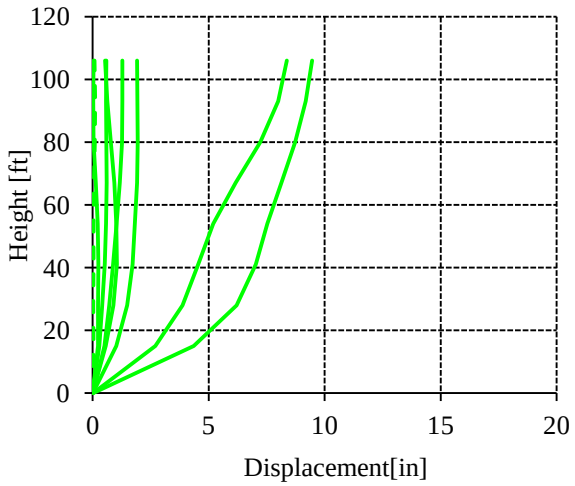

Figure 16: *Sample of building displaced shape at different times for the 8-story non-ductile building subjected to a Northridge ground motion time history*

3.4 Assumptions and limitations

As described in Section 3.2.1, the simulations used in this study were developed as ground velocity time histories, converted to ground acceleration time histories for input to structural analysis models. This was done using a linear conversion to estimate the ground acceleration at a given time step. However, this assumption of using a linear conversion introduces a certain level of error into the acceleration tine history. Also, if the time step is large, the linear approximation misses key aspects of the velocity time history.

This study is also limited in that it is valid only for a specific type of structure, namely reinforced concrete space frames which are regular in plan. Also, the periods of the buildings studied are between 0.63s and 2.2s and, while a large percentage of the world building inventory falls into this period range, this study can draw no conclusions about buildings with shorter or longer periods. However, while explicit results cannot be used, the methodology and broader implications in terms of seismic risk assessment can be applied in future studies to different types of buildings as well as short or long period structures.

Lastly, the older non-ductile building models do not consider shear failure modes, as will be discussed later. While the trends within the results in terms of the building response between various events are valid, the numerical values obtained for collapses and collapse risk should not be directly used for drawing conclusions about the seismic risk of the current building inventory without further analysis.

3.4.1 Sources of uncertainty

This study has two types of uncertainty: aleatory and epistemic. Aleatory uncertainty is that which is attributed to inherent randomness and cannot be reduced. Epistemic uncertainty is uncertainty resulting from a lack of knowledge or poor modeling and which, in the case of this study, could be likely reduced with further research (Champion, 2010).

Due to record to record variability, aleatory uncertainty is an inherent part of seismic research. This study attempts to limit the effects of ground motion variation through the use of generalized sets based on a number of ground motion records, this helps to normalize and account for any record to record variability. Use of confidence intervals to describe ranges in which we are confident that the true value lies with a certain probability also help to quantify aleatory uncertainty. Epistemic uncertainty in this study results mainly from the modeling processes. The building models themselves contain epistemic uncertainty regarding important seismic characteristic including, strength, stiffness, ductility and yield displacement. The ground motion simulation process also contains epistemic uncertainty. While the rupture scenarios are developed in an attempt to accurately model ground motions for which we have data, the modeling process itself is still uncertain. The geological models, while based on extensive testing, may not contain all the information necessary to accurately model the seismic wave propagation. The fault rupture and slip distribution are also developed to try and reproduce results seen in past earthquakes, but again contain a level of both epistemic and aleatory uncertainty.

Chapter 4: Concrete Frame Building Models, Design and Modeling

4.1 Introduction to modeling reinforced concrete buildings

This study focuses on the response of two types of reinforced concrete (RC) moment resisting frame structures. The buildings are designed to be archetypical RC frames in that they may be used to represent a general set of real buildings. While they do not take into consideration features such as setbacks, weak stories, vertical irregularities etc. that may be found in real buildings, they are designed as a sample building representing a broader representation of a class of buildings typically found in the California building inventory. Using computer simulation models, the buildings are analyzed to quantify seismic performance and, in particular, assess collapse risk. This study uses three modern (ductile) code conforming buildings of varying heights, and three older (non-ductile) RC frame structures also of varying heights. This variation allows us to gain insights into how differences in building periods, ductility and structural design parameters affect response to ground motions. A key advantage to using these building models is that they are based on past and present building code provisions and are representative of designs used in industry (Champion 2010).

4.1.1 Modeling approach

This study uses nonlinear dynamic analysis to analyze the response of RC frame buildings to earthquake ground motion time histories. This analysis requires a robust nonlinear analysis model which is capable of capturing key aspects of strength and stiffness deterioration as the structure becomes damaged (Liel and Deierlein 2008). The analysis is conducted in the OpenSees modeling platform, a software platform developed by researchers at PEER. The buildings are modeled in two-dimensions (2-D) to include both lateral and gravity systems. These building models were developed as past research by Haselton et al (2007) and Liel et al. (2008).

The RC frames used for this study are idealized using a 2-D, 3 bay lateral force-resisting system which is shown in **Figure 17**. This configuration, while simple, can be utilized to represent the response of actual RC frame buildings because it contains both interior and exterior columns and joints (Haselton and Deierlein 2007). Aspects of key nonlinear elements used in

modeling are also depicted in **Figure 17,** including the lumped beam-column elements, and joint shear springs. The figure also shows how geometric nonlinearities (P-delta effects) are accounted for with a leaning column. The frame configuration focused on in this study is the space frame system, whereby each frame line is designed to carry a combination of both gravity and lateral loads, a sample of which can be seen in **Figure 18**.

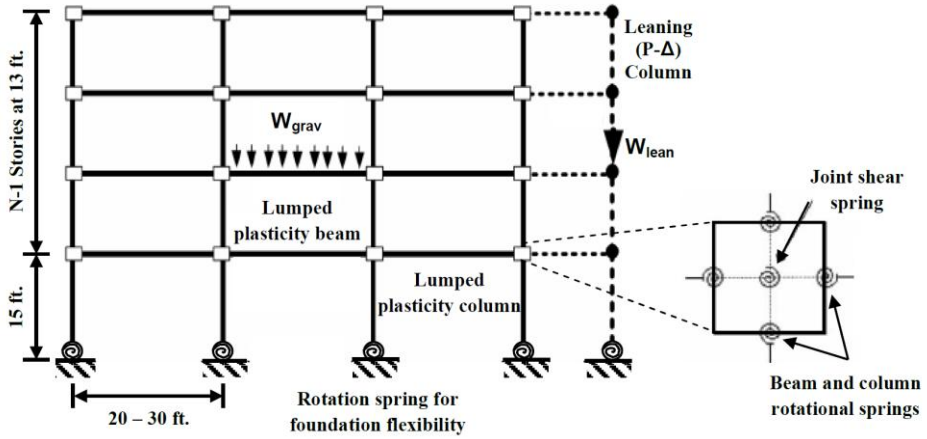

Figure 17: *View of structural model* **(Haselton, Liel, et al. 2010)**

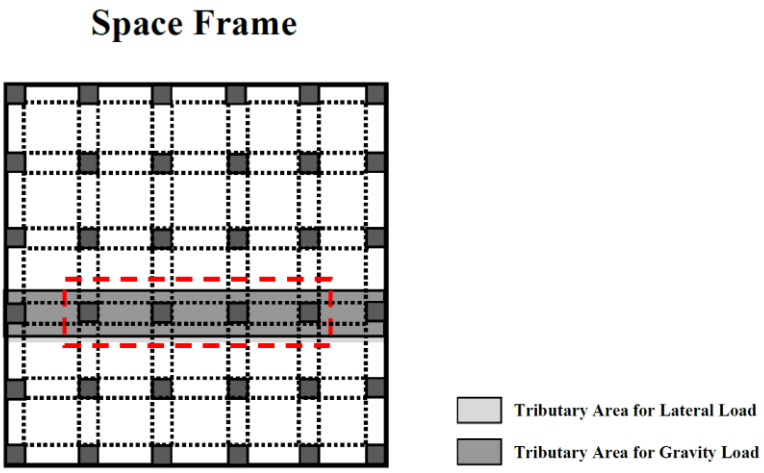

Figure 18: *Tributary areas for the space frame system* **(Champion 2010)**

4.2 Building model overview

Two sets of building models were used in this study for a total of six different building models. Three of the buildings are ductile modern buildings of 2, 4 and 8-stories and the remaining three are older non-ductile buildings, also with 2, 4 and 8 stories. The important information for all the buildings is summarized in **Table 3**. The modern, ductile building models were designed by Haselton et al. (2007) while the older non-ductile building models were designed by Liel et al. (2008). Important design parameters used in the creation of these models include ductility, base shear capacity and overstrength, and are summarized for the buildings in **Table 3**. Ductility capacity (μ) can have a major impact on the seismic performance of a building. Ductility is a measure of a system's ability to withstand inelastic deformations. For RC frames, the ductility of the structure is closely related to the detailing of the structural components. This study computes ductility by following FEMA P695 which requires a static pushover analysis to determine a maximum base shear capacity (V_{max}), a yield displacement (d_y) and the ultimate displacement (d_{ult}); ductility capacity is the ratio of d_{ult} to $d_{y.}$ Overstrength (Ω) represents the ratio of the ultimate base shear (from pushover analysis) to the design base shear, and provides an indicator of the level of conservatism in the design, indicating the structure exceeds code minimum strength requirements.

Table 3: *Design information for RC frame structures* (Champion 2010)

	Building ID	No. of Stories	T_1[a] (sec)	Design Base Shear Coefficient[b]	Ω[c]	μ[d]	d_y[e]
Modern (ductile)	1001	2	0.6	0.125	3.5	15.0	0.952
	1008	4	0.91	0.092	2.7	10.7	1.44
	1012	8	1.81	0.05	2.3	6	3.11
Older (non-ductile)	3001	2	1.03	0.086	1.9	3.29	0.953
	3004	4	1.92	0.068	1.4	2.29	2.18
	3016	8	2.23	0.054	1.5	2.25	3.01

a) The first mode building period determined by eigenvalue analysis

b) The ratio of the design base shear to effective seismic weight (V_{design}/W_s)

c) Overstrength as determined by nonlinear static pushover analysis

d) Ductility capacity as determined by nonlinear static pushover analysis

e) Yield displacement used for S_{di} calculation

Modern buildings were designed by Haselton and Deierlein (2007) to meet all current code provisions (strong column weak beam ratio, deflection limits etc.) for special RC moment frames as outlined in the 2003 International Building Code (IBC), ASCE 7-05 and ACI 318-02. They are designed with 20 ft bays, a first story of 15 ft. tall and subsequent floors heights of 13 ft. The 2 and 4-story building models are 120 ft. x 180 ft. in plan while the 8-story building is 120 ft x 120 ft. The modern buildings were designed for a site in the northern area of Los Angeles for which the Maximum Considered Earthquake (MCE) value of S_{MS}=1.5g and S_{M1}=0.9g. Soil conditions were assumed to be soil site class D (Haselton and Deierlein 2007).

Older buildings were designed to conform to the minimum requirements of the 1967 Uniform Building Code (UBC) using the ultimate strength design method. The older design code had numerous difference from current building codes, namely in the amount and detailing of steel reinforcement, which can cause brittle failure of structural elements. These buildings consist of 25 ft. bays with a first story height of 15 ft and subsequent story heights of 13 ft. For these buildings the 2 and 4 story buildings are 125 ft. x 175 ft. in plan and the 8-story building is 125 ft. x 125 ft. in plan. The older buildings were also designed for the same site in the Los Angeles region and using the 1967 seismic classification of zone 3 (Liel and Deierlein 2008).

Chapter 5: Results Comparing Building Response to Simulated and Recorded Motions

Chapter 5 provides the results from this study. It focuses on building 3016, the 8-story non-ductile frame, and also addresses general trends seen in building response for all buildings. Building 3016 was selected because it and building 3004 are the only buildings for which ground motions from all of the earthquakes caused at least some collapses. Of those two, building 3016 exhibited some interesting trends in building response to examine.

Section 5.1 addresses the quantitative results, including collapse and interstory drift results, collapse fragility functions and drift level exceedance fragility functions. This section also focuses on quantifying the aleatory uncertainty inherent in seismic analysis by defining confidence intervals in an attempt to determine whether the simulated ground motions exhibit significantly different building response from the recorded ground motions.

Section 5.2 examines what may be causing the differences seen in building response between all the earthquakes by looking at the frequency and time domains. Looking at the frequency domain entails examining the elastic response spectra, and considering inelastic spectral response. Features examined in the time domain include looking at building displaced shapes and modal phasing, as well as energy content and earthquake duration.

Section 5.3 addresses the implications of the results. It also examines what effects a study such as this may have in the broader spectrum of seismic building analysis and the use of simulated ground motions for engineering purposes.

5.1 Building response

After running all six nonlinear building models with both the recorded and simulated ground motions, important building response metrics were recorded and analyzed. Result summaries for all buildings and both recorded and simulated ground motions can be found in Appendix A.1. **Table 4** summarizes some of the important building response metric outputs for building 3016 when subjected to both the recorded and simulated ground motions. For the non-collapsed results, because interstory drifts and peak floor accelerations (PFA) are not directly comparable because ground motion levels from a particular earthquake may vary widely in

spectral intensities, they are normalized by the spectral acceleration (*Sa*) to provide a more direct comparison.

Table 4: *Results summary for 8-story non-ductile concrete frame*

			Collapsed Results				Non-Collapsed Results	
	Earthquake	M_w	Collapses	% Collapse	Median $Sa(T_1)$ causing collapse [g]	Ln Std Dev	Average IDR / Average $Sa(T_1)$	Average PFA / Average $Sa(T_1)$
Recorded	Generalized set	6.5-7.6	N/A	N/A	0.29	0.39		
	Northridge	6.7	12	3.8	0.41	0.34	0.0984	4.01
	Loma Prieta	6.9	6	3.7	0.27	0.34	0.1252	3.51
	Chi-Chi	7.6	80	9.5	0.22	0.36	0.1147	2.06
Simulated	ShakeOut	7.8	192	26.1	0.19	0.25	0.0994	0.94
	1906	7.8	328	19.0	0.24	0.40	0.1011	2.24
	Puente Hills	7.2	302	34.5	0.25	0.34	0.0596	1.78

a) The std deviation represents the value of the logarithmic standard deviation

b) Numbers in gray are uncertain because fewer than 10 collapses occurred indicating insufficient data for logistic regression

Figure 19 shows the relationship between spectral acceleration (ground motion intensity) level and interstory drift for building 3016 subjected to all the earthquakes (similar plots for all six buildings can be found in Appendix A.3). The plot was created by computing the average IDR versus spectral acceleration curve for ground motions from each earthquake, as described in Section 3.3.1. This plot reveals that, for this building, the Northridge earthquake produces lower drifts for a given spectral acceleration than any of the other earthquakes. For levels of low spectral acceleration, the drift responses of the earthquakes were all relatively linear and also had similar slopes and values. Yet, the value of spectral acceleration for which the relationship becomes non-linear is much higher for the Northridge earthquake. This indicates higher ground motion intensities before severely nonlinear behavior occurs. Once collapse occurs, interstory drifts are meaningless, so the flat part of the curve is obtained by plotting the median spectral acceleration for collapse vs. the median drift causing collapse for that building. The median collapse value was obtained from logistic regression as described in Chapter 3.

Figure 20 is a graphical representation of the collapse fragility functions for building 3016 and was obtained from the logistic regression of the building analysis collapse results. Data from each earthquake are treated separately. Fragility functions for all buildings can be found in

Appendix A.3. The fragility functions for building 3016 reveals that the ShakeOut simulation causes collapse at much lower spectral accelerations than any of the other earthquakes studied. The Northridge earthquake does not cause collapse until larger ground motion intensities. The percent difference between the median spectral accelerations for the Northridge and the ShakeOut earthquakes is 78%, while the percent difference between the General Set and the Chi-Chi earthquake, which have the second largest difference, is only 27%.

The standard deviations for the 1906 earthquake and ShakeOut earthquake are the largest and smallest and the group, with logarithmic standard deviations for collapse of 0.40 and 0.25, respectively. The 1906 earthquake has the largest standard deviation and the ShakeOut has the smallest. This implies that the 1906 earthquake has the greatest variability in values of $Sa(T_1)$ causing collapse while the ShakeOut earthquake has the lowest variability in values of $Sa(T_1)$ which cause collapse. These differences are due to variability in ground motion frequency content and other characteristics that are not captured by $Sa(T_1)$.

Examining the interstory drift versus spectral acceleration plots (found in Appendix A.2) for all six buildings reveals that the Northridge earthquake consistently causes lower drifts for a given level of spectral acceleration than the other earthquakes, while the ShakeOut earthquake consistently causes higher drifts for a given spectral acceleration level. Thus, while the response varies from building to building, all buildings show less drift at a given spectral acceleration level for the Northridge and more drift at a given spectral acceleration level for the ShakeOut earthquake. Looking at the collapse fragility functions for all six buildings reveals that in general, the Northridge recordings caused collapse only at higher levels of spectral acceleration. However, since many of the structures did not collapse in the Northridge earthquake ground motions, this trend cannot be extended to the modern buildings. The collapse fragility function plots also show that the ShakeOut earthquake causes collapse at lower values of $Sa(T_1)$ for all the buildings except the modern 2-story for which there was not enough collapse data to create the collapse fragility functions. Whether these differences in response are due to properties of the various spectral shapes, higher mode effects, etc will be examined further in Section 5.2.

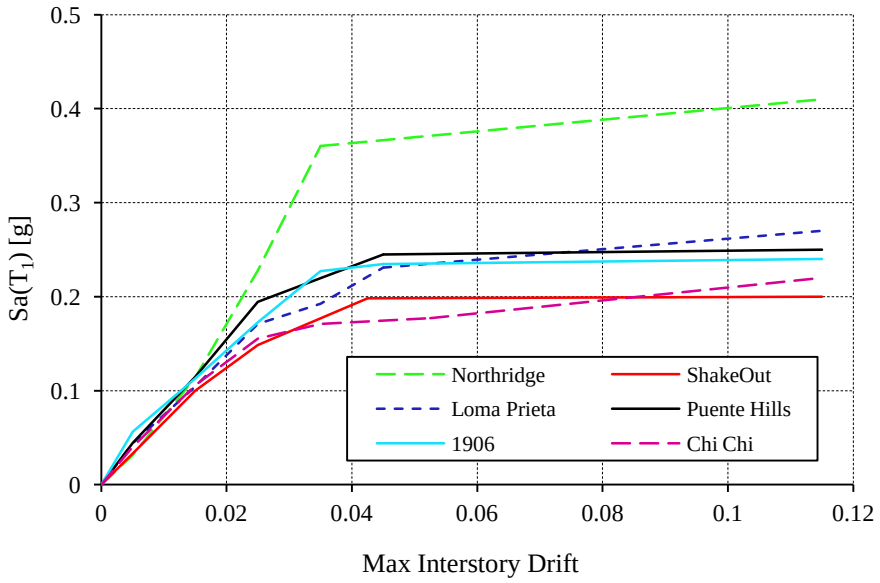

Figure 19: *Relationship between ground motion spectral acceleration and interstory drifts in the 8-story non-ductile frame, for the six different earthquakes*

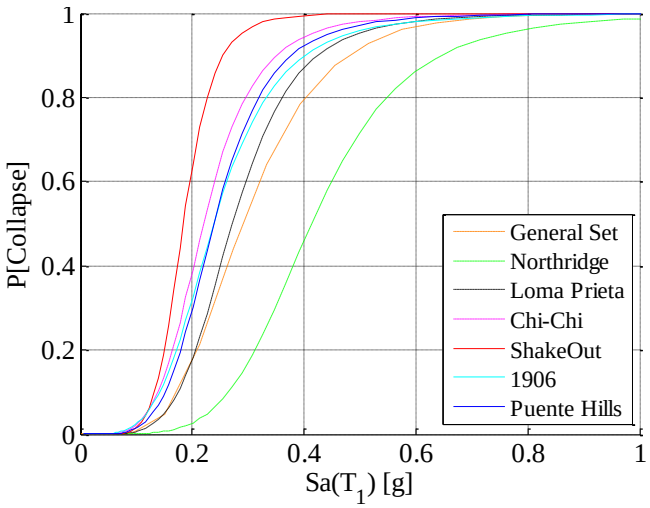

Figure 20: *Collapse fragility functions for the 8-story non-ductile frame*

Another interesting aspect of the results to examine is the probability of exceeding certain drift levels, i.e. fragility functions representing the probability of exceeding a given drift level. **Figure 21** shows the curves representing the probability of exceeding 2, 4, 6 and 8% interstory drift for the 8 story non-ductile frame. The median spectral acceleration causing exceedance of these drift levels was calculated from logistic regression predictions and can be found in **Table 4**. For all four drift levels, the ShakeOut simulation causes exceedance at lower spectral accelerations than any of the other earthquakes, which is consistent with the results seen for collapse. Also consistent with the collapse fragility function, the Northridge earthquake exceeds

the given drift levels at much higher spectral accelerations than the other buildings. The percent difference between the ShakeOut and the Northridge earthquake increases as we look at higher drift levels; the percent difference is 38% for 2% drift, 71% for 4% drift, 76% for 6% drift and 78% for 8% drift.

However, this does not hold true for the other earthquakes. For example, the Chi-Chi earthquake exceeds 2% interstory drift at a lower $Sa(T_1)$ than the Puente Hills simulation, but the Puente Hills simulation exceeds 4% interstory drift at a lower $Sa(T_1)$ than the Chi-Chi earthquake. In general though, all the earthquakes except the ShakeOut and Northridge have median spectral accelerations causing collapse within a range of 20% difference.

Table 5: *Median $Sa(T_1)$ causing exceedance of interstory drift levels for the 8-story non-ductile frame*

		$Sa(T_1)$ causing exceedance of 2% drift [g]	$Sa(T_1)$ causing exceedance of 4% drift [g]	$Sa(T_1)$ causing exceedance of 6% drift [g]	$Sa(T_1)$ causing exceedance of 8% drift [g]
Recorded	Northridge	0.18	0.36	0.41	0.41
	Loma Prieta	0.15	0.25	0.27	0.27
	Chi-Chi	0.13	0.22	0.22	0.22
Simulated	ShakeOut	0.12	0.17	0.18	0.18
	1906	0.14	0.24	0.24	0.24
	Puente Hills	0.15	0.21	0.24	0.24

Looking at the probability of exceeding given drift levels for all the buildings (found in Appendix A.2) reveals similar trends to those seen for building 3016. For building 3001 (the 2-story nonductile frame with T_1=1.03s), the ShakeOut again has the lowest median spectral acceleration causing exceedance of given drift levels and the Northridge has the highest. However, for this building, the Chi-Chi earthquake is much closer to the Northridge earthquake in median probability of exceedance for all drift levels. For building 3004 (the 4-story non-ductile frame with T_1 = 1.92s), the Loma Prieta actually has the highest value of median spectral acceleration causing exceedance of 6 and 8% drifts while the Northridge has the second highest and the ShakeOut again has the lowest. The three modern buildings show similar trends with the ShakeOut having the lowest probability of exceedance of given drift levels. For building 1001 (the ductile 2-story frame with T_1= 0.6s), the Loma Prieta and Northridge earthquakes again have higher values of spectral acceleration causing exceedance of 2% drift. However, because of the modern detailing and design and the relatively low spectral intensities of the Northridge and

Loma Prieta ground motions, these ground motions do not cause exceedance of the higher drift levels. Again, the ShakeOut has the lowest values of spectral acceleration causing exceedance. For building 1008 (the ductile 4-story frame with T_1= 0.91s), the trend is slightly different, the Chi Chi earthquake has the highest value of spectral acceleration causing exceedance followed next by the Northridge. Once again the ShakeOut has the lowest value of spectral acceleration causing exceedance of all the drift levels. Lastly, for building 1012 (the ductile 8-story frame with T_1= 1.81s), the Northridge earthquake has the highest value of spectral acceleration causing exceedance while the ShakeOut has the lowest. However, the modern buildings experience less drifts overall so there is a lack of data regarding the probability of exceeding drift levels for the earthquakes with lower shaking intensities, namely the Loma Prieta and Northridge.

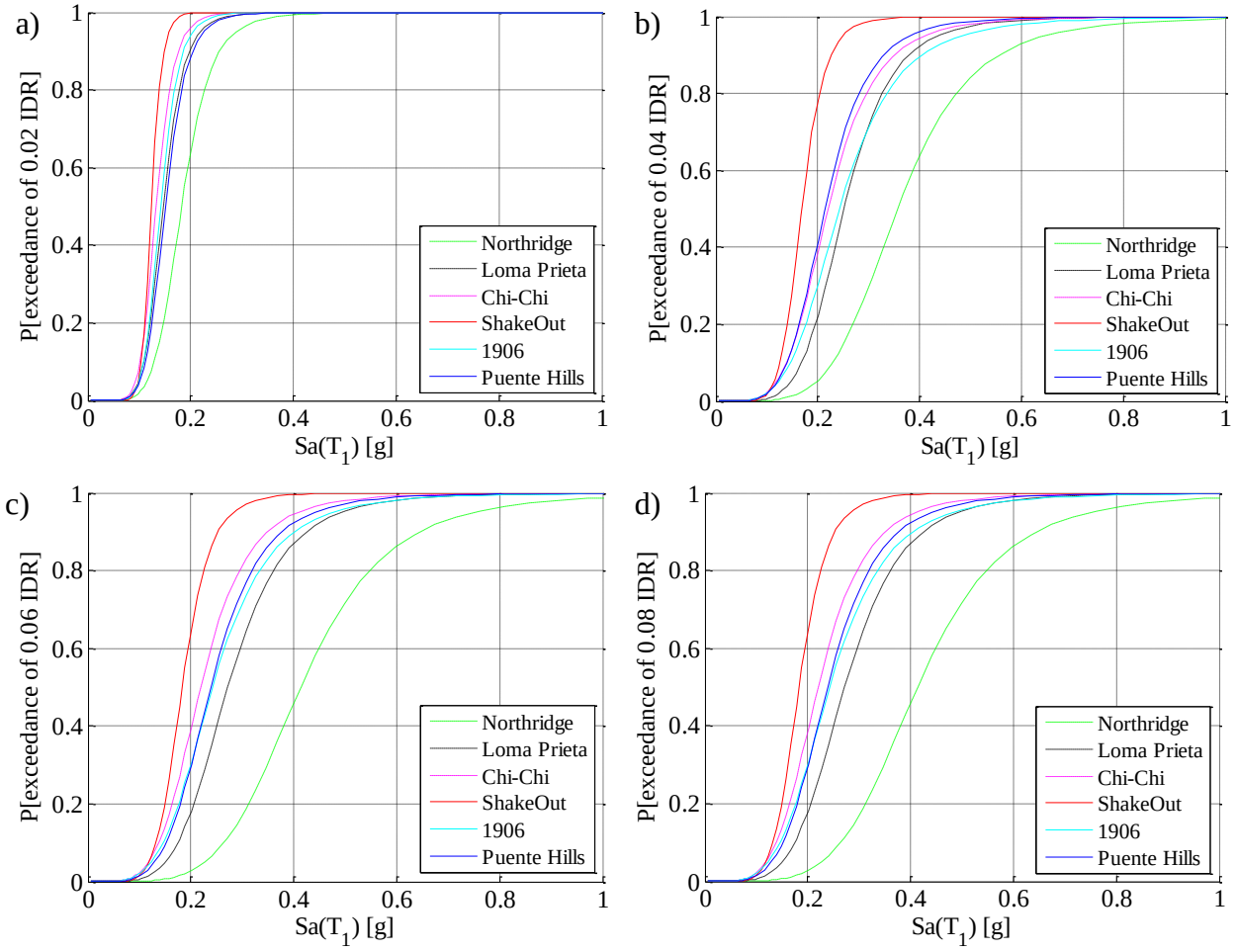

Figure 21: *Probability of exceeding a) 2% b) 4% c) 6% and d) 8% interstory drift for the 8-story non-ductile frame*

After looking at the building response to all the individual earthquakes, it was important to quantify an expected range for building response due to past recorded earthquakes. This allows for a comparison of the recorded and simulated earthquakes and offers valuable information about whether building responses due to simulated earthquakes are significantly different than we would expect from actual earthquakes. To create a mean response curve for the recorded ground motions, the collapse and spectral acceleration results for all the recorded ground motions were combined into a single "*recorded set*." The fragility function for this *recorded set* was then obtained by performing logistic regression. **Figure 22a** depicts the fragility function for the *recorded set* in comparison to the ground motions used to create it. Because it is a direct aggregation of all the recorded ground motions, we see that it is a weighted average response of the three recorded earthquakes used in this study.

Figure 22a also indicates that the Northridge earthquake yields significantly different results than the other two recorded earthquakes; reasons for the variations in the building response to real earthquakes will also be examined in Section 5.2. **Figure 22b** shows a comparison between the fragility functions obtained from the general set of large ground motions and the *recorded set*. While the fragility curve for the average of the recorded ground motions is shifted slightly left, and has a slightly different standard deviation than the general set, the difference is minor enough to imply that the set of recorded ground motions utilized in this study is representative of results expected to be seen from a general set of real earthquakes. The difference in the two curves can be attributed to the expected variation in building response due to differences in ground motions for different earthquakes.

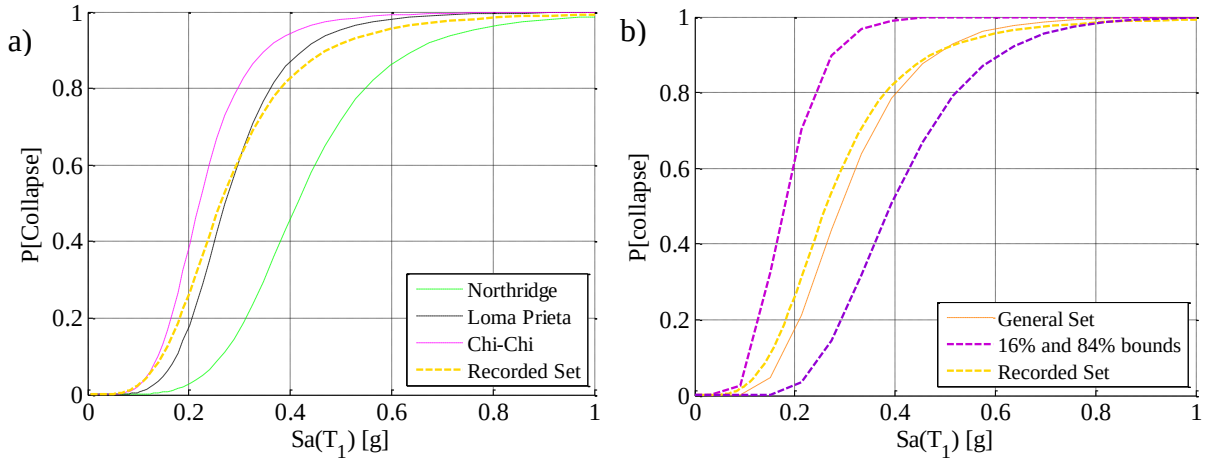

Figure 22: "*Recorded Set" a) calculation b) comparison to general set*

Confidence intervals are used to statistically examine the differences seen in building response. In this case, the general set is taken as the baseline response and the confidence intervals quantify the likelihood that the fragility functions obtained from the other ground motion records came from the same distribution. To be precise, in this case we are defining 68% confidence intervals around the median, obtained from the *recorded set*, and defining bounds on the median. If the fragility curve developed from ground motions from a different earthquake falls outside the bounds defined by the confidence interval, we expect that there is only a 32% chance it came from the same distribution as the data obtained from the other ground motion sets. **Figure 22b** shows the confidence bounds of 16% and 84% for the fragility function based on the general suite of ground motions. These confidence bounds assume a coefficient of variation (COV) of 0.5. This is used as an estimate of the COV for the 5% damped spectral response at collapse, which is unknown. This number is assumed to be a reasonable number for analysis of real earthquakes, though further research could provide a better estimate for the COV (Liel, et al. 2009). Even though the variance is only an estimate and therefore unknown, because the number of trials used was relatively large, the t-distribution is assumed to approach the standard normal distribution and therefore the equation to determine the upper and lower confidence bounds is:

$$\mu_{(1-\alpha)=0.68} = (\bar{x} - \sigma * t_{\frac{\alpha}{2}}; \bar{x} + \sigma * t_{\frac{\alpha}{2}})$$

where the standard deviation σ is:

$$\sigma = \sqrt{\ln(1 + COV^2)}$$

and μ is the mean of the lower or upper confidence bound, $\bar{x}$ is the mean ln($Sa(T_1)$) causing collapse calculated from the *general set*, and $t_{\frac{\alpha}{2}}$ is the value taken from a standard normal probability table for the desired confidence range. Using the mean for the upper and lower bounds, the curves were plotted using the same standard deviation as the fragility function for the general set of ground motions. The upper and lower bounds in this case represent a 16% and 84% confidence interval, or the 68% confidence that the true median lies in that region. Again, as seen in **Figure 22b**, the *recorded set* lies well within the probable region in which the mean is expected to be found based on a general set of earthquakes. Using this information we assume that the *recorded set* of ground motions analyzed for this study can also be used to reasonably

represent an expected value with which to compare the response of the simulated ground motions.

Having determined that the *recorded set* of ground motions yields similar building response results as a general set of large ground motions, we can now look at how well the simulations seem to fit the trends seen in building response during the recorded earthquakes. **Figure 23** shows the recorded set with 16% and 84% bounds calculated and compared to the simulated earthquakes. The first interesting trend is that the simulations are all to the left of the *recorded set* indicating that all the simulations are predicting collapse at lower accelerations than what we see with recorded earthquakes. Also, the 1906 San Francisco simulation and the Puente Hills simulation seem to yield very similar fragility functions, with the same value for median $Sa(T_1)$ causing collapse for Puente Hills and the 1906 simulation, and with standard deviations of 0.35 and 0.40 respectively. The median value of the Puente Hills and 1906 earthquakes is also only 9.5% different than the *recorded set*. We also see that these two simulations are distinctly within the one standard deviation confidence interval defined from the *recorded set*. We can also see that the ShakeOut simulation causes collapses at lower ground motion intensities than the *recorded set* and the other two simulations. However, the collapse fragility curve from the ShakeOut earthquake remains within the confidence bounds. The standard deviations though are quite different with the ShakeOut having a standard deviation of 0.25, while the recorded set has a standard deviation of 0.4, indicating that there is more variability in the collapse capacity data data of the *recorded set* than the ShakeOut. We do see that building response to actual earthquakes and the ShakeOut simulation are different and the reasons these differences may exist will be examined in Section 5.2

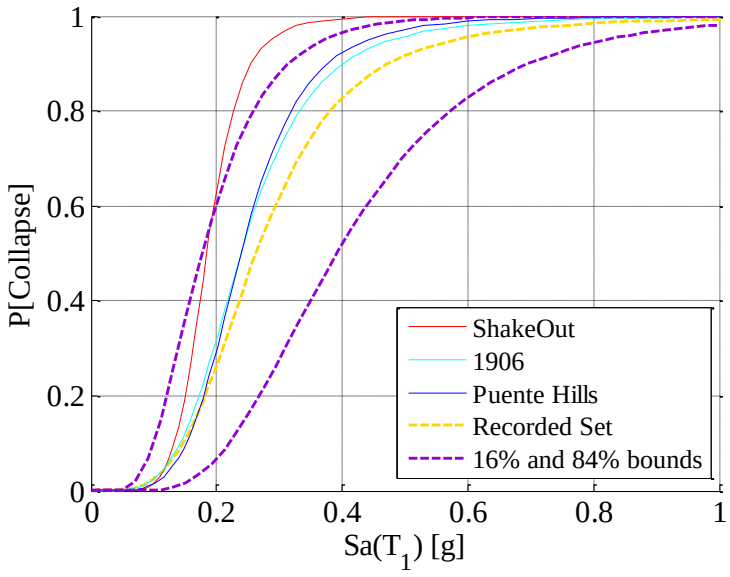

Figure 23: *Collapse fragility functions for recorded set and simulated ground motions for building 3016*

The probability of exceeding given drift levels can also be examined for the simulated earthquakes in comparison to the recorded set. In this case, some interesting trends appear. At high levels of drift (4% and higher) the probability of exceedance fragility functions for the simulations are all to the left of the curve for the *recorded set*. This implies that, when subjected to the simulations, the buildings are more vulnerable (fragile) than when subjected to the recorded ground motions. However, for exceedance of 2% interstory drift, the Puente Hills and 1906 earthquake both predict higher spectral accelerations before the specified drift level is exceeded than the *recorded set*, implying less vulnerability or fragility. Again, the ShakeOut simulation predicts exceedance of all drift levels at significantly lower spectral accelerations than the other earthquakes. What properties of the ShakeOut simulation cause this phenomenon, and what implications this has, will be examined in Sections 5.2 and 5.3.

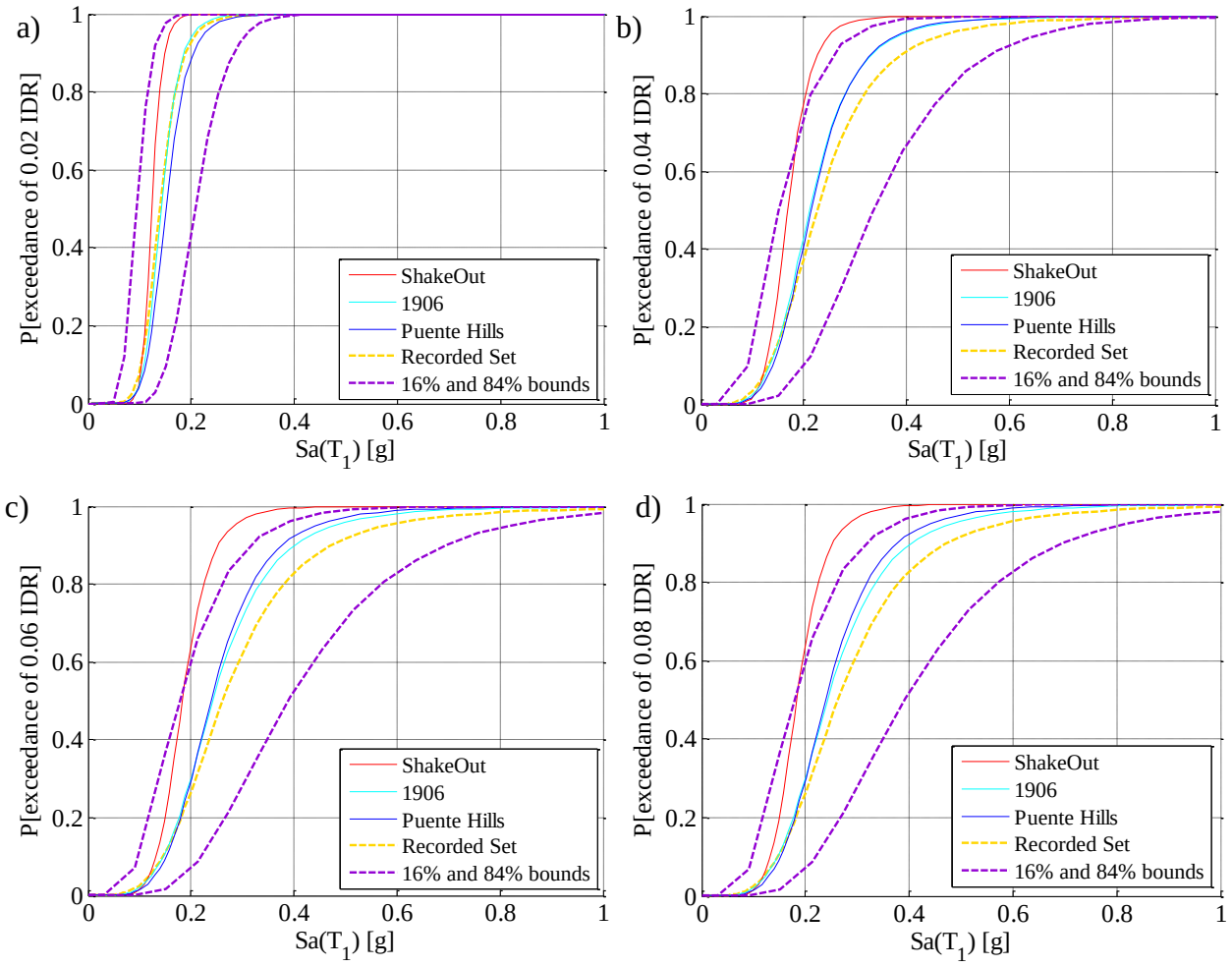

Figure 24: *Probability of exceeding a) 2% b) 4% c) 6% and d) 8% interstory drift for building 3016*

Examining the building response to both recorded and simulated ground motion time histories does yield differences in building response for all the earthquakes. Yet, in general the fragility functions and building response metrics for the simulations are within the confidence bounds of 16% and 84%. This indicates that they all may come from the same distribution as the recorded earthquakes. However, it is important to investigate what properties of the ground motion time histories are causing differences in building response. This can benefit engineers who may be using these simulated ground motions and also help researchers to possibly further improve the simulation process to bring it closer in line with observed results.

5.2 Reasons for variations in building response

5.2.1 Examining response spectras

The elastic spectral acceleration is a parameter that represents the elastic response due to an earthquake ground motion of an SDOF oscillator with a given period. Variations in the elastic spectra cause important differences in building response. Therefore, comparison of response spectra is an important place to start in examining the reasons for the differences in building response which were observed in Section 5.1. All the response spectra in this study, elastic and inelastic, were created with a 5% damping ratio.

The ShakeOut and Northridge earthquakes exhibited the most significant differences in collapse based on **Figure 20**, so to attempt to explain these differences we compared their elastic spectra. **Figure 25** shows the average response spectras for ground motions from the ShakeOut and Northridge earthquakes which have a $0.25g < Sa(T_1=2.2sec) < 0.28g$. The period of interest, 2.20sec, is the fundamental period of the 8-story non-ductile building. These values were selected because it is above the median $Sa(T_1)$ causing collapse for the ShakeOut ground motions but less than median $Sa(T_1)$ causing collapse for the Northridge ground motions. Therefore, for each earthquake, some of the ground motions included within the selected range caused collapse and some did not.

The average spectra offer insight into the observed building response. In this case, the Northridge earthquake has considerably more energy at shorter periods which would excite higher modes. This earthquake would be more likely to cause damage and collapse if higher mode effects significantly affect building response. Higher mode effects are examined and discussed in Section 5.2.3. The ShakeOut earthquake ground motions, on the other hand, have close to three times the energy of the Northridge spectra at longer periods (i.e. $T_1 > 3$ sec). This suggests that differences seen the building response may be due to the lengthening of the first mode building period as it is damaged. As the period of the building lengthens, the higher level of energy at that period causes more damage. Since the ShakeOut ground motions appear to have higher energy at longer periods than the Northridge records, this may be one of the reasons that the ShakeOut earthquake had approximately a 22% higher rate of collapse at this spectral acceleration level than the Northridge earthquake. If the high energy content at long periods is affecting the building response, we can expect to see less difference in the building response

when we examine it in relation to the inelastic spectral displacement; S_{di} is examined in detail in Section 5.2.2.

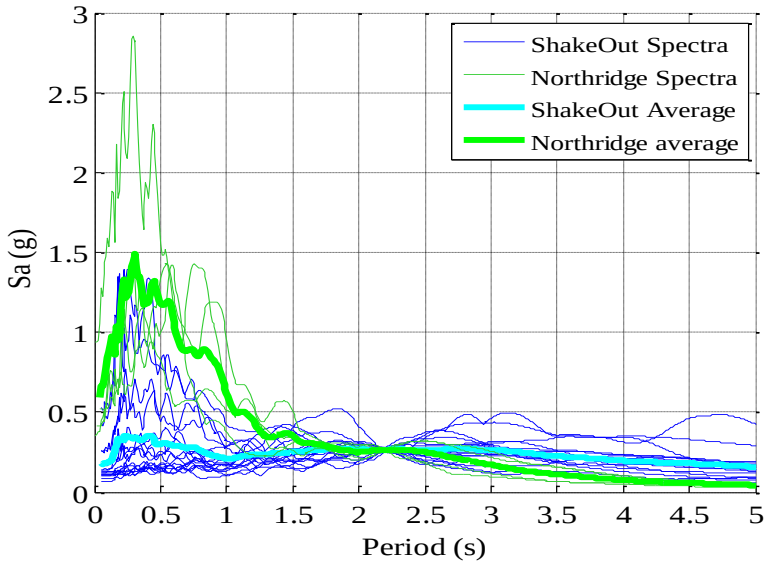

Figure 25: *Response spectra from ground motions for the Northridge and ShakeOut earthquake sites with 0.25g< Sa(T_1 = 2.2 sec) <0.28g*

Extending the comparison above to all the earthquakes yields **Figure 26**, which displays the average response spectra of sites with 0.25g< *Sa*(T_1 = 2.2 sec) <0.28g and 0.39g< *Sa*(T_1= 2.2 sec) < 0.42g for all the earthquakes. The range of 0.39g< *Sa*(T_1= 2.2 sec) < 0.42g was selected because it was a range which contained the median spectral value causing collapse for the Northridge earthquake (0.41g) and it was thought looking at this range may offer information regarding the cause of the significantly higher value of *Sa* required to cause collapse.

For both these spectral acceleration ranges, the Northridge earthquake records exhibit the highest energy of all the earthquakes at shorter periods. This would imply that if higher mode effects were causing differences in building damage, the Northridge should experience a higher level of collapse than the other earthquakes; however, conclusions about higher mode effects will not be drawn until further examination. The ShakeOut earthquake also exhibits the lowest energy at short periods of any of the earthquakes, but the highest at long periods. Because the ShakeOut earthquake has the lowest median *Sa*(T_1) causing collapse, the spectra plots imply that the high energy at long periods may be the reason for the difference in median response. Interestingly, the Chi-Chi earthquake average spectra very closely resembles the ShakeOut spectra for the range of 0.25g< *Sa*(T_1) <0.28g. These two earthquakes also exhibited the closest median spectral acceleration causing collapse (only 15% different). Overall, for both ranges, the

Puente Hills and 1906 simulations have similar spectras though the Puente Hills does contain approximately 60% more energy between periods of 0.5sec to 1.5sec for 0.39g< $Sa(T_1)$ < 0.42g, implying that higher mode effects could affect building response in this region. These two earthquakes were also only 4% different in their median spectral acceleration causing collapse, the closest two considered.

Many aspects of the response spectras seen below are consistent with the collapse fragility curves generated. In particular, similarities in spectras generally indicate that the building response to those two spectral ranges selected was similar. The long period energy is generally lower for those building with a higher level of $Sa(T_1)$ causing collapse. Based on the short periods though, we would expect the Northridge earthquake to have a lower value of $Sa(T_1)$ causing collapse if higher modes played a significant role in the building response.

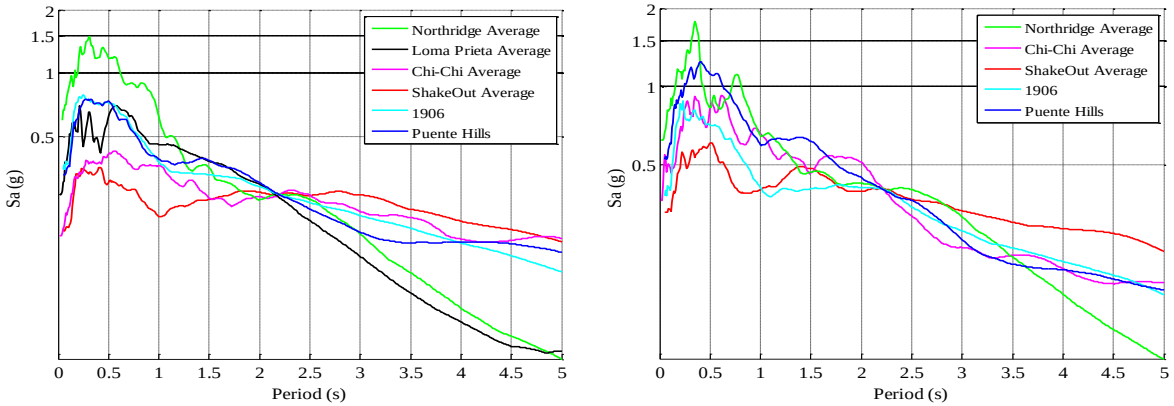

Figure 26: *Average response spectras for ground motions between a) 0.25g< Sa(T_1 = 2.23sec) <2.8g b) 0.39g< Sa(T_1 = 2.23 sec) <0.42g for all earthquakes.* (The Loma Prieta earthquake is excluded in (b) because there are no ground motions with spectra falling in this range.)

5.2.2 Examining inelastic spectral displacement (S_{di})

Examining the inelastic spectral response of the building when subjected to the ground motions offers valuable information about what aspects of the earthquake spectra are causing the differences in building response. If analyzing building response in comparison to the inelastic spectra rather than elastic spectra yields results with medians which are closer, this is an indication that the energy contained at longer periods is contributing to the differences in building response. This is because S_{di} uses a bilinear oscillator to predict response of a single degree of freedom system, accounting for the lengthening of the building period and thereby taking into consideration longer period spectral characteristics. By taking this into consideration,

we are essentially normalizing the response to account for inelastic behavior. For this examination, the inelastic spectral displacement was calculated for all the earthquake simulations, as well as the recorded ground motions. The elastic spectral displacement (S_{de}) was also calculated using the relationship:

$$S_{de} = \frac{Sa(T_1)}{\omega^2}$$

where $\omega = \frac{2\pi}{T}$ is the natural frequency of the building. Comparing the elastic and inelastic spectral displacements offers a more direct comparison than examining $Sa(T_1)$ and S_{di}. By plotting the simulated earthquakes along with the *recorded set* and the 16% and 84% confidence bounds we can examine whether the differences in building response are due to energy content at long periods.

Figure 27 below shows the average spectral response for all earthquakes in the range 9.8in<S_{di}(T_1=2.23s)<11in. This range was chosen because a majority of the earthquakes have a median S_{di} value causing collapse in this range. The Northridge earthquake has the highest inelastic spectral displacement value for periods less than 2s and one of the lowest for periods after about 2s. The ShakeOut earthquake has the lowest inelastic spectral displacement value for periods less that about 2s and the highest for periods after 2s. The Loma Prieta earthquake and the Northridge earthquake both exhibit a drop in the value of spectral acceleration at periods longer than 2s, while the other earthquakes have values of S_{di} which continue to increase at periods longer than 2s. This figure shows that the inelastic spectral response spectra follow the same trends as the collapse fragility curves created using inelastic spectral displacement, seen in **Figure 29,** for the earthquakes. This indicates that the inelastic spectrum of the various earthquakes does play a key role in the building response.

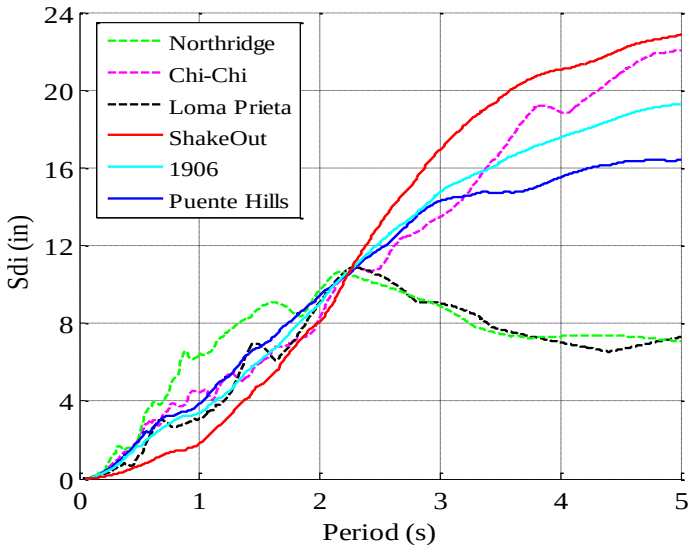

Figure 27: *Average response spectra for ground motions between (9.8in<S_{di}(T_1=2.23s)<11in) for all earthquakes*

Figure 28 shows the relationship between maximum interstory drift and S_{di}. When compared with **Figure 19**, which plotted maximum interstory drift versus $Sa(T_1)$, we see that all the curves have moved much closer. The curve for the Northridge earthquake, in particular, has moved much closer to those of the other earthquakes. This again indicates that the long period energy content of the Northridge earthquake is particularly distinct from the other records.

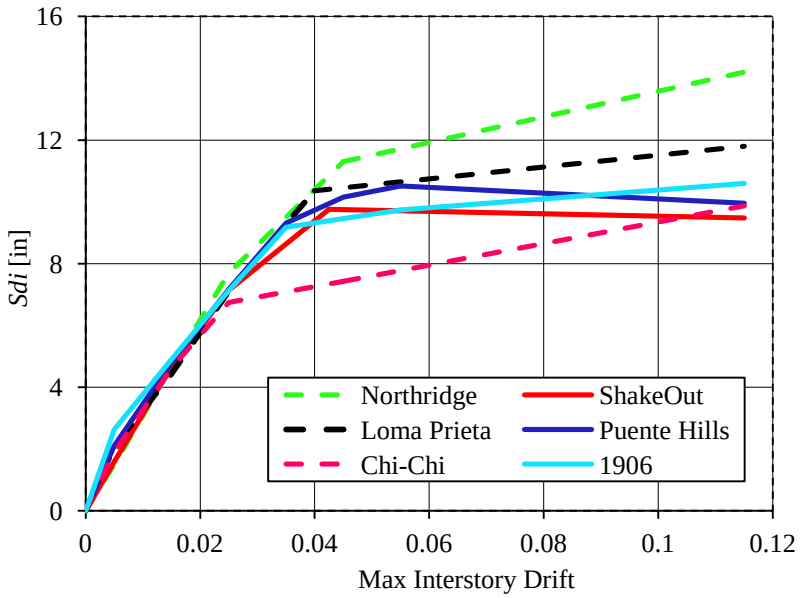

Figure 28: *Relationship between inelastic spectral displacement and interstory drifts in the 8-story non-ductile frame*

As seen in **Figure 29**, the collapse fragility functions using the inelastic spectral displacement have much closer medians than those plotted against the elastic spectral displacement. The percent difference in median collapse probability between the Northridge and ShakeOut earthquakes changes from 77% when looking at S_{de} to 40% when looking at S_{di}. **Table 6** shows the median value of S_{di} causing collapse for all the earthquakes taken from the collapse fragility curves in **Figure 29** versus the median value of S_{de} causing collapse. This table again reveals that the Northridge earthquake experiences the greatest shift in median spectral displacement causing collapse from using only the elastic response to using the inelastic response. The Chi-Chi earthquake experiences the least difference from examining building response in terms of inelastic versus elastic spectral displacement. **Table 6** also shows the ratio of S_{di} to S_{de} for each earthquake. The closer this ratio is to one, the less the building response has been affected by inelastic behavior. Again, the Northridge earthquake record appears to be the one most affected by inelastic building response, while Chi-Chi is least affected, implying that the building response is actually very sensitive to the long period energy content of the Northridge earthquake and not very sensitive to the long-period energy of the Chi-Chi records.

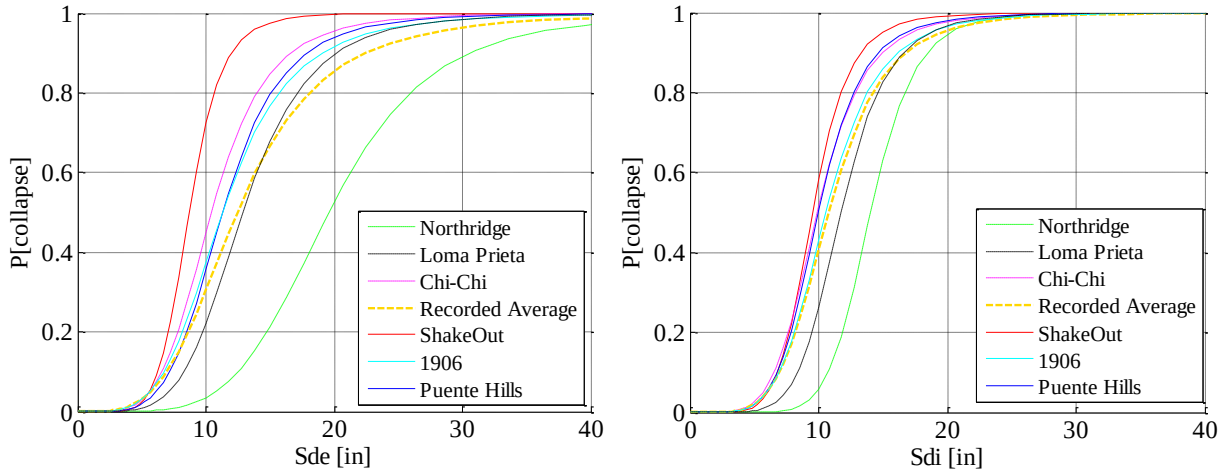

Figure 29: *Collapse fragility functions for the 8-story non-ductile frame structure representing a) elastic spectral displacement and b) inelastic spectral displacement*

Table 6: *Comparing median S_{de} and S_{di} causing collapse in the 8-story non-ductile frame structures*

		Median S_{de} causing collapse [in]	Median S_{di} causing collapse [in]	S_{di} /S_{de}	% difference between medians S_{de} and S_{di}
Recorded	Northridge	19.6	14.2	0.89	-28
	Loma Prieta	12.9	11.8	0.97	-8.5
	Chi-Chi	10.4	9.9	0.98	-4.8
Simulated	ShakeOut	8.68	9.5	1.04	+9.4
	1906	11.3	10.6	0.97	-6.2
	Puente Hills	11.3	9.96	0.95	-12

a) Numbers in grey are uncertain because fewer than 10 collapses occurred indicating insufficient data for logistic regression

Collapse fragility functions plotted versus S_{di} for all the earthquakes can be found in Appendix A.3. For all the buildings, the collapse fragility curves created using S_{di} are much closer together than those based on $Sa(T_1)$ implying that, for all the buildings examined, the inelastic spectrum plays a key role in the building response. We also see that various earthquakes are affected by the inelastic spectrum in different ways. For example, with the 2-story nonductile building when normalized by S_{di}, the ShakeOut earthquake actually has the highest value of median inelastic spectral displacement causing collapse and the Northridge has the second smallest value of spectral displacement causing collapse. In contrast, for the 4-story nonductile building, the Loma Prieta has the highest value of spectral displacement causing collapse and the Puente Hills earthquake has the lowest. This illustrates the point that buildings with different fundamental periods are susceptible to the long period energy content of an earthquake in different ways. Since each earthquake has different content in the long period energy region, the building response when normalized by S_{di} is different than when considering only *Sa*. Similar to the results for elastic spectral acceleration versus probability of collapse, the modern buildings did not experience enough collapses for the all the earthquake scenarios to draw general trends regarding the difference between various earthquakes and in fact the ductile 8-story building did not have enough collapses for any of the earthquakes to create fragility curves. We did see that S_{di} is a potentially better normalization for all buildings for which we had enough collapse data because all the collapse fragility curves moved closer together.

Figure 30, for the 8-story nonductile building, shows a comparison of the simulated earthquakes plotted with the *recorded set* and the 68% confidence interval for both S_{de} and S_{di}.

The confidence bounds were found in the same manner as the confidence bounds for the collapse fragility functions versus *Sa*. These confidence bounds are also calculated with an estimated COV of 0.5. While this number is used, further research may be able to improve the estimate for COV. Theoretically, the COV for S_{di} should be smaller than the COV for *Sa* but because of a lack of information about the true value of COV, we continued to use the value of 0.5. The figures show that when examining only elastic response, analysis with the ShakeOut earthquake leads to a fragility curve that is near the confidence interval boundary. Conversely, when using inelastic spectral displacement, the ShakeOut earthquake falls well within the confidence interval. Interestingly, while the ShakeOut earthquake does move more to the right, the r*ecorded set* collapse fragility curve also moves substantially to the left. This again implies that the real earthquakes, particularly the Northridge earthquake, are significantly affected by representing ground motion intensity by the inelastic response parameter.

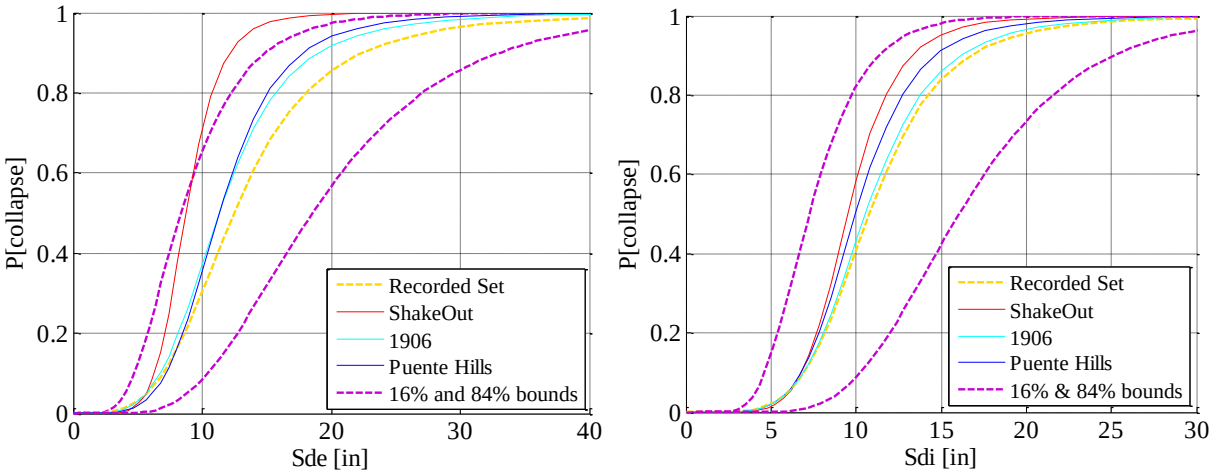

Figure 30: *Collapse fragility functions comparison of simulated earthquakes and "Recorded Set" for a) elastic spectral displacement b) inelastic spectral displacement*

5.2.3 Examining higher mode effects

Examining the relationship between building response and the inelastic parameter S_{di}, rather than *Sa* or S_{de}, resulted in a substantial decrease of the differences in median response between earthquakes; this implies that the differences in long period energy do have a large effect on building response. However, differences in median response still exist, even after normalizing by S_{di}, leading us to ask what other features of the ground motion are affecting

building response and causing these differences. The next avenue we chose to explore was higher mode effects. Thus far, the relationships examined between $Sa(T_1)$, S_{de}, S_{di} and building response, have been based on the first mode building period; however, during an earthquake, excitement of higher modes can also contribute to damage, particularly in more flexible structures. This is because excitement of higher modes may cause more nonlinear behavior and deformation at the top of the structure.

To examine whether higher modes are affecting building response and causing differences between recorded and simulated earthquakes, it is useful to look at the displaced shape of the building, as it evolves over the duration of the ground motion time histories. The laterally displaced shape of each building was created by taking displacement data for one node per floor along a single column line at ten discrete times throughout selected ground motion time histories. All ten time steps were superimposed on a single plot to show the trends of displaced shape throughout the length of the ground motion record. The displaced shape was plotted for each earthquake at one collapsed site and at one non-collapsed site in the range of $0.25g < Sa(T_1) < 0.28g$ and can be seen in **Figure 31** to**Figure 36**. It is important to note that for the collapsed sites, the later displaced building shapes exhibit runaway (very large) interstory drifts. For all the earthquakes and sites, the collapsed buildings experienced high concentration of interstory drifts in the lower floors, but often very little interstory drift for the upper floors. This could imply the presence of a soft or weak story as well as a high base shear levels combined with P-delta effects. All the earthquake sites examined, both collapsed and non-collapsed, also exhibited minor higher mode effects.

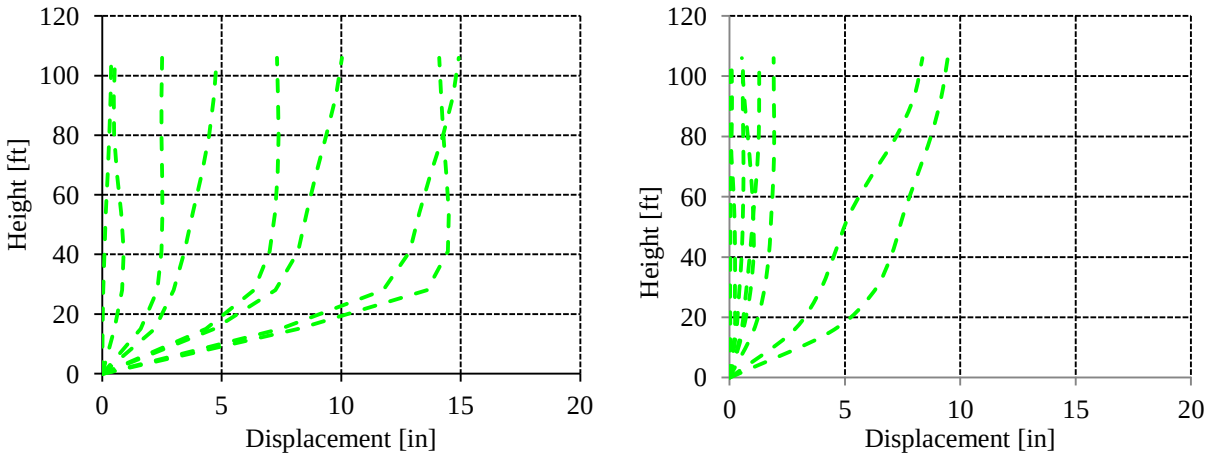

Figure 31: *Northridge earthquake building displaced shape at a) collapsed site, Sa(T_1)=0.26g and b) non-collapse site, Sa(T_1)=0.27g*

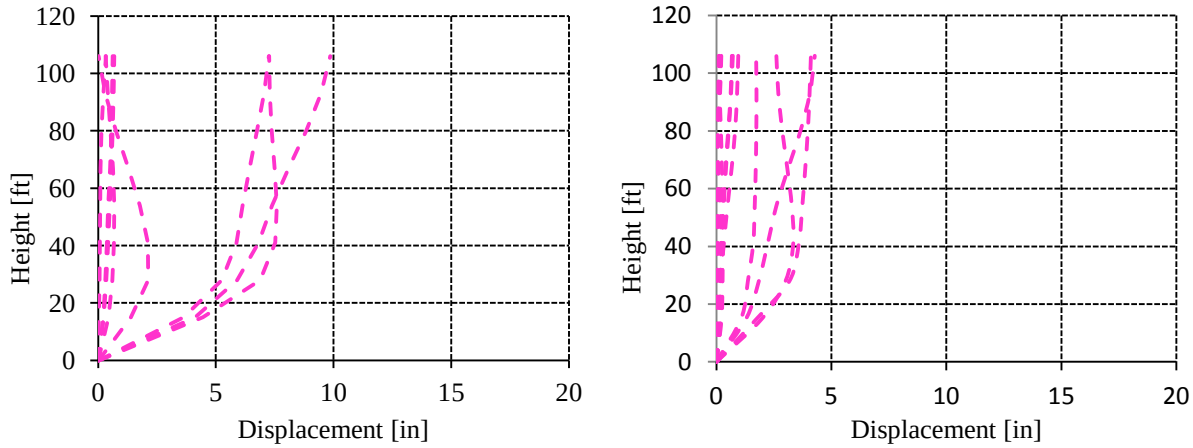

Figure 32: *Chi-Chi earthquake building displaced shape at a) collapsed site, Sa(T_1)=0.25g and b) non-collapse site, Sa(T_1)=0.25 g*

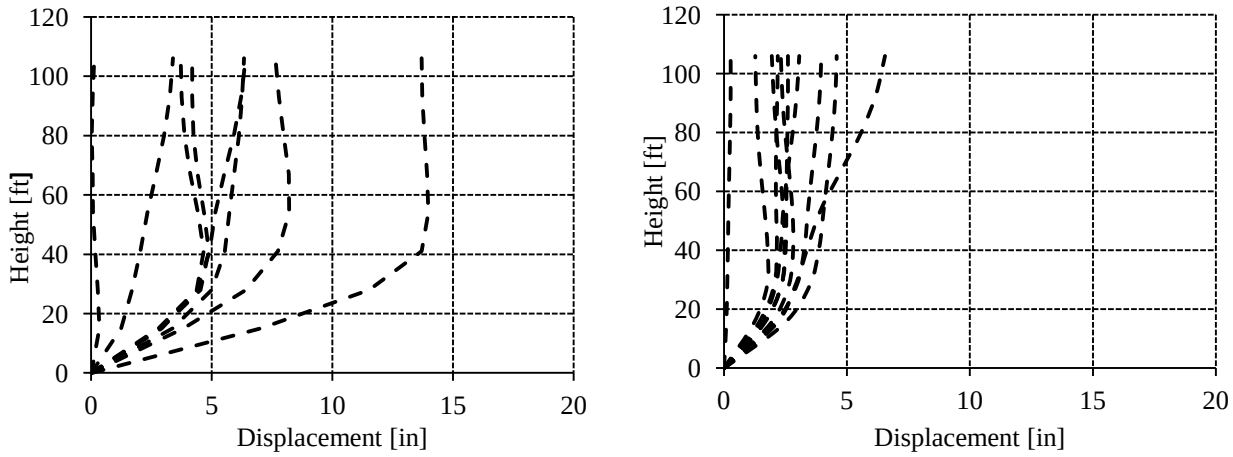

Figure 33: *Loma Prieta earthquake building displaced shape at a) collapsed site, Sa(T_1)=0.26g and b) non-collapsed site, Sa(T_1)=0.25g*

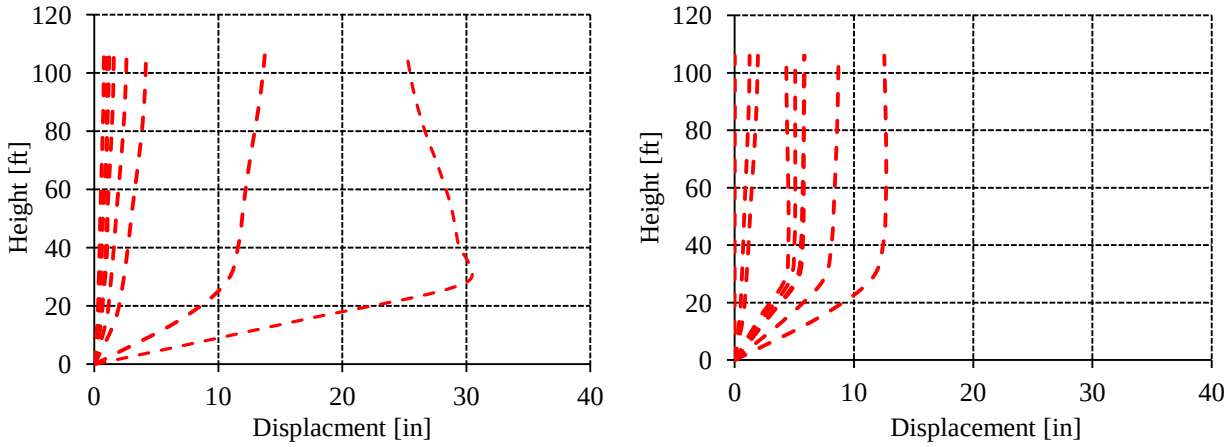

Figure 34: *ShakeOut simulation building displaced shape at a) collapsed site, Sa(T_1)=0.26g and b) non-collapsed site, Sa(T_1)=0.27g*

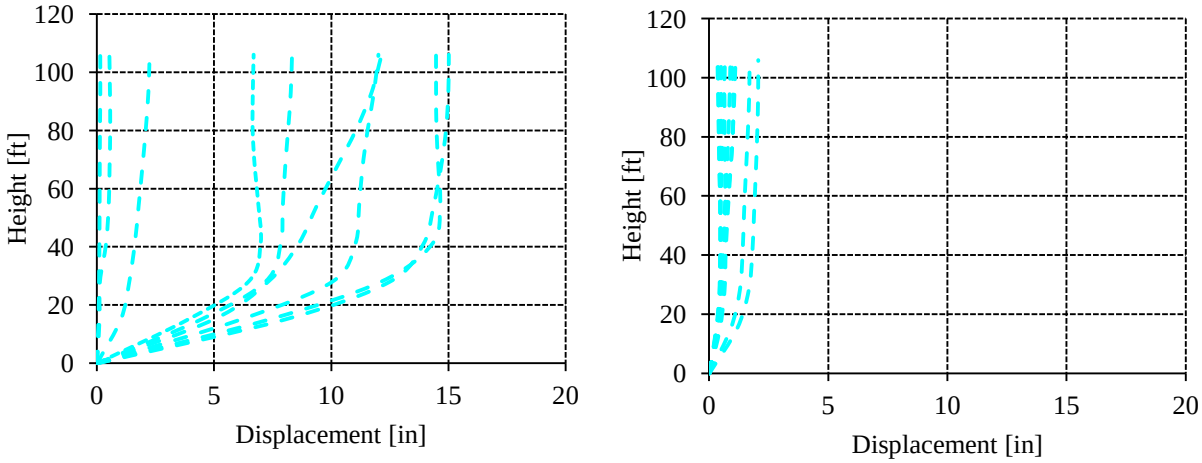

Figure 35: *1906 simulation building displaced shape at a) collapsed site, Sa(T_1)=0.25g and b) non-collapsed site, Sa(T_1)=0.25g*

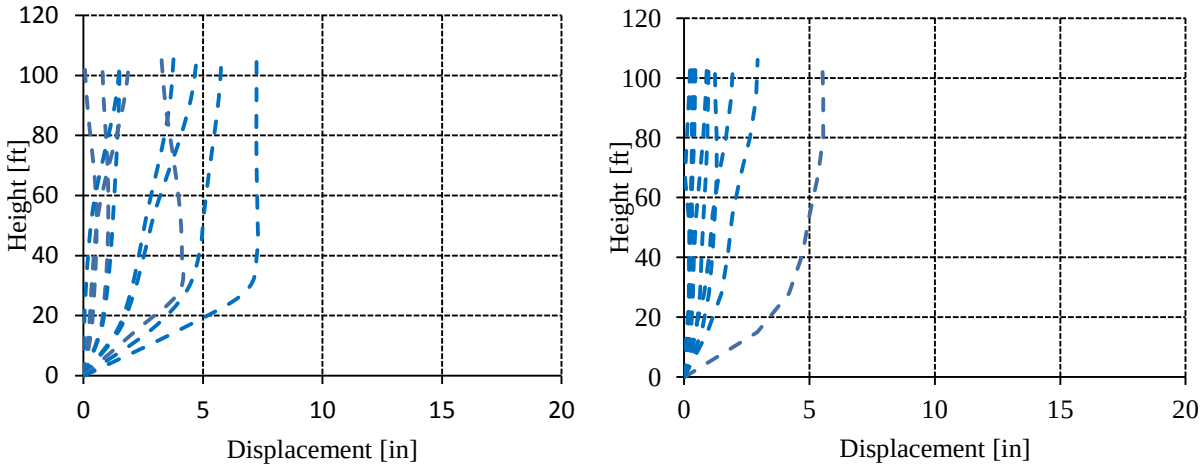

Figure 36: *Puente Hills simulation building displaced shape at a) collapsed site, Sa(T_1)=0.25g and b) non-collapsed site, Sa(T_1)=0.26g*

To examine trends in displaced shape between all the earthquakes, the displaced shapes were compared for each earthquake and plotted in **Figure 37**. To reduce the record to record variability, these displaced shapes are for non-collapsed sites in the range of 0.25g< Sa(T_1) <0.28g, and the building response which yielded the maximum roof displacement over the time history from each record were averaged. This plot shows an interesting trend regarding the distribution of damage over the height of the building. For all three of the simulated earthquake scenarios and the Northridge recorded ground motion, the damage appears to be concentrated primarily in the lower three stories while for the two other recorded earthquakes, the damage is distributed more evenly over the total building height. These two recorded earthquake also cause the lowest drifts overall for the selected spectral acceleration level. This trend is apparent in **Figure 38**, which shows the interstory drifts at each story. The simulated ground motions exhibit levels of interstory drift higher than the recorded ground motions at the bottom three floors and lower interstory drifts at the all the remaining floors except the roof. If higher modes are significantly affecting building response, we would expect to see higher levels of drift in higher stories. We also see that the ShakeOut earthquake incites the largest interstory drifts for the first level and also exhibits the most variability in interstory drift across the height of the building. This may be because the range of *Sa* used to examine building response was significantly higher than the median value causing collapse for the ShakeOut (which was 0.19g). This range was chosen because it was about, or slightly higher than, the median *Sa* causing collapse for all earthquakes except the Northridge. The Northridge was excluded from dictating

the choice of range because of its significantly higher *Sa* causing collapse. Interestingly though, despite the low level of *Sa*, in this case the building response to the Northridge earthquake is the least different from the simulated building responses. This is of note also because when analyzing the collapse metrics, the Northridge earthquake consistently had the highest percent difference from the simulated ground motions in terms in median response. The Northridge earthquake also exhibited the highest frequency content of any of the earthquakes in short periods which would imply that buildings subjected to the Northridge ground motions should be most affected by higher mode effects. However, this does not seem to be the case as the interstory drifts for the Northridge earthquake are relatively low in the higher stories.

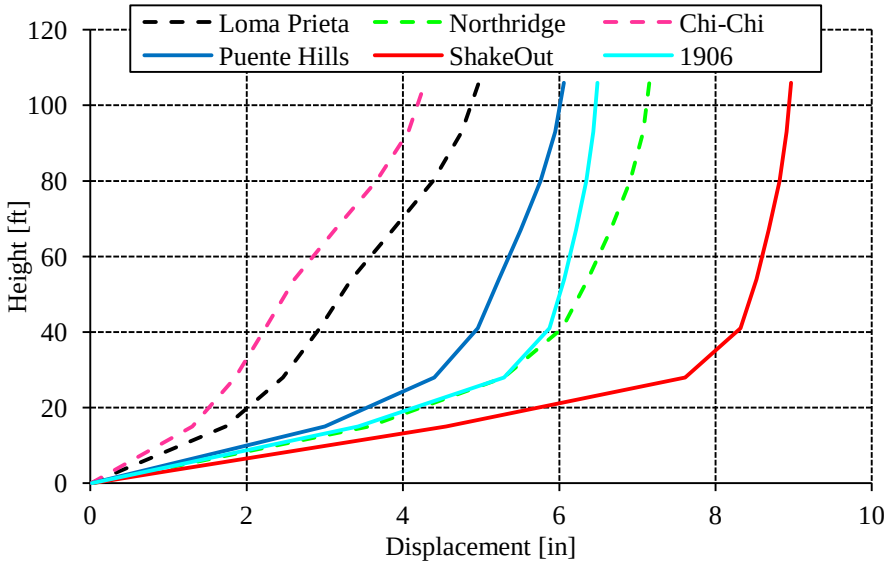

Figure 37: *Building displaced shape yielding maximum roof displacement, averaged over all non-collapsed sites with 0.25g< Sa(T_1) <0.28g*

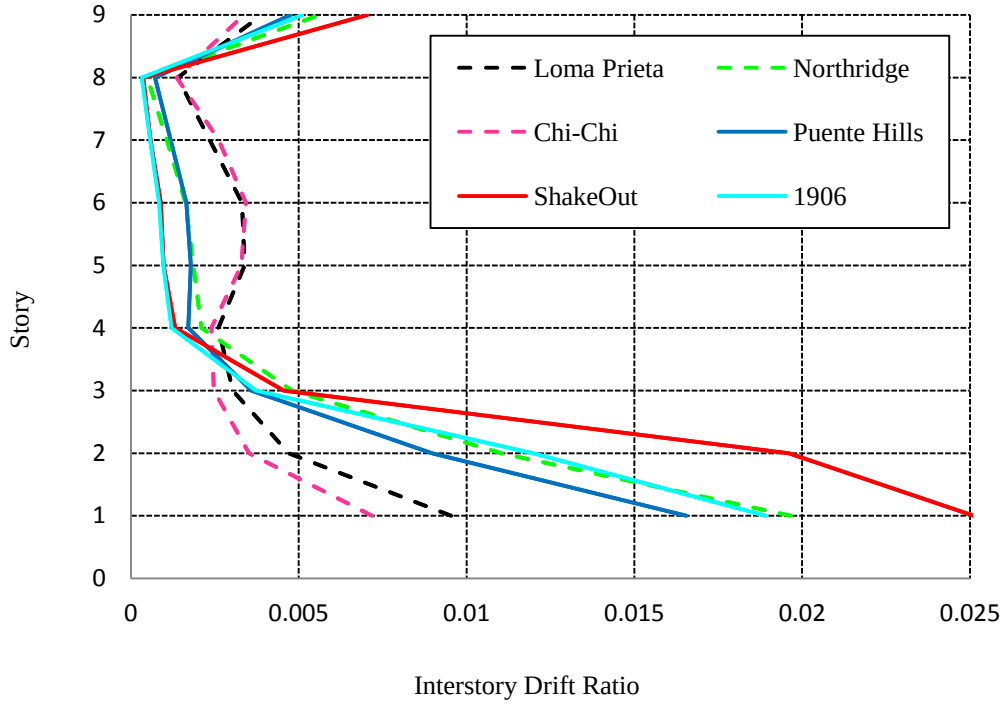

Figure 38: *The maximum interstory drift ratio recorded at each story then averaged for all earthquakes in the range 0.25g< Sa(T_1) <0.28g.*

While the trends in buielding displaced shape for the various recorded and simulated earthquakes are important when considered in the context of using simulated ground motions to analyze building response, they do not seem to offer an explanation for the differences in median collapse response. The next aspect of the ground motions examined to try and explain these differences is energy content and earthquake duration.

5.2.4 Examining energy content and duration

We have examined the frequency domain of all the earthquakes, by looking at the response spectra and the inelastic spectral response and are still finding differences. The next step was to examine the time domain of the earthquakes. A major component of the time domain which may cause differences in building response has to do with the energy of the ground motion. The rate at which energy accrues as well as the total energy of the ground motion can play a role in how the building responds to the ground motion. To look at energy content we will first examine Arias intensity (I_a) which is a measure of the intensity of a ground motion based on

the integral of the square of the ground acceleration over the length of the ground motion (Kramer 1996). It is known to be an indicator of damage potential. From the Arias intensity, Husid plots can be created which represent both the earthquake duration and the accrual of energy during the ground motion time history, independent of the absolute amplitude of the Arias intensity (Somerville, 2002). Husid plots are made by normalizing the Arias intensity at each time step by the total Arias intensity over the duration of the ground motion. In this case, the time was also normalized using the total ground motion duration so that the rate of energy accumulation could be compared for all the earthquakes despite varying durations. Care was taken to select records with an $Sa(T_1)$ value as close as possible to each other in the range $0.25g < Sa(T_1) < 0.28g$, to ensure a level of consistency. It should be noted though, that the Arias intensity and Husid plots are all made using only one record, meaning that record to record variability is not considered here.

First, the Arias intensity is examined; **Figure 39** shows the Arias intensity versus the total duration for building 3016 taken from the same ground motion records as those used in Section 5.2.3. These plots are then normalized by time, as shown in **Figure 40**. The relative duration of the various ground motion time histories is apparent in **Figure 37**; for example, the Northridge earthquake has the shortest duration (20s) followed by the Loma Prieta (40s), the Puente Hills (60s), the Chi-Chi (70s), the ShakeOut (81s), and finally the 1906 simulation (175s). This figure shows that the 1906 simulation record has significantly higher absolute Arias intensity for both the collapsed and the non-collapsed sites than the rest of the ground motions. In addition, the 1906 simulated record reaches close to the maximum Arias intensity very early on in the total duration of the earthquake implying that, after the initial period of high intensity shaking, there is a long period of low shaking intensities. For these two sites, the ShakeOut ground motions exhibit the lowest Arias intensity, the 1906 is approximately 4 times higher for the collapsed site and approximately 12 times higher for the non-collapsed site. While the Arias intensity offers interesting information regarding the total intensity of the various ground motions, it does not seem to reveal the reason for the remaining differences in the values of median S_{di} causing collapse.

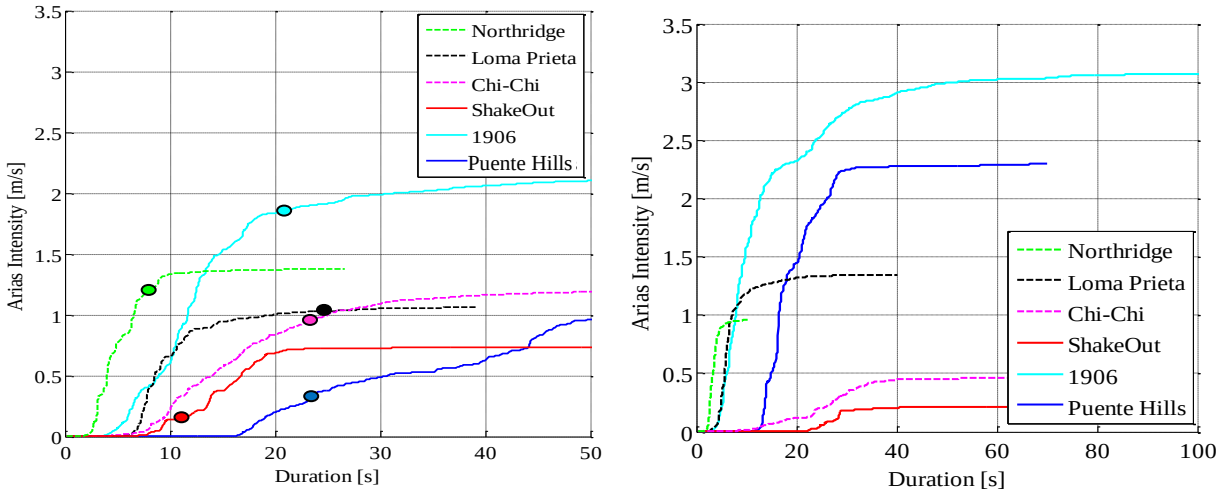

Figure 39: *Accumulation of Arias intensity over time for representative ground motion time histories from each earthquake for one a) collapsed site (dots represent time when the building collapsed) b) non-collapsed site within the range* $0.25g < Sa(T_1) < 0.28g$

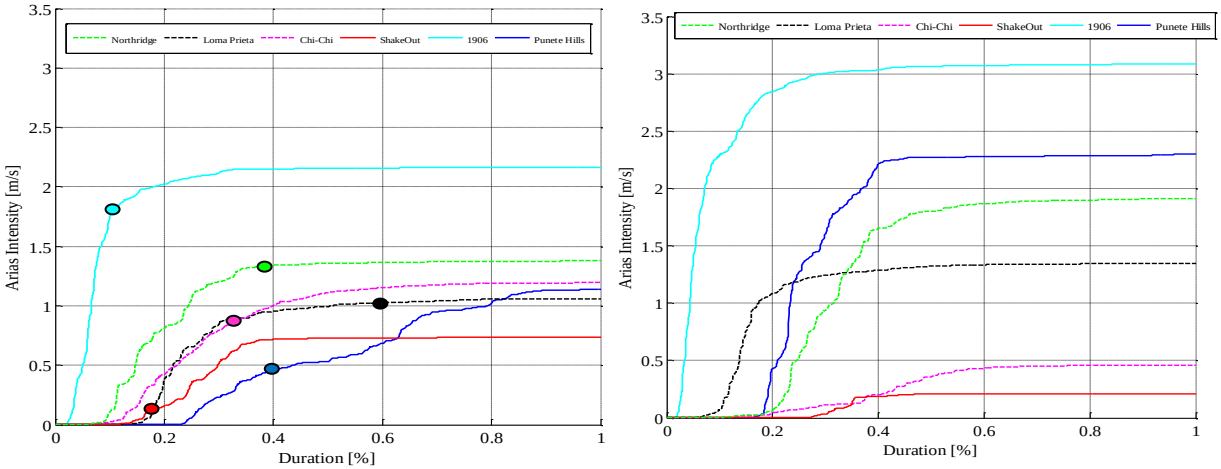

Figure 40: *Accumulation of Arias intensity over time for representative ground motion time histories from each earthquake for one a) collapsed site (dots represent time of collapse) b) non-collapsed site within the range* $0.25g < Sa(T_1) < 0.28g$

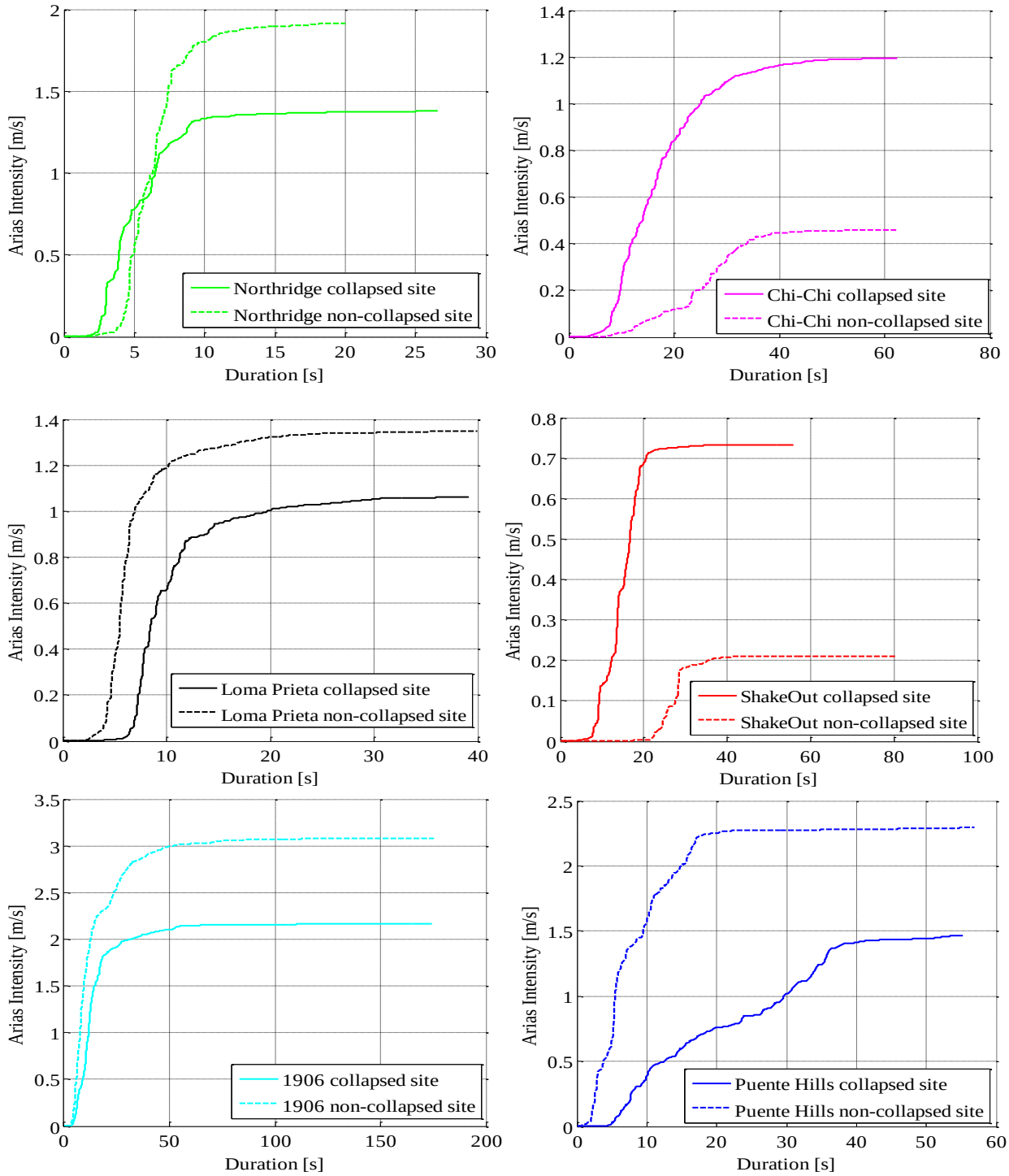

Figure 41: *Accumulation of Arias intensity over time for ground motion time histories from each earthquake for one collapsed site and one non-collapsed site within the range* $0.25g < Sa(T_1) < 0.28g$

The next measure of energy content examined was the rate of accumulation of the Arias intensity over the duration of the ground motion records. **Figure 42** shows the Husid plots for one site for each of the earthquakes. **Figure 43** illustrates the Husid plots for the ground motions corresponding to those used for Arias intensity and for the displaced building shapes plots in Section 5.2.3 providing a comparison of the difference in energy accumulation between the collapsed and non-collapsed sites for each earthquake. Again, the Husid plot shows only one site for each earthquake within a range $0.25g < Sa(T_1) < 0.28g$ which means they may not be representative of all the recorded sites. To quantify the rate of energy accumulation, we can look at the slope of the Husid plots. The curves with a steep slope are accumulating energy quicker (relative to the total length of the ground motion) which could potentially affect the building response. In **Figure 42a**, we see that the Puente Hills ground motion accumulates energy at a significantly lower rate than the other earthquakes. The Puente Hills ground motion takes approximately half its total duration (or 30 s) to reach 50% energy accumulation while the 1906 ground motion reaches 50% energy accumulation only about 6% of the way (10.5 s) through the total earthquake duration. Also, based on the collapse results we saw, we would expect the Northridge and ShakeOut earthquakes to be the most different in terms of significant duration and rate of energy accrual, however we do not find this to be the case. Although, it is interesting to note that the ShakeOut earthquake does cause collapse much earlier in the record than ground motion time history than the other earthquakes. However, the record duration and rate of energy accrual do not seem to follow the trends seen in building response. This implies that the rate of accumulation of energy is likely not the cause of differences in the building response.

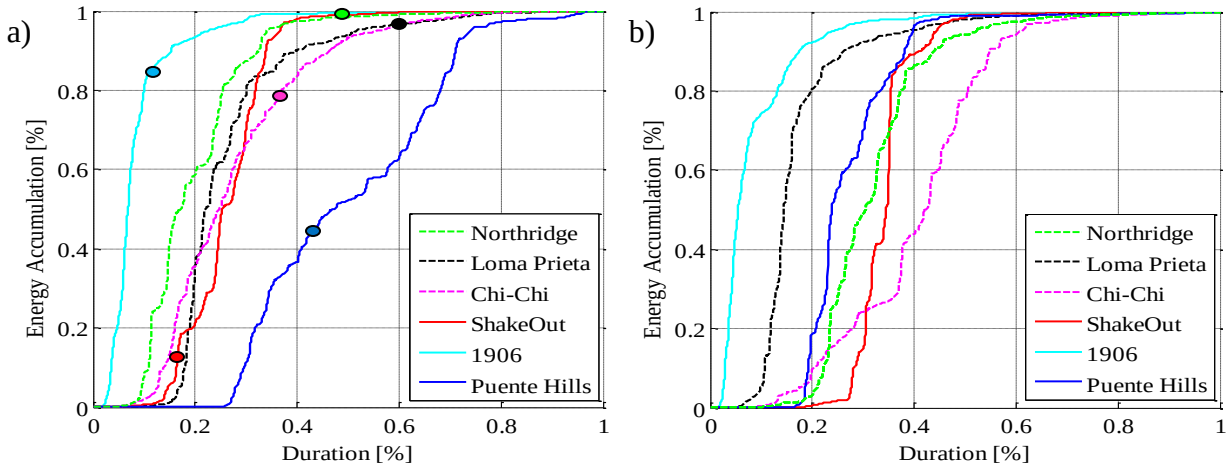

Figure 42: *Husid plots for representative ground motions from earthquakes for a) one collapsed site and b) one non-collapsed site within the range* $0.25g < Sa(T_1) < 0.28g$

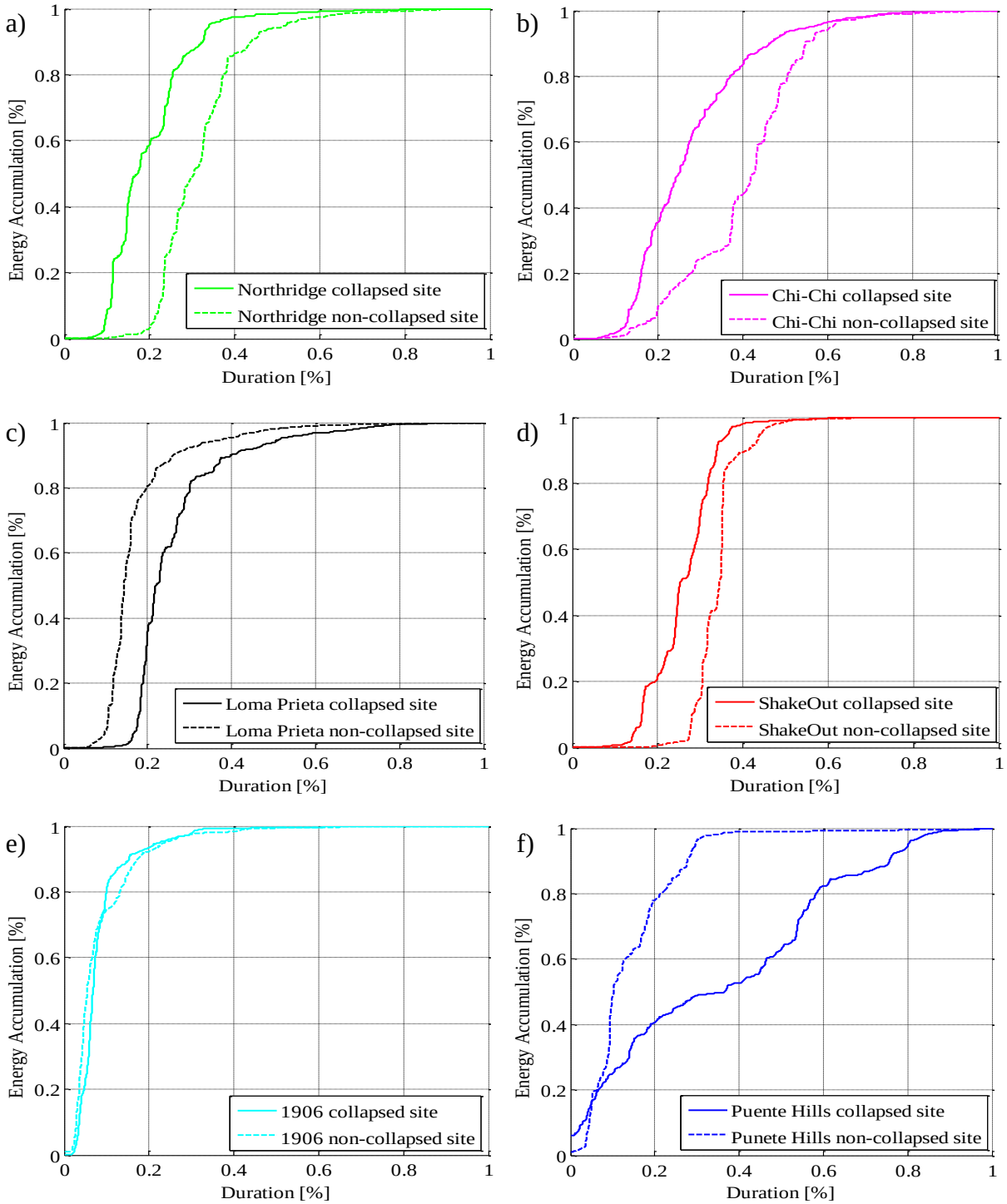

Figure 43: *Husid plots for one collapsed and one non-collapsed site for a) Northridge b) Chi-Chi c) Loma Prieta d) ShakeOut e) 1906 and f) Puente Hills within the range* $0.25g < Sa(T_1) < 0.28g$

5.2.5 Conclusions regarding variations in building response

As seen in Section 5.1, building response exhibited significant differences between ground motions from the different earthquakes: particularly, the metrics of interstory drift for

given levels $Sa(T_1)$, median values of $Sa(T_1)$ causing collapse and median values of the probability of exceeding certain drift levels. Confidence intervals showed that the ShakeOut, Puente Hills and SongMod simulations are potentially statistically related. We also determined that, while other simulations have median values of collapse which are closer to that of the recorded ground motion set, there were still significant percent differences between all the earthquakes.

In attempting to determine the source of the differences, we looked at the relationship between building response and inelastic response rather than simply elastic response as in Section 5.1. Examining building response in the context of inelastic response significantly decreased the percent difference in response between all the earthquakes. This implies that the long period energy significantly affects the building response for all the earthquake scenarios. We can conclude that it is important to consider inelastic response of buildings rather than simply the elastic response. However, there were still differences between the building responses when quantified in terms of inelastic spectral displacement. To try to determine why these existed, we looked at the response spectra for the different earthquakes, examined higher mode effects, and energy content. While the building response to all the earthquakes exhibited some higher mode effects, higher modes did not seem to play an integral role in the differences between earthquakes. The energy content was then examined through Arias intensity and Husid plots. While the energy content and rate of energy accumulation offers valuable information about the recorded and simulated ground motions, there does not seem to be any distinct trends which indicate that the energy content or rate at which the energy is accumulating plays an important role in the remaining differences seen in building response.

With regard to the objective of determining whether differences exist in building response to simulated versus recorded ground motions, this study concludes that potentially significant and quantifiable differences do exist. While differences in building response are to be expected between different earthquakes, this study finds that when considering the elastic response spectras of the simulated and recorded ground motions, potentially significant differences in collapse probabilities and drift ratios exist for all recorded and simulated ground motions. However, once the building response was analyzed in the context of inelastic spectral properties, the median building responses for all records were much closer together. This observation implies that the frequency content at long periods is having an effect on the building response. When plotting the spectras for the ShakeOut scenario, in general the ShakeOut spectra

contains relatively lower levels of energy at short periods but high levels at long periods (reference **Figure 26**). Whether this long period energy is characteristic of rupture patterns in this area or whether it is a product of the simulation process should be explored further. Ongoing research is being done by Kalkan and Hatayama (2010) about long period, strong ground motions. Using acceleration time histories recorded in the Los Angeles basin during the 7.2 Mw 2010 El Mayor-Cucapah earthquake, they have determined that the soft-sediment of the basin significantly amplifies the long period energy. These findings may indicate whether the long period energy of the ShakeOut records is reasonable.

5.3 Implications for Risk Assessments

This research has implications in terms of the broader area of seismic risk assessment regarding probabilistic building analysis. Probabilistic building analysis is used to determine median expected elastic or inelastic measures of ground motion intensity causing collapse for an archetypical building. By using collapse and drift exceedance fragility curves similar to those developed for this study, designers and researchers can predict, with relatively good accuracy, anticipated regions of vulnerability for certain building types. For example, for the ShakeOut earthquake, we used the program ArcGIS to plot the building sites, seen in **Figure 44a,** which collapsed after performing nonlinear dynamic analysis. In **Figure 44b**, we plotted all sites that have higher spectral acceleration values than the median collapse spectral acceleration from the ShakeOut earthquake ground motions. Next, we identified all sites that have higher Sdi values than the median value of S_{di} predicted to cause collapse for the ShakeOut, as shown in **Figure 44c**. These plots reveal that using only the $Sa(T_1)$ or S_{di} value of a given site, without doing the nonlinear dynamic analysis, we can predict regions of vulnerability and that in general, the median value $Sa(T_1)$ or S_{di} causing collapse offer a good metric for predicting collapse.

To analyze whether this trend was valid for all the earthquakes examined, results for all earthquakes can be found in **Table 7**. For all earthquakes, except the Loma Prieta (for which there were fewer than 10 collapsed sites indicating insufficient data for logistic regression), the median $Sa(T_1)$ predicts the number of collapsed sites within a few percent. The earthquakes for which there was more data, yielded closer estimates of collapse based on the Sa value with the Puente Hills estimating collapse values within 2%. Using S_{di} as a predictor of collapse was at least as good as using $Sa(T_1)$, and in most cases was even better. The Puente Hills simulation again has the closest prediction value at less than 1% difference.

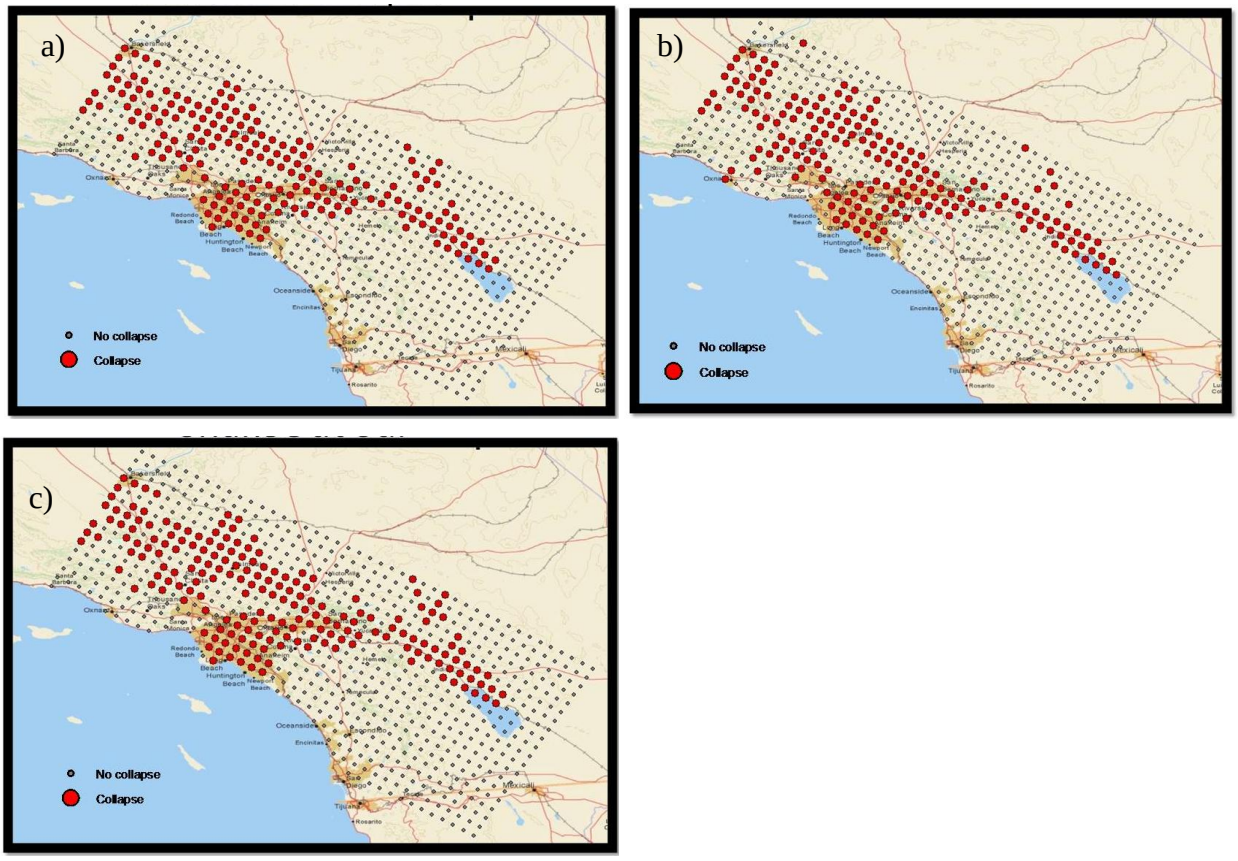

Figure 44: *ShakeOut collapse sites a) from nonlinear analysis, b) based on median Sa(T_1=2.23s) for ShakeOut c) based on median S_{di} for ShakeOut*

Table 7: *Comparison of actual collapse results to estimates based on Sa(T_1) and S_{di}*

		Num. of Collapsed Sites obtained through nonlinear analysis	Num. of Collapsed Sites estimated by *Sa*	% diff from collapse results [%]	Num. of Collapsed Sites Collapse estimated by S_{di}	% diff from collapse results [%]
Recorded	Northridge	9	8	-11	8	-11
	Loma Prieta	6	2	-67	5	-17
	Chi-Chi	57	46	-19	46	-19
Simulated	ShakeOut	193	187	-3	195	1
	1906	327	293	-10	308	-6
	Puente Hills	302	296	-2	301	0

Next we evaluated what implications these probabilistic analyses may have for areas and sites where we do not have simulated ground motions. To do this we took the median $Sa(T_1)$ value causing collapse for the General Set, and plotted the sites which exceeded this median spectral acceleration causing collapse. **Figure 45a** shows that, while the regional risks seem to be similar for the actual collapse results and those estimated using the generalized set, there is a substantial underestimate of the number of sites that will collapse. This makes sense because the results implied that the ShakeOut simulation estimated median collapse at a significantly lower (34%) spectral acceleration value than the generalized set. Expected collapse trends using the median inelastic spectral displacement were also determined and can be found in **Figure 45b**. This shows that using the inelastic response from a general set of recorded earthquakes offers a much better predictor of what happens due to the simulated event. When using median *Sdi* as a predictor of collapse, the difference between the number of actual and predicted collapses was only 19% and as seen in **Figure 45**, the patterns of locations which experienced collapse were also well predicted when using the median *Sdi*. This implies that perhaps using predicted values of inelastic spectral displacement for predicting seismic risk could be a helpful metric for evaluating vulnerability.

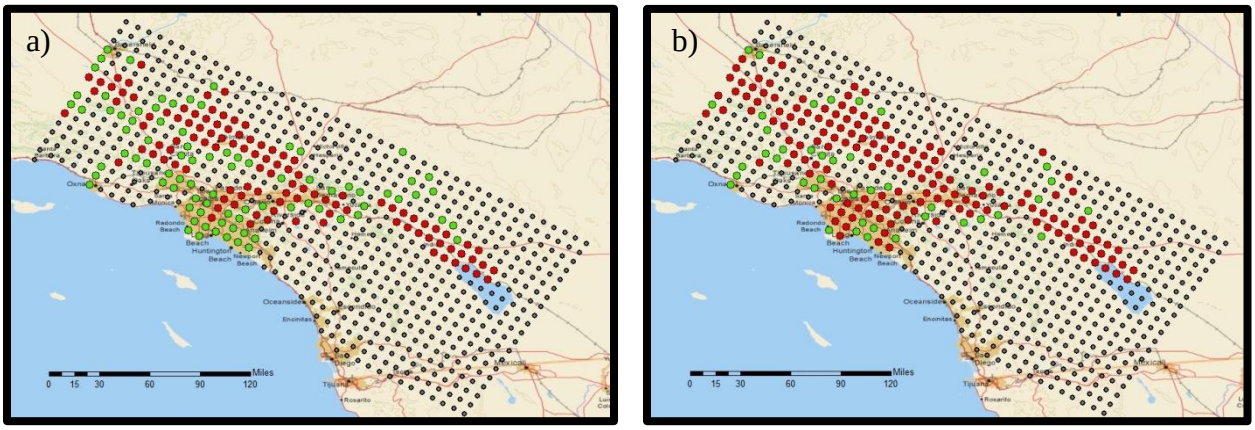

Figure 45: *Collapses predicted for the ShakeOut earthquake from a) General Set $Sa(T_1)$ b) Recorded Set S_{di}. (Green spots represent those which collapse during the ShakeOut simulation, but are not predicted by the general set. Red indicate those sites which did collapse due to the ShakeOut simulation and are predicted to collapse by the median of the general set.)*

The final predictor that we examined which may have implications in terms of evaluating seismic risk was using the *Recorded Set* to come up with a predictor of probability of collapse. **Figure 46** below shows the probabilities of collapse predicted from the spectral displacement

Recorded Set fragility curve. For example, if a site has an inelastic spectral displacement of 10 in., it has a 40% probability of collapse based on the collapse fragility curve for the *Recorded Set* and so it is plotted in the 40-49.9% probability of collapse range. We find that overall this offers a good predictor of the trends seen in collapse results for the ShakeOut earthquake. Using a study such as this may allow researchers to draw conclusions about the vulnerability of buildings to large ground motions. Potentially, for places that we do not have simulations, we could create collapse fragility curves from a generalized set of large ground motions and use that to predict the probability of collapse of buildings with relatively good accuracy.

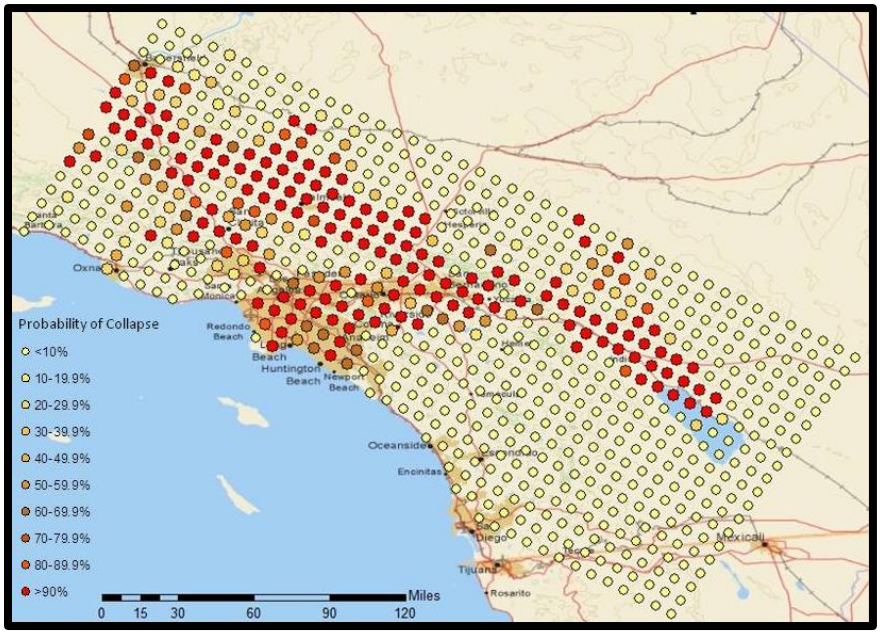

Figure 46: *Probability of collapse predicted for the ShakeOut earthquake using* S_{di}

Chapter 6: Conclusions

This study evaluates the use of physics-based ground motion simulations for nonlinear analysis of MDOF systems. It does this by examining, probabilistically, response of ductile and non-ductile concrete frame buildings to simulated earthquake scenarios and recorded ground motions from past earthquakes. Building response parameters examined include: interstory drift, probability of collapse, probability of exceedance and building displaced shapes. Probabilistic analysis is used to create fragility functions which help to quantify some of the building responses obtained from the nonlinear analysis. Using statistical methods, the building responses are compared to a general set of ground motions, which is assumed to be representative of response expected due to actual earthquakes. This comparison offers valuable information about whether, given modeling uncertainty, the sets of data for the various earthquakes likely came from the same distribution. The confidence intervals developed can indicate whether the data for the simulated earthquakes seems to be related to the data we have recorded from actual events. This study next tries to determine what ground motion characteristics may be causing the differences in building response. Aspects examined include: the elastic response spectra, inelastic response, building displaced shape and energy content for the various ground motions. Combining the investigation of all of these, this research attempts to determine whether there are aspects of the simulated ground motions which are causing these differences in building response. Finally, this study also attempts to examine a method of using probabilistic analysis to aid in seismic risk assessment.

This research shows that the mere fact that some of the events were simulated rather than recorded did not produce significant differences in the fragility functions in terms of $Sa(T_1)$, yet differences did exist in the fragility curves of all six events examined. The probability of collapse for various simulations and recorded earthquakes varied significantly in some cases, particularly between the Northridge recorded ground motions and the ShakeOut simulation. Statistical analysis showed that, when looking at probability of collapse in terms of the 5% damped elastic spectral acceleration response, the ShakeOut simulation had a 32% probability of not being from the same distribution as a general set of recorded large magnitude ground motions. However, when the probability of collapse was examined in relation to the 5% damped

inelastic spectral displacement response, statistical analysis indicated that the data sets for all the simulated and recorded events came from the same distribution. Looking at building response in relation to *Sdi* also decreased the percent difference between the various median values causing collapse. This indicates that the long period energy content of the various ground motions has a significant effect on the building response. Examining higher building displaced shape indicated that higher mode effects were not playing a part in the differences in probability of collapse. Looking at higher mode effects showed that the Loma Prieta and Chi-Chi ground motions excited higher modes as indicated by the increased story drifts in the higher stories; but that the Northridge, ShakeOut, Puente Hills and 1906 ground motions were not exciting higher modes. Examining energy content and earthquake duration also indicated that this was not the cause of the differences in building response. While difference existed in the total energy content, the rate of energy accruement and the earthquake significant duration, the trends do not follow the trends seen in collapse results.

This study also has implications in the broader area of seismic risk analysis. Using the probabilistic analysis outlined in the study, we examine the applicability of using collapse results from a generalized set of recorded ground motions to determine seismic risk of a particular type of structure. We compare the estimated collapse results using to the actual results of building collapse from the simulated ground motions to look at whether this type of analysis may be useful for regions where we do not have simulated or recorded events. This may offer a useful framework to evaluate seismic vulnerability of buildings.

References

Aagaard, Brad, et al. "Ground-Motion Modeling of the 1906 San Fransico Earthquake, Part II: Ground-Motion Estimates for the 1906 Earthquake and Scenario Events." *Bulletin of the Seismological Society of America,* 2008: 1012-1046.

Aagaard, Brad, et al. "Data Files for Ground-Motion Simulations of the 1906 San Fransico Earthquake and Scenario Earthquakes on the Northern San Andreas Fault." 2009.

Aagaard, Brad, et al. "Ground-motion modeling of the 1906 San Francisco earthquake, Part I: validation using the 1989 Loma Prieta earthquake." *Bulletin of Seismological Society of America* 98 (2008): 989-1011.

Abrahamson, N A, and W J Silva. "Summary of Abrahamson and Silva NGA ground motion relations." *Earthquake Spectra*, 2008.

Applied Technology Council. *Quantification of Building Seismic Performance Factors, ATC-63 Project Report (FEMA P695).* Redwood City: FEMA, 2008.

Atkinson, Gail, and Katsuichiro Goda. "Inelastic seismic demand of real versus simulated ground-motions records for Cascadia subduction earthquakes." *Bulletin of Seismological Society of America* 100 (2010): 102-115.

Baker, Jack. "Conditional mean spectrum: tool for ground motion selection." *Journal of Structural Engineering*, 2011: 322-331.

Baker, Jack, and Allin Cornell. "Spectral shape, epsilon and record selection." *Earthquake Engineering and Structrual Dynamics* 35 (2006): 1077-1095.

Boore, D M, and G M Atkinson. "Grounf motion prediction equations for the average horizontal component of PGA, PGV, PGD and 5%-damped linear elastic response spectra ranging from 0.01 to 10 s." *Earthquake Spectra*, 2008.

Brocher, et. al. "The new USGS 3D seismic velocity model for Northern California." *Seismological Letters* 77 (2006): 271.

Brune, J.N. "Tectonic stress and spectra of seismic shear waves from earthquakes." *Journal of Geophysical Research* (J. Geophysics. Res.) 75 (1970): 4997-5009.

Campbell, K W, and Y Bozorgnia. "NGA ground motion model for the geometric mean horizontal component of PGA, PGV, PGD and 5% damped liner elastic response spectra for periods ranging from 0.01 to 10s." *Earthquake Spectra*, 2008: 139-171.

Champion, Casey. "The effect of near-fault directivity on building seismic collapse risk." Master's Thesis, 2010.

Chiou, B S, and R R Youngs. "Chiou and Youngs PEER-NGA emperical ground motion model for the average horizontal component of peak acceleration and pseudo-spectral acceleration for spectral periods from 0.01 to 10 s." *Earthquake Spectra*, 2008.

Graves, R W, B T Aagaard, K W Hudnut, L M Star, J P Stewart, and H T Jordan. "Broadband simulations for Mw 7.8 southern San Andreas earthquakes: Ground motion sensitivity to rupture speed." *Geophysical Research Letter*, 2008.

Graves, Robert. *BroadBand Ground Motion Simulations for the Puente Hills Thrust System.* USGS, 2005.

Haselton, C B, A B Liel, G G Deierlein, B S Dean, and J H Chou. "Seismic collapse safety of reinforced concrete buildings: I. Assessment of ductile moment frames." *Journal of Structural Engineering*, 2010: (accepted).

Haselton, C B, and G G Deierlein. *Assessing seismic collapse safety of modern reinforced concrete frame buildings.* Technical report No 156, Blume Center, 2007.

Husid, R. Analisis de terremotos:Analisis General, *Revista del IDIEM* 8, 21-42, 1969.

Jayaram, N, N Shome, and H Krawinkler. "A statistical analysis of the response of tall buildings to recorded and simulated ground motions." *SCEC annual meeting.* 2010.

Jones, L.M., et al. *The ShakeOut Scenario, U.S. Geological Survey Open File Report 2008-1150.* Preliminary Report 25, USGS, 2008.

Kramer, S L. *Geotechnical Earthquake Engineering.* Pearson Education, 1996.

Krishnan, Swaminathan, Chen Ji, and Dimitri Komatitsch. "Performance of two 18-story steel moment-frame buildings in southern California during two large simulated San Andreas earthquakes." *Earthquake Spectra* 22, no. 4 (2006): 1035-1061.

Liel, A B, and G G Deierlein. *Assesing the collapse risk of California's existing reinforced concrete frame structures: Metrics for seismic safety decisions.* Technical report No 166, Blume Center, 2008.

Liel, Abbie B, Curt B Haselton, G G Deierlein, and Jack W Baker. "Incorperating Modeiling Uncertainties in the Assesment of Seismic Collapse Risk of Buildings." *Structural Safety* (Struc), 2009.

Luco, Nicolas, and Paolo Bazzurro. "Do scaled and spectrum-mathced near-source racords produce biased nonlinear structrual results?" *Proceedings of the 8th U.S. national conference on earthquake engineering.* San Francisco, 2006.

Luco, Nicolas, and Paolo Bazzurro. "Does amplitude scaling of ground motion records result in biased nonlinear structural drift responses?" *Earthquake Engineering and Structural Dynamics* 36 (2007): 1813-1835.

Lynch, Kathryn, Kristen Rowe, and Abbie Liel. "Seismic performance of reinforced concrete frame buildings in southern California." *Earthquake Spectra*, 2011.

McCann, Martin W, and David M Boore. "Variability in ground motions: Root mean square acceleration and peak acceleration for the 1971 San Fernando, California earthquake." *BSSA*, 1983: 615-632.

Olsen, Anna, Brad Aagaard, and Thomas Heaton. "Long-period building response to earthquakes in the San Francisco Bay area." *Bulletin of Seismological Society of America* 98, no. 2 (2008): 1047-1065.

PEER ground motions database. n.d. http://peer.berkeley.edu/peer_ground_motion_database (accessed June 6, 2011).

Star, Lisa M, J P Stewart, R W Graves, and K W Hudnut. "Validation against NGA emperical Model of simulated motions fro M7.8 ruptrue of San Andreas Fauly." *Conference on earthquake engineering.* Beijing, China, 2008.

Stewart, Jonathan, Lisa Star, and Robert Graves. *Validation against empirical model of simulated motions for M7.15 rupture of Puente Hills Fault.* Berkeley: University of California, 2008.

USGS. *USGS Earthquake Hazards Program. ground motion simulations background.* 2009. http://earthquake.usgs.gov/regional/nca/1906/simulations/background.php (accessed February 2011).

Wald, D.J, B.C. Worden, V Quitoriano, and K.L. Pankow. "Rupture model of the 1989 Loma Prieta earthquake from the inversion of strong-motion and broadband teleseismic data." *Bulletin of Seismological Society of America*, 1991: 1540-1572.

Zareian, F, and P Jones. "Simulated vs. Recorded Ground Motions." *2010 SCEC Annual Meeting.* 2010.

Zareian, Farzin, and Pierson Jones. "Simulated vs. recorded ground motions: a comparison between reponse of tall buildings to recorded and simulated ground motions in an extreme hazard level." *2010 SCEC Annual Meeting.* 2010.

Appendix

A.1 Dynamic analysis results

Northridge results (recorded)

					Collapsed Results			Non-Collapsed Results	
	Bldg	# of Stories	Period	Collapses	% Collapse	Median Sa causing collapse [g]	Std Dev[a]	Average IDR/ Average Sa	Average PFA/ Average Sa
Modern	1001	2	0.63	0	0	N/A	N/A	0.0169	1.72
	1008	4	0.94	0	0	N/A	N/A	0.0240	1.70
	1012	8	1.80	0	0	N/A	N/A	0.0564	3.52
Older	3001	2	1.08	27	8.6	0.56	0.27	0.0385	1.40
	3004	4	1.98	16	5.1	0.39	0.34	0.1187	2.80
	3016	8	2.20	12	3.8	0.41	0.34	0.0984	4.01

a) The std deviation represents the value of the logarithmic standard deviation

Loma Prieta results (recorded)

					Collapsed Results			Non-Collapsed Results	
	Bldg	# of Stories	Period	Collapses	% Collapse	Median Sa causing collapse [g]	Std Dev[a]	Average IDR/ Average Sa	Average PFA /Average Sa
Modern	1001	2	0.63	0	0	N/A	N/A	0.0150	1.83
	1008	4	0.94	0	0	N/A	N/A	0.0229	1.48
	1012	8	1.80	0	0	N/A	N/A	0.5175	3.06
Older	3001	2	1.08	0	0.0	N/A	N/A	0.0764	1.83
	3004	4	1.98	5	3.1	0.42	0.48	0.1507	2.69
	3016	8	2.20	6	3.7	0.27	0.34	0.1252	3.51

a) The std deviation represents the value of the logarithmic standard deviation
b) Numbers in grey are uncertain because fewer than 10 collapses occurred indicating insufficient data for logistic regression

Chi-Chi Taiwan results (recorded)

				Collapsed Results				Non-Collapsed Results	
	Bldg	# of Stories	Period	Collapses	% Collapse	Median Sa causing collapse [g]	Std Dev[a]	Average IDR/ Average Sa	Average PFA /Average Sa
Modern	1001	2	0.63	1	0.12	N/A	N/A	0.0040	0.47
	1008	4	0.94	3	0.36	2.68	0.54	0.0045	0.28
	1012	8	1.80	4	0.47	0.96	0.4	0.0058	0.23
Older	3001	2	1.08	41	4.9	0.54	0.32	0.0086	0.22
	3004	4	1.98	74	8.8	0.26	0.39	0.0147	0.01
	3016	8	2.20	80	9.5	0.22	0.36	0.1147	2.06

a) The std deviation represents the value of the logarithmic standard deviation
b) Numbers in grey are uncertain because fewer than 10 collapses occurred indicating insufficient data for logistic regression

General set results (recorded)

				Collapsed Results			
	Bldg	# of Stories	Period	Collapses	% Collapse	Median Sa causing collapse [g]	Std Dev[a]
Modern	1001	2	0.63	N/A	N/A	4.32	0.44
	1008	4	0.94	N/A	N/A	1.94	0.372
	1012	8	1.80	N/A	N/A	0.81	0.384
Older	3001	2	1.08	N/A	N/A	0.51	0.30
	3004	4	1.98	N/A	N/A	0.32	0.30
	3016	8	2.20	N/A	N/A	0.29	0.39

ShakeOut results (simulation)

				Collapsed Results				Non-Collapsed Results	
	Bldg	# of Stories	Period	Collapses	% Collapse	Median Sa causing collapse [g]	Std Dev[a]	Average IDR/ Average Sa	Average PFA /Average Sa
Modern	1001	2	0.63	4	0.54	2.02	0.38	0.0044	0.53
	1008	4	0.94	18	2.45	0.87	0.31	0.0051	0.34
	1012	8	1.80	51	6.93	0.56	0.44	0.0083	0.21
Older	3001	2	1.08	95	12.9	0.32	0.27	0.0042	0.10
	3004	4	1.98	176	23.9	0.20	0.15	0.0079	0.07
	3016	8	2.20	192	26.1	0.19	0.25	0.0994	0.94

a) The std deviation represents the value of the logarithmic standard deviation
b) Numbers in grey are uncertain because fewer than 10 collapses occurred indicating insufficient data for logistic regression

1906 San Francisco results (simulation)

				Collapsed Results				Non-Collapsed Results	
	Bldg	# of Stories	Period	Collapses	% Collapse	Median Sa causing collapse [g]	Std Dev[a]	Average IDR/ Average Sa	Average PFA /Average Sa
Modern	1001	2	0.63	0	0.0	N/A	N/A	0.0075	1.82
	1008	4	0.94	3	0.3	1.50	0.32	0.0247	1.92
	1012	8	1.80	19	1.6	0.86	0.30	0.0123	0.53
Older	3001	2	1.08	209	18	0.37	0.27	0.0118	0.44
	3004	4	1.98	293	25	0.32	0.42	0.0254	0.04
	3016	8	2.20	328	28	0.24	0.40	0.1011	2.24

a) The std deviation represents the value of the logarithmic standard deviation
b) Numbers in grey are uncertain because fewer than 10 collapses occurred indicating insufficient data for logistic regression

Puente Hills results (simulation)

				Collapsed Results				Non-Collapsed Results	
	Bldg	# of Stories	Period	Collapses	% Collapse	Median Sa causing collapse [g]	Std Dev[a]	Average IDR/ Average Sa	Average PFA /Average Sa
Modern	1001	2	0.63	1	0.11	N/A	N/A	0.0111	1.33
	1008	4	0.94	24	2.74	1.8	0.45	0.0120	0.63
	1012	8	1.80	72	8.23	0.81	0.43	0.0136	0.53
Older	3001	2	1.08	272	31.1	0.39	0.34	0.0114	0.41
	3004	4	1.00	298	34.1	0.27	0.43	0.0186	0.38
	3016	8	2.20	302	34.5	0.25	0.34	0.0596	1.78

a) The std deviation represents the value of the logarithmic standard deviation

A.2 Dynamic analysis results plots by building

Building 3001

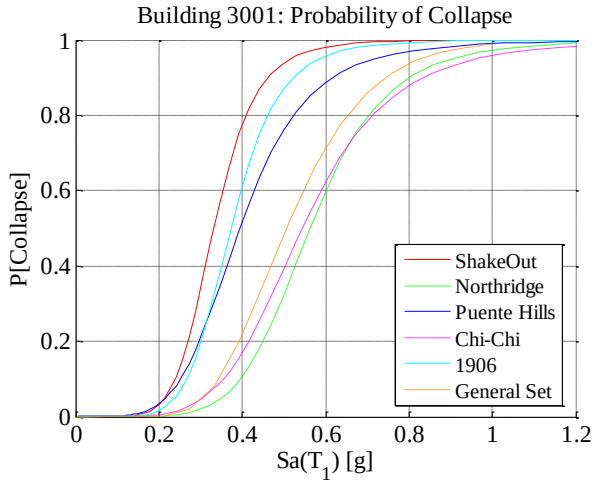

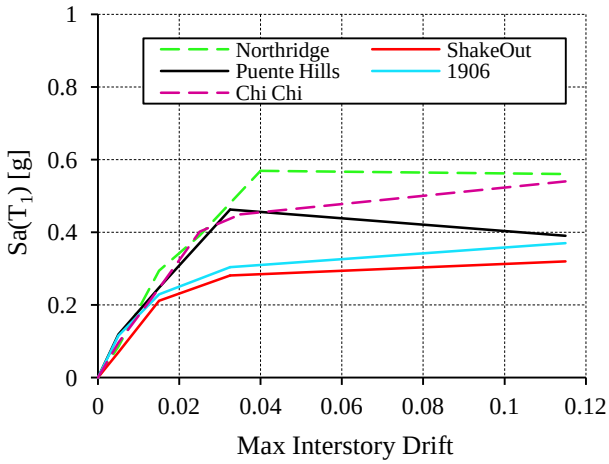

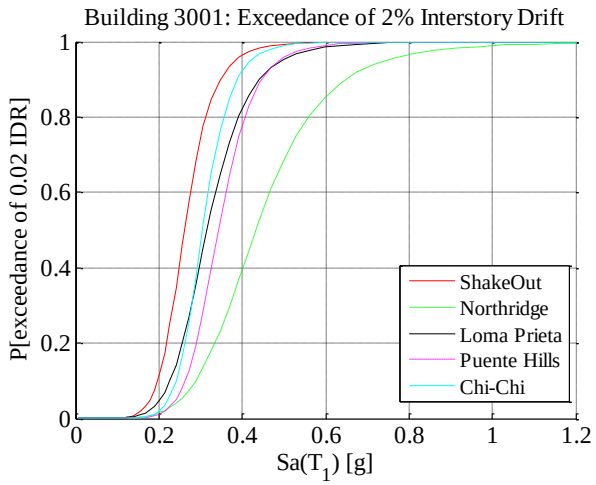

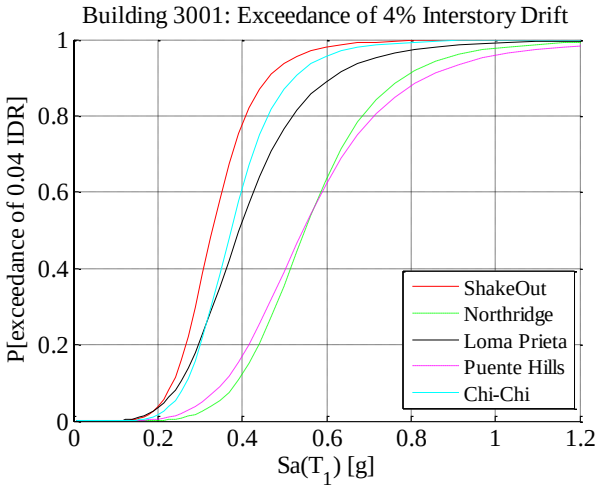

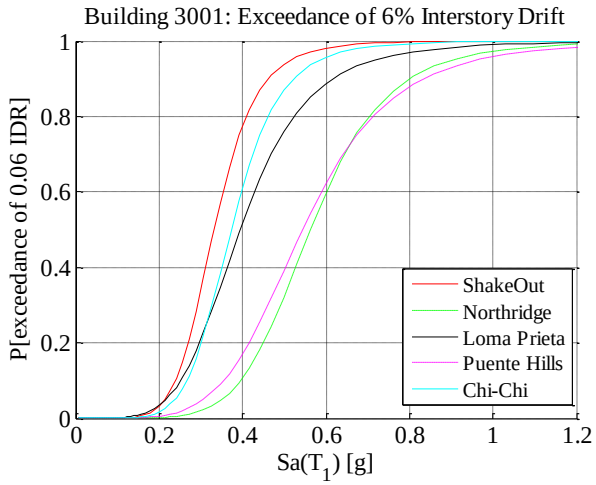

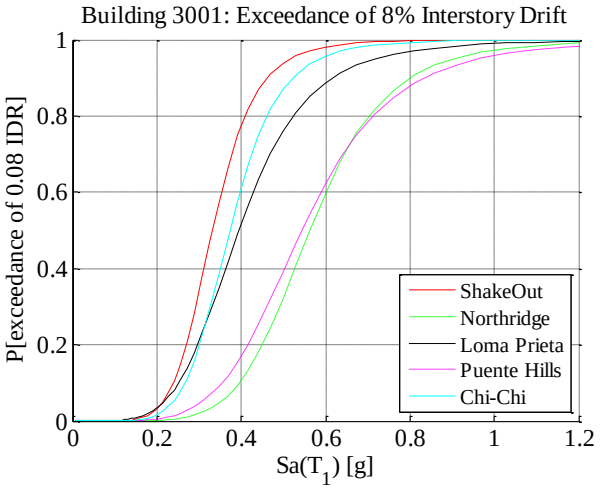

Building 3004

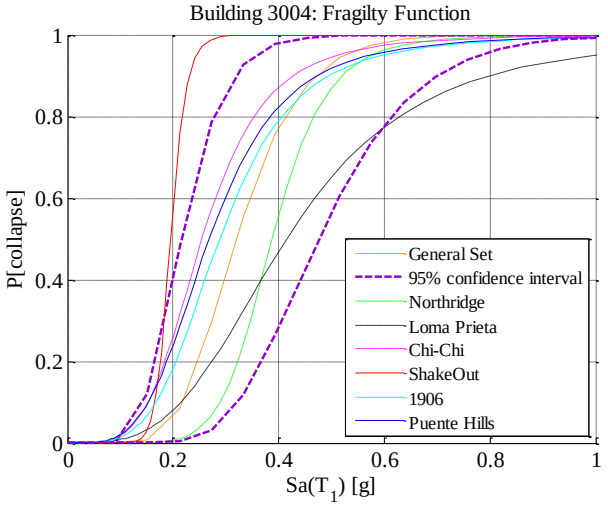

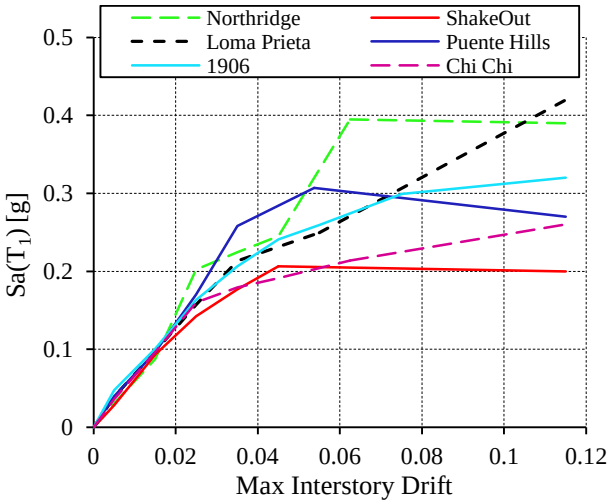

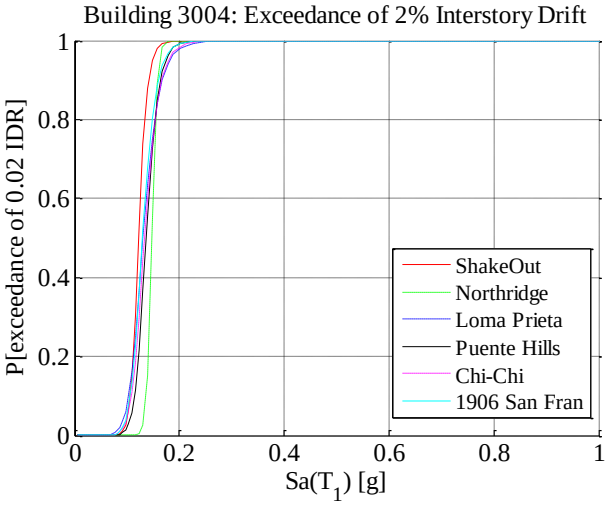

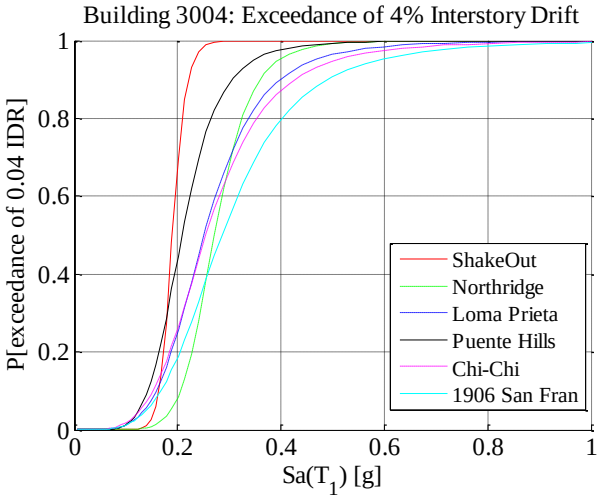

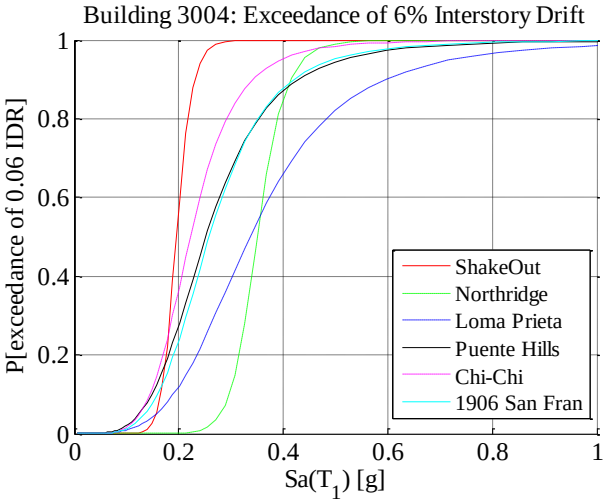

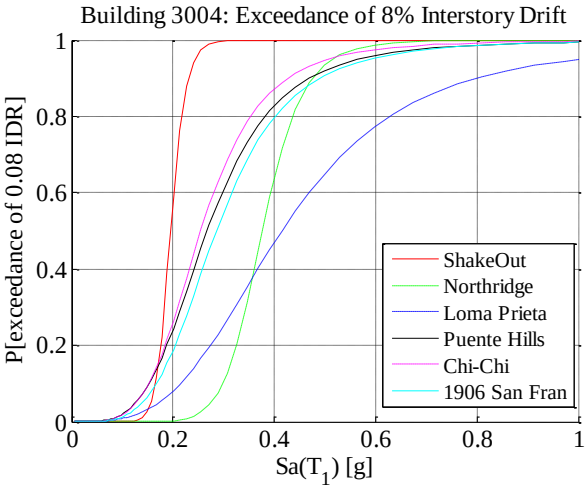

Building 3016

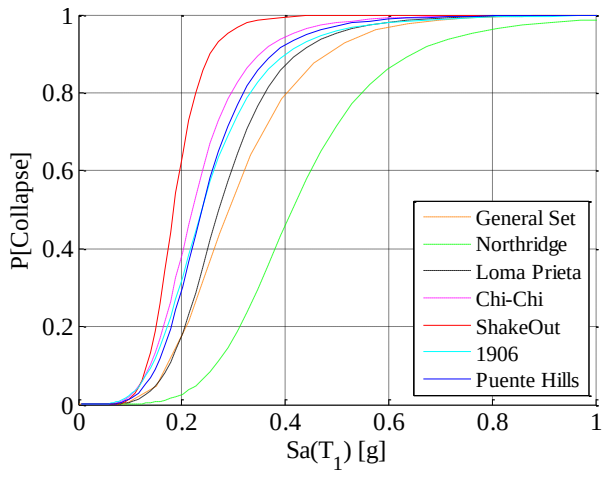

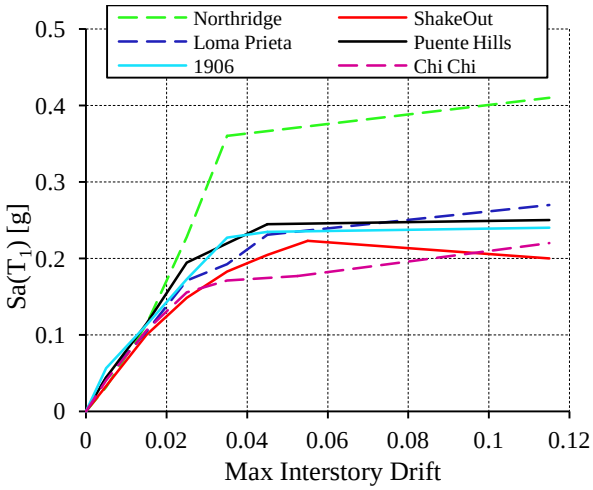

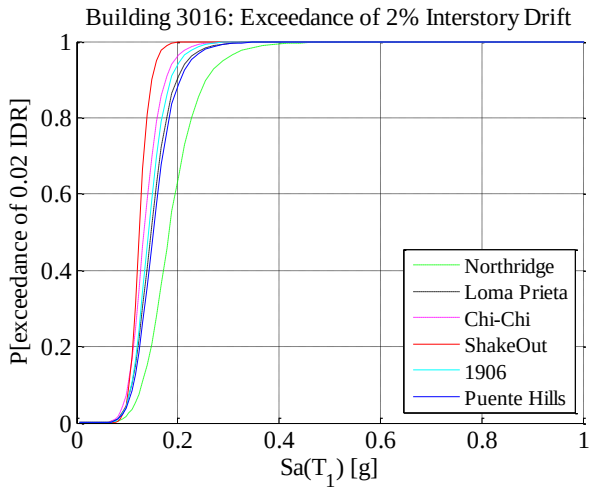

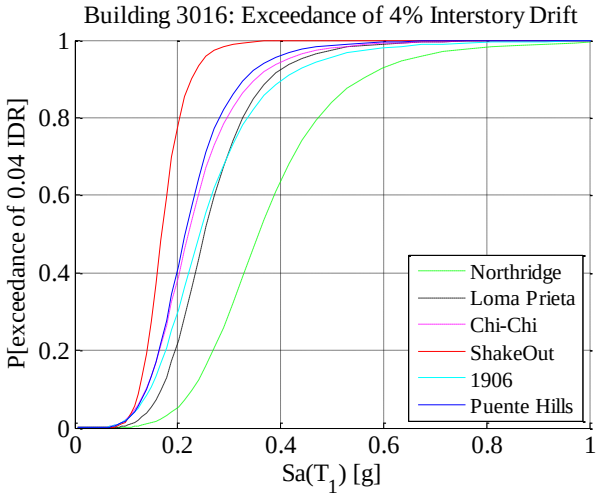

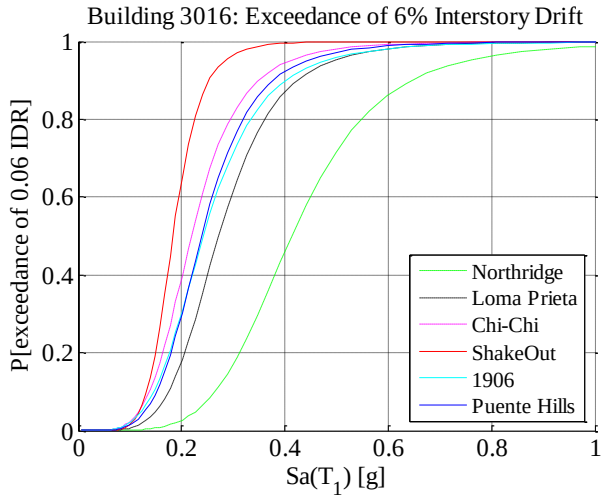

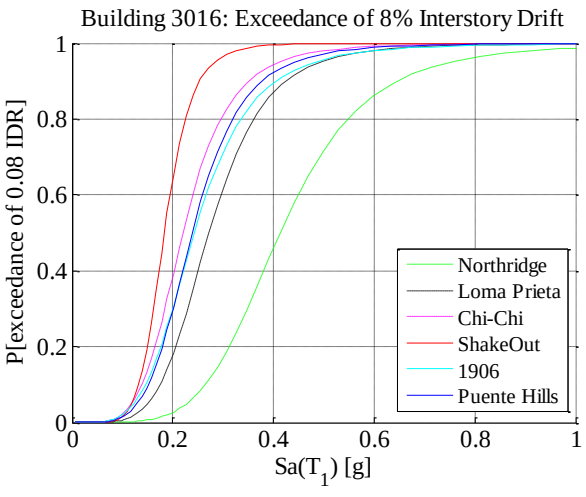

Building 1001 (Due to limited collapses, logistic regression could not be performed, therefore collapse fragility curve cannot be created)

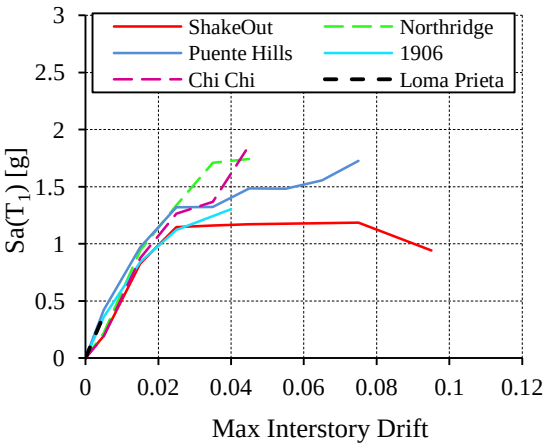

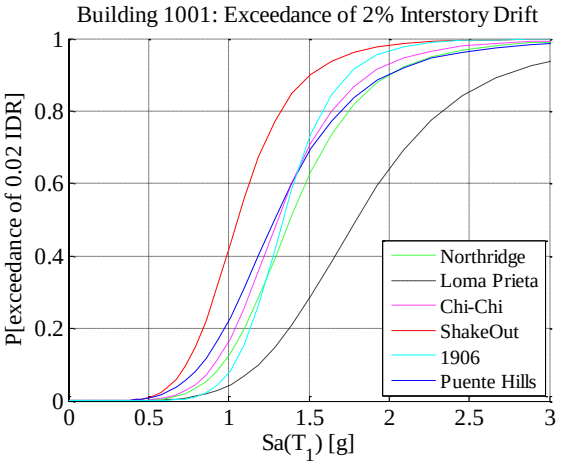

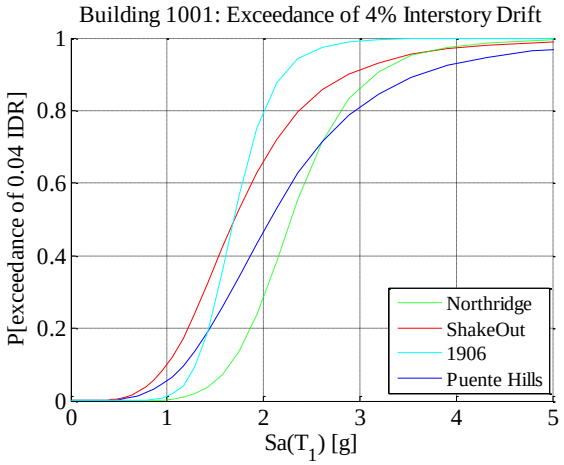

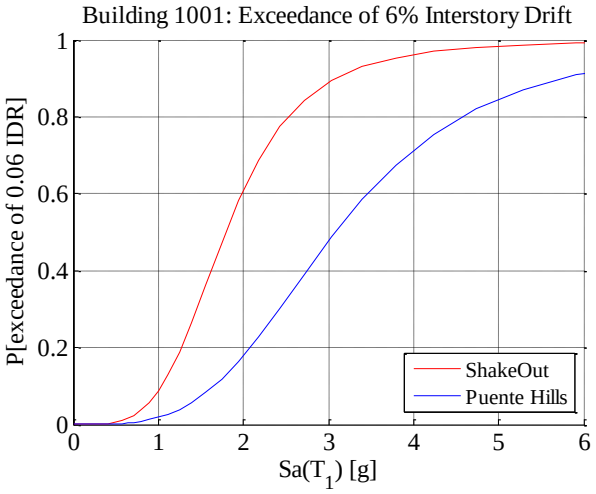

Building 1008

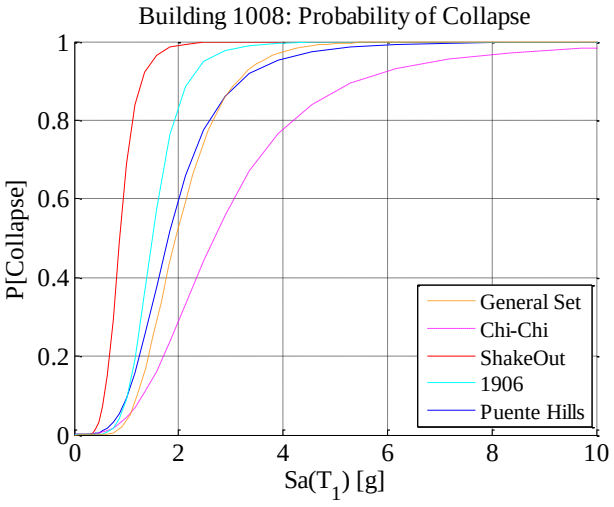

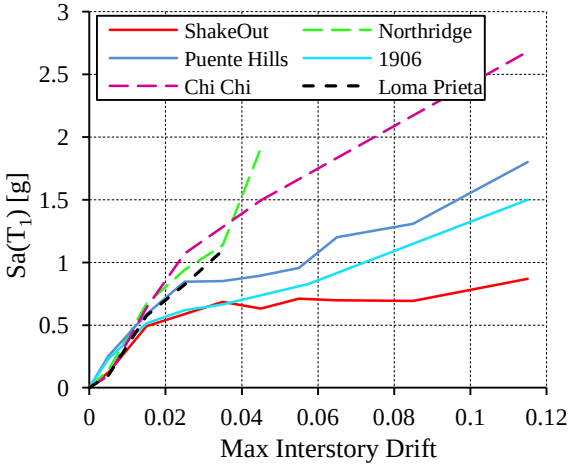

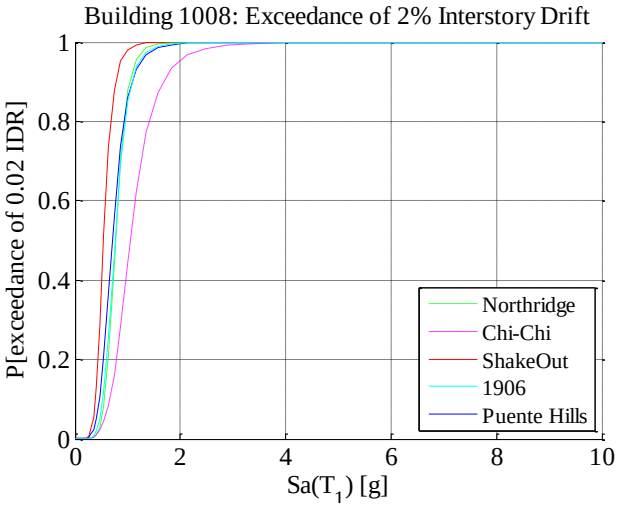

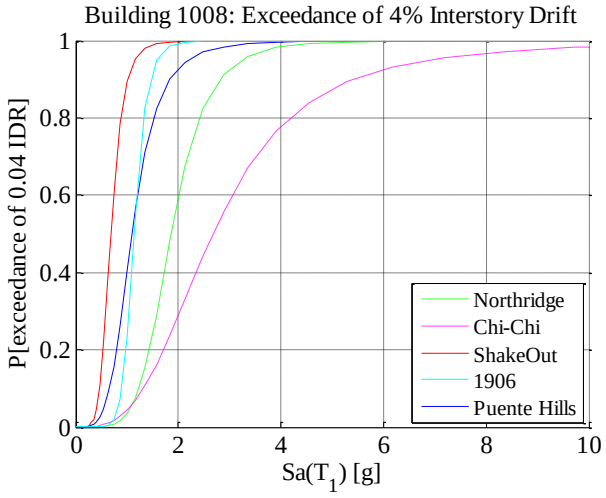

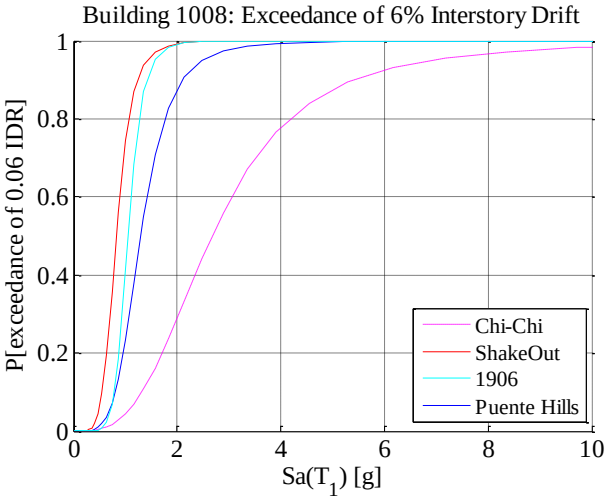

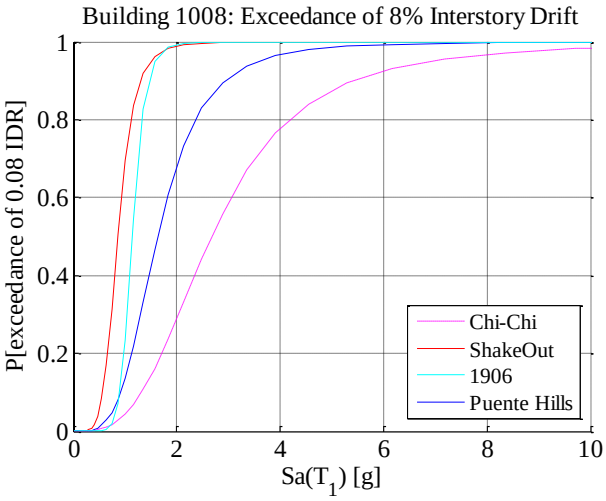

Building 1012

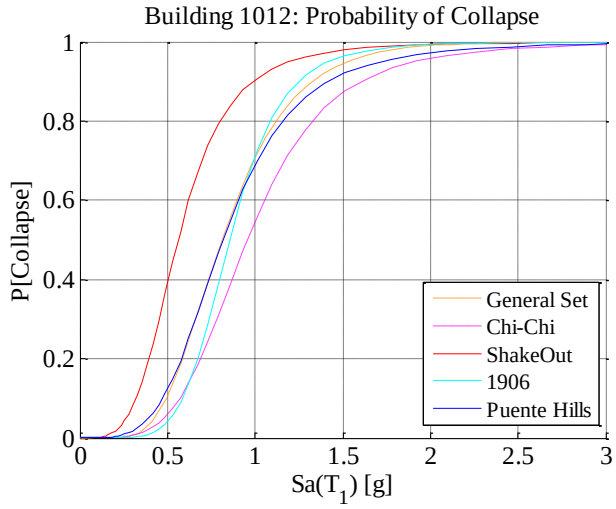

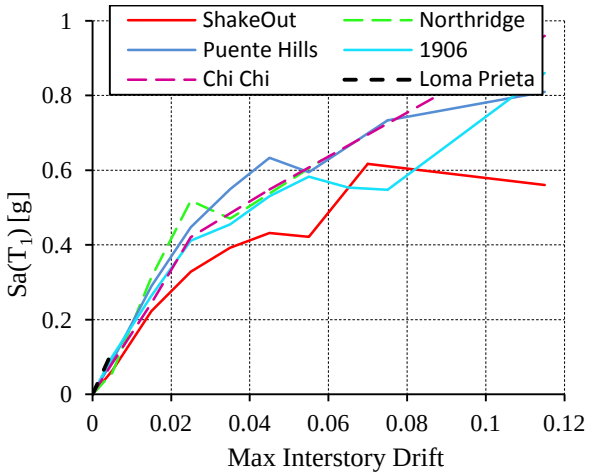

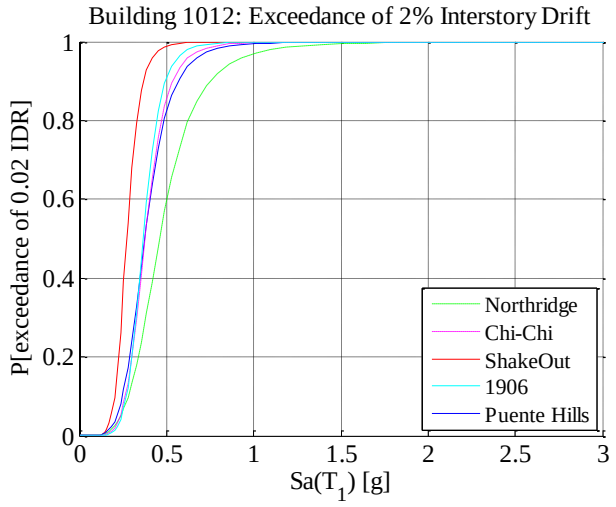

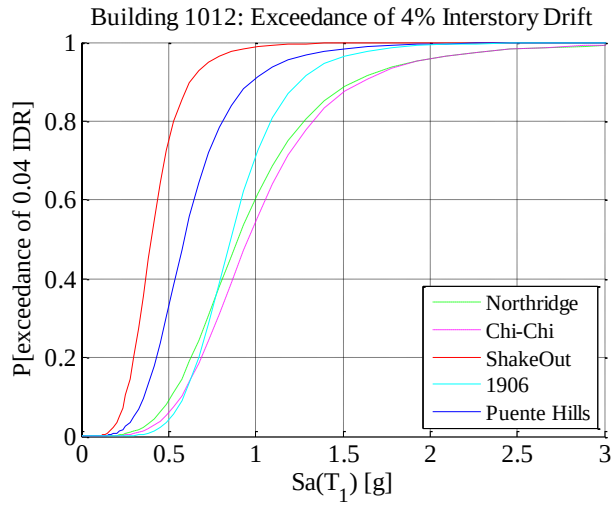

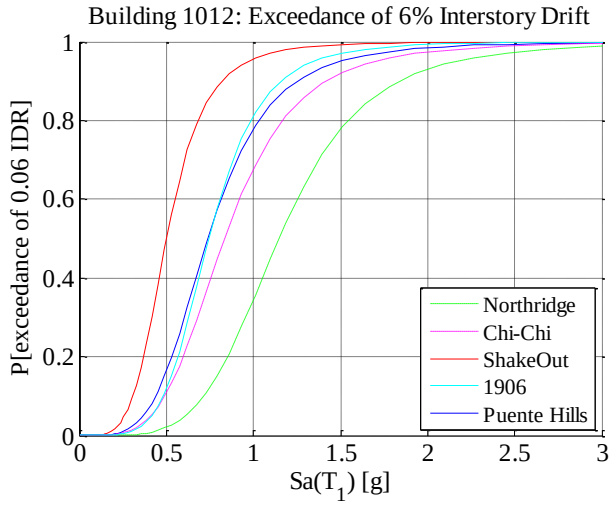

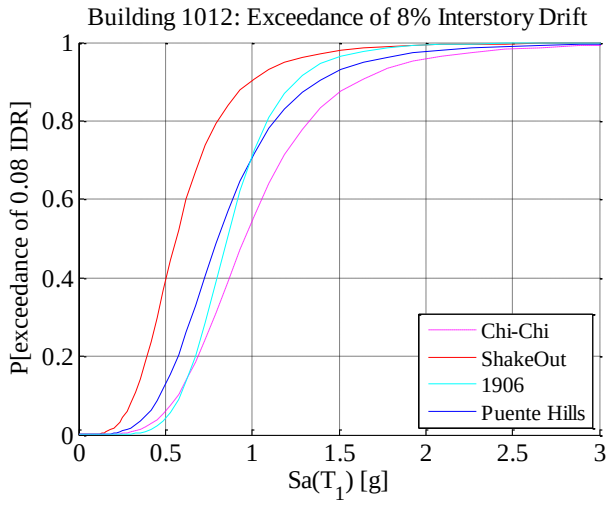

A.3 Examining *Sdi* by building

Building 3001

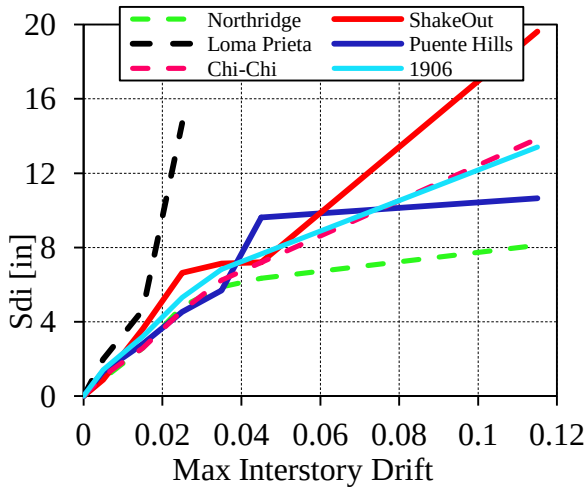

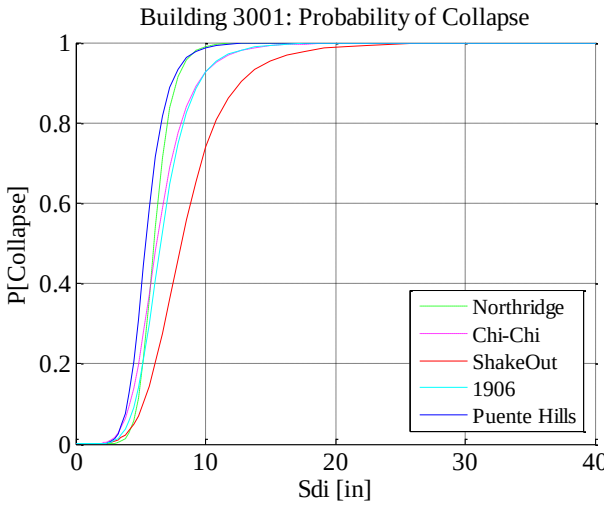

Building 3004

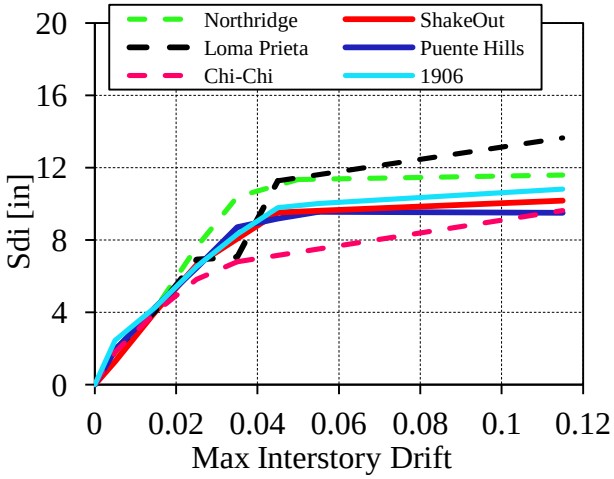

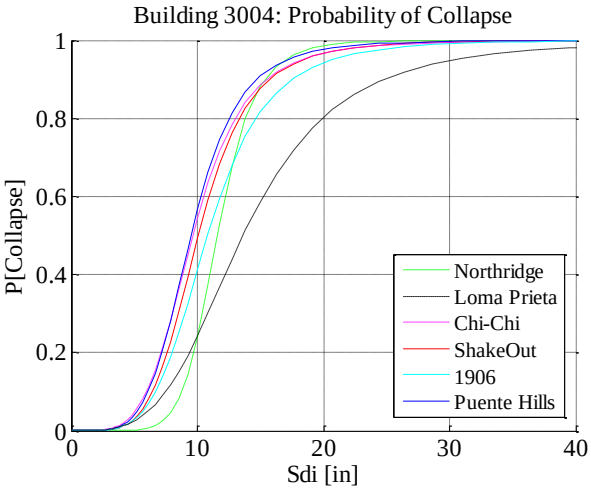

Building 3016

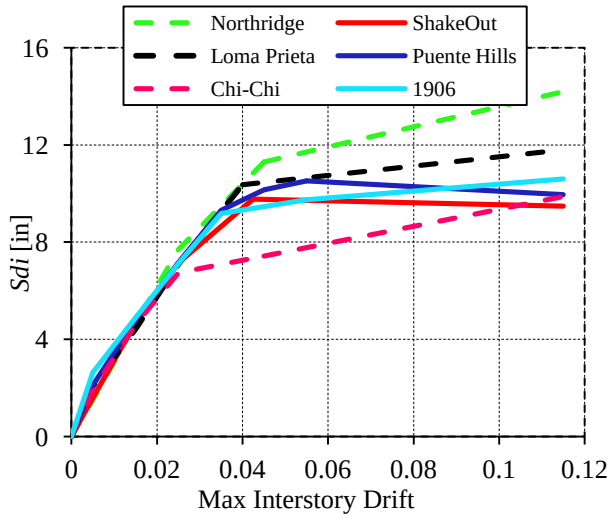

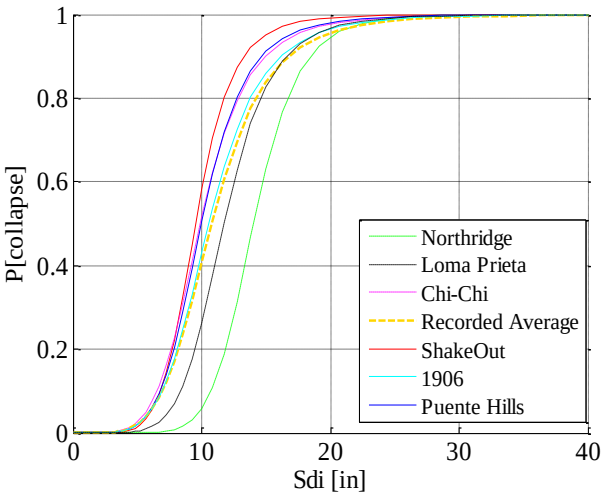

Building 1001 (Due to limited collapses, logistic regression could not be performed, therefore collapse fragility curve cannot be created)

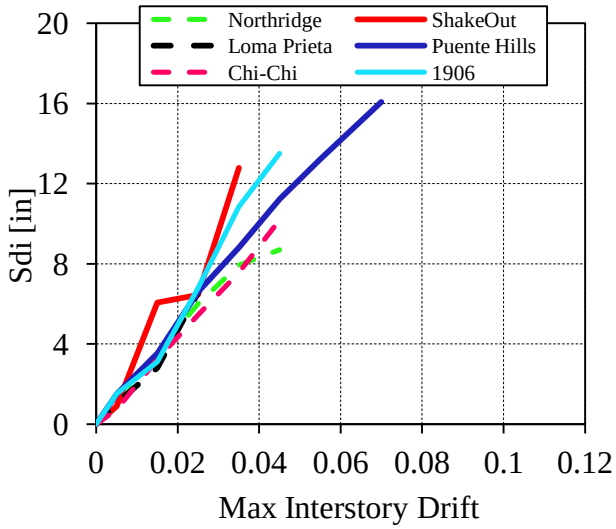

Building 1008

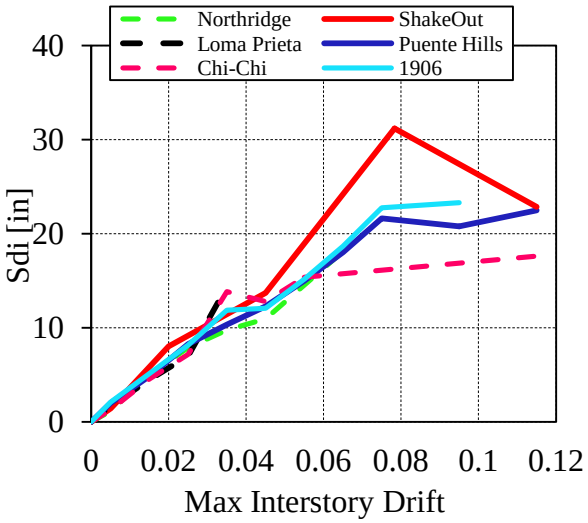

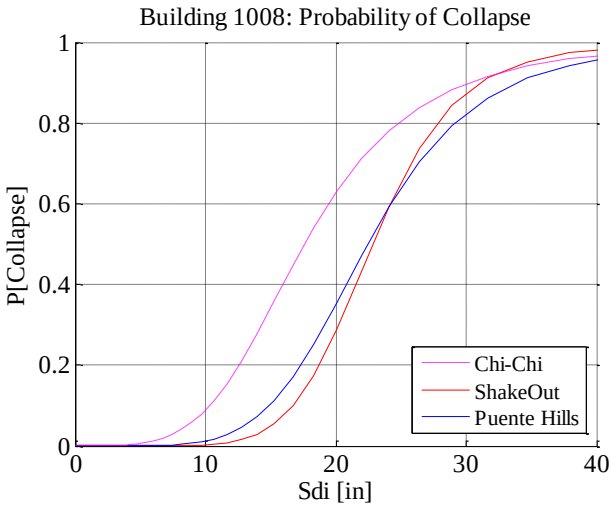

Building 1012